Pacific Northwest
NATIONAL LABORATORY

PNNL-38085

Evaluation of Howard A. Hanson Dam Juvenile Fish Passage and Survival Study

Final Report for the Live Fish Injury Assessment, Sensor Fish, and BioPA Modeling Tasks

January 2026

Stephanie A Liss Larson, Rajesh K. Singh, Brett D Pflugrath, Tao Huang, Jade M Carver, Eric S Fischer, Margaret J Giggie, Ryan A Harnish, Aljon L Salalila, Antonio Lopez Guzman, Kyle R DeSomber, Z. Daniel Deng

U.S. DEPARTMENT of ENERGY

Prepared for the U.S. Department of Energy
under Contract DE-AC05-76RL01830

DISCLAIMER

PACIFIC NORTHWEST NATIONAL LABORATORY
operated by
BATTELLE
for the
UNITED STATES DEPARTMENT OF ENERGY
under Contract DE-AC05-76RL01830

Printed in the United States of America

Available to DOE and DOE contractors from
the Office of Scientific and Technical Information,
P.O. Box 62, Oak Ridge, TN 37831-0062
www.osti.gov
ph: (865) 576-8401
fox: (865) 576-5728
email: reports@osti.gov

Available to the public from the National Technical Information Service
5301 Shawnee Rd., Alexandria, VA 22312
ph: (800) 553-NTIS (6847)
or (703) 605-6000
email: info@ntis.gov
Online ordering: http://www.ntis.gov

PNNL-38085

Evaluation of Howard A. Hanson Dam Juvenile Fish Passage and Survival Study

Final Report for the Live Fish Injury Assessment, Sensor Fish, and BioPA Modeling Tasks

January 2026

Stephanie A Liss Larson, Rajesh K. Singh, Brett D Pflugrath, Tao Huang, Jade M Carver, Eric S Fischer, Margaret J Giggie, Ryan A Harnish, Aljon L Salalila, Antonio Lopez Guzman, Kyle R DeSomber, Z. Daniel Deng

Prepared for
the U.S. Department of Energy
under Contract DE-AC05-76RL01830

Pacific Northwest National Laboratory
Richland, Washington 99354

Preface

This study was funded by the U.S. Army Corps of Engineers (Corps) – Seattle District. It was led by Stephanie Liss Larson (509-375-2988) from Pacific Northwest National Laboratory. The USACE technical lead for the study was Fenton Khan (503-808-4777).

The structure of this final report includes four of the six tasks within the Evaluation of Howard A. Hanson Dam Juvenile Fish Passage and Survival Study. The report begins with a combined introduction to all four tasks. Sections are then structured by individual task, with each section presenting the corresponding objectives, methods, and results. A dedicated section to incorporating the findings from the four tasks into the Biological Performance Assessment toolset (BioPA) is also included.

At the end, a conclusion section synthesizes survival estimates across all four tasks. A separate document contains the appendices associated with this final report to minimize file size. These appendices provide detailed information supporting the four tasks.

This report should be cited as follows:

Liss Larson SA, Singh RK, Pflugrath BD, Huang T, Carver JM, Fischer ES, Giggie MJ, Salalila A, Lopez A, Deng ZD, DeSomber KR. 2025. *Evaluation of Howard A. Hanson Dam Juvenile Fish Passage and Survival Study*. PNNL-38085. Final Report for the Live Fish Injury Assessment, Sensor Fish, and BioPA Modeling Tasks submitted by the Pacific Northwest National Laboratory to the U.S. Army Corps of Engineers, Seattle, Washington.

Executive Summary

The United States Army Corps of Engineers (Corps) is designing a downstream fish bypass system at Howard A. Hanson Dam (HAHD) on the Green River in Washington State. To support the design of the bypass, the Corps requested assistance from Pacific Northwest National Laboratory (PNNL) to evaluate the expected survival rates of fish during passage through the new proposed design. This evaluation used a combination of live fish injury and survival testing, Sensor Fish measurements, Computational Fluid Dynamics (CFD) modeling, and application of the Biological Performance Assessment toolset (BioPA). PNNL recently proposed novel strike metrics based on velocity (M_V) measured by the Sensor Fish to quantify the biological effects of strikes/collisions and shear effects between live fish and hydraulic structures in hydroturbine passage. The threshold value of M_V for fish injury/mortality can vary by hydraulic structure as well as species; therefore, it can't be directly applied. Accordingly, PNNL has performed studies to calculate the M_V threshold for the HAHD tunnel as well as a high head steep slope fish bypass system at Green Peter Dam (GPR; located on the Santiam River in Oregon). Velocity-based strike metrics were applied to estimate fish survival and to relate hydraulic conditions to observed biological responses. By adhering to these velocities and through this project's assessment of the impact effects to live fish, the resultant design will allow for a high probability of survival upon the project's completion. Six tasks were used to develop the findings for the evaluation of HAHD juvenile fish passage and survival study. This report presents a summary of four of the six tasks, and methods for determining results. Results of the other two tasks were delivered in separate reports. For this report, tasks included:

- Evaluating and comparing direct live fish injury and survival, associated hydraulic conditions (Sensor Fish), and CFD modeling performed under laboratory conditions (shear tank testing; Section 2.0)
- Performing a direct live fish injury and survival and associated hydraulic conditions (Sensor Fish) study at GPR (Section 3.0)
- Performing a direct live fish injury and survival and associated hydraulic conditions (Sensor Fish) study at HAHD (Section 4.0)
- CFD modeling of GPR and HAHD for BioPA (Sections 2.0, 3.0, and 4.0)

Study tasks were conducted by researchers from PNNL. To achieve study objectives for each of the four tasks, field work occurred at GPR to evaluate the highest elevation fish intake horn of the steep slope bypass pipe and at HAHD to evaluate baseline conditions of the 19-foot (ft) horseshoe tunnel. Laboratory work occurred at PNNL's Aquatic Research Laboratory (ARL) to evaluate simulated dam passage conditions (i.e., shear forces and collision in the shear tank).

At each of these locations, live fish injury and survival assessments of fish tagged with and without balloon tags or passive integrated transponder (PIT) tags were correlated with Sensor Fish to determine thresholds. The BioPA CFD modeling analyses were then performed, and the computed values were compared to the corresponding measured values of Sensor Fish data. The results of the overall injury and survival of live fish were also used in the validation of the CFD modeling method. Each of these tasks estimated survival rates that were derived from laboratory-calibrated threshold values of *a* velocity-based strike metric *(M_V)*. Collectively, the results will aid in future modeling of fish passage at HAHD. Results from these tasks can be used by biologists, engineers, resource managers, and regional decision-makers to inform baseline conditions under current operations and the engineering design of the new fish passage facility (FPF) at HAHD.

This final report contains data and results from the four tasks. Table S-1, Table S-2, and Table S-3, and Figure S-1, Figure S-2, and Figure S-3, depict the CFD modeling findings for the fish

horn of the steep slope bypass pipe at GPR, the HAHD 19-ft horseshoe tunnel, and shear tank laboratory testing. Table S-4, Table S-5, and Table S-6 depict the Sensor Fish findings for the fish horn of the steep slope bypass pipe at GPR and the HAHD 19-ft horseshoe tunnel. Table S-9 and Table S-10 show the biological response models (derived from models developed from shear and collision laboratory testing), and Table S-11 shows the biological response model for rapid decompression for juvenile Chinook salmon (Brown et al. 2012), all of which were used to conduct BioPA analysis.

In the field, the HAHD live fish field studies incorporated a range of species and sizes. The primary species of interest was Chinook salmon (*Oncorhynchus tshawytscha*). However, coho salmon (*O. kisutch*) were used in field testing during times of the year when Chinook salmon were too small for evaluation. At GPR, live fish field studies used Chinook salmon of two age classes and sizes (fry and subyearling). As a result, both species and multiple sizes of fish were evaluated during laboratory testing. Laboratory shear exposure testing provided valuable insights into juvenile salmonid responses to hydraulic stressors, revealing trends where survival decreased with increasing exposure intensities. Specifically, fish size and species played significant roles in survival outcomes.

In laboratory collision tests, coho salmon exhibited 100% immediate and 48-hr survival at 40 fps jet velocities but survival dropped to 90.7% at 50 fps (n = 30–54 fish per treatment). This indicated that velocities around 50 fps began to induce mortality through strike impacts and calibrated a mortal velocity-based strike metric (M_V) threshold of 4.45 m/s from CFD. Laboratory shear tests also demonstrated high immediate survival (> 95%) for both coho and Chinook salmon up to 50 fps, with no mortalities attributed to shear, though survival trended lower at velocities exceeding 50 fps, and Chinook salmon proved more resilient than coho salmon to these forces. Field tests at GPR showed consistently high immediate (> 98%) and 48-hr survival (98.8% for Chinook salmon fry, 97.2% for subyearlings; n = 179–190 fish per treatment) through the steep slope bypass at 985 ft elevation and 100% flow control gate opening. At the HAHD tunnel, immediate survival for coho salmon remained high (> 90%) across test conditions, but 48-hr survival varied from 75.9% to 100% (n = 20–107 fish per treatment), trending lower at higher forebay elevations (e.g., 1164–1168 ft) and intermediate flow control gate openings (17–21 in) due to operational influences on hydraulic conditions.

Based on pressure nadir values from Sensor Fish measurements and CFD analyses, barotrauma is likely negligible for fish passage at both HAHD and GPR under the evaluated conditions, although a portion of nadir values at GPR reached levels that may pose concern for depth-acclimated fish. The testing was effective in establishing conservative survival baselines to inform bypass designs, despite field limitations such as balloon tag challenges at HAHD—including the lack of depth acclimation prior to release, balloon tag retention failures resulting in recovered tags without fish or fish without tags, and unrecovered individuals in general—and recovery issues at GPR's juvenile fish collector. Balloon tag presence increased mortality probability, rendering observed survival rates conservative relative to non-tagged wild fish.

Sensor Fish measurements were used to identify the hydraulic mechanisms associated with observed live fish survival trends by quantifying strike/collision, shear, and pressure-related stressors during passage. Across laboratory testing, GPR, and HAHD, collision-related acceleration events were the dominant stressor, while shear exposure was infrequent and pressure effects were minimal under the evaluated conditions. Laboratory shear testing showed that peak accelerations increased with jet velocity, and a statistically significant tag effect was observed, with tagged Sensor Fish exhibiting lower peak accelerations than non-tagged units ($p < 0.01$). Shear-related strike metrics (M_V) were consistently low and not associated with predicted

mortality, supporting live-fish observations that shear was not a primary injury mechanism under tested conditions.

At GPR, Sensor Fish data revealed substantially higher collision severity in the 24-in steep slope bypass pipe compared to the horizontal 12-in pipe, with mean maximum accelerations increasing from 101 g_0 to 193 g_0 and severe acceleration events increasing from 46% to 100% of releases. Collision severity quantified using the velocity-based strike metric (M_V) was consistently higher in the 24-in pipe, while all M_V values in the 12-in pipe remained below calibrated collision thresholds. Approximately 80% of predicted mortal collision events in the 24-in pipe occurred within the bend region (bottom of the steep slope pipe), identifying this area as the primary contributor to collision risk.

At HAHD, Sensor Fish results showed that severe acceleration events were infrequent at the gate opening, indicating minimal collision occurrence at the radial gate, while the upstream tunnel transition and tunnel regions exhibited higher acceleration magnitudes and elevated M_V values. A collision mortal threshold of M_V = 1.27 m/s was calibrated using the coho salmon survival data, and showed strong agreement between Sensor Fish predictions and live-fish survival in the upstream tunnel transition region (r = 0.86, p = 0.005), identifying this region as the dominant contributor to predicted injury and mortality. Consistent with live-fish observations, collision severity increased with higher forebay reservoir elevations.

The predicted survival outcomes from the CFD modeling were compared to the field and laboratory tests. The CFD predictions agreed strongly with the Sensor Fish data. Additionally, the predicted live fish survival rates, calculated using the laboratory-calibrated threshold values of the velocity-based strike metric—M_V—were reasonably consistent with the survival rates observed in the live fish field studies and Sensor Fish outcomes for GPR. However, the survival rates predicted by both CFD simulations and Sensor Fish studies were higher than those recorded in live fish field studies conducted at HAHD.

Extensive investigations were conducted to examine the disparities in M_V values between HAHD predictions and laboratory experiments—values that were significantly lower from field studies at HAHD—thereby facilitating the establishment of an appropriate M_V threshold. The M_V threshold derived from laboratory collision testing was applied to historical spillway passage data from other dams in the Pacific Northwest (presented in Appendix I). The fish survival rates calculated using this threshold demonstrated good agreement with those obtained directly from the laboratory shear tank collision tests. Subsequently, multiple hydraulic stressors influencing fish survival at HAHD were thoroughly evaluated for their potential synergistic effects. Analyses revealed that shear, collision, and nadir pressure acted collectively to determine individual fish survival. Nadir pressure variations remained within ranges that were unlikely to pose a mortality risk to surface-acclimated fish.

Table S-1. Data summary for CFD-particle studies for severe events and strike metrics, with live fish for GPR (2023).

Bypass Pipe Elevation (ft)	Gate Opening (%)	Number of Particles Released	Percentage of particle with Severe Events (≥ 95 g_0)	Strike Metric (M_V) (m/s) – [fps]		48-hr Survival Rate[1]	Live Fish – Chinook Salmon			
							Live Fish Releases (*n*) for Treatment & Control		48-hr Survival Rate (%)	
				95th Percentile	Max Value		Fry	Subyearling	Fry	Subyearling
985	100	600	100	3.65 – [11.97]	5.49 – [18.01]	98.60	179 & 175	190 & 186	98.8	97.2

[1] Estimated from Mortal Threshold of Strike Metrics ($M_V = 4.21\ m/sec$) calibrated from laboratory collision tests (coho salmon) with a jet velocity of 50 fps and a 20° plate angle in 2025.

Mortal threshold predicted from the laboratory collision testing setup can pe applied to high head fish passage. This threshold value closely aligns with findings from a recent study that combined Sensor Fish and live fish testing with yearling Chinook salmon at the removable spillway weir of Ice Harbor Dam in 2015 (Duncan et al., 2018). The study identified a threshold M_V of 4.25 m/s.

The CFD-predicted survival rate corresponds closely with observations from live fish field studies. However, survival rates can vary significantly depending on the species, which are specific to the species evaluated, their size class, and the hydraulic conditions under consideration.

Table S-2. CFD-particle data summary for HAHD field testing (2023–2024).

Forebay Reservoir Elevation (ft)	Gate Opening (in)	Fish Strike Metric (M_V) at 95% cumulative exposure (based on CFD modeling; vertical dashed line in Figure S-1)[1]		48-hr Survival Rate from CFD, using estimates from Sensor Fish Strike Metric (M_V) and Mortal Threshold (1.78 m/s) Calibrated from Collision Lab Tests (Coho) in 2025 (see Table 1.3)[2]	Live Fish – Coho Salmon	
		Overall Region (m/s) – [fps]	Max M_V for Overall Region (m/s) – [fps]	Overall Tunnel Region[3] (%)	Live Fish Releases (*n*) for Treatment & Control	48-hr Survival Rate (%)
1089.2	10	1.25 – [4.10]	2.28 – [7.48]	99.2	48 & 57	92.3
1089.9	20	1.02 – [3.34]	1.63 – [5.35]	100	45 & 55	95.6
1090	32	1.37 – [4.49]	1.89 – [6.20]	99.45	42 & 38	85.7
1137.8	8	2.13 – [6.99]	2.77 – [9.09]	80.03	30 & 30	85
1137.4	16	1.93 – [6.33]	5.10 – [16.73]	93.5	20 & 20	100
1137.8	24	1.97 – [6.46]	4.10 – [13.45]	91.95	30 & 30	100
1168.1	17	1.86 – [6.10]	3.89 – [12.76]	94.05	50 & 50	77.8
1164.8	21	1.72 – [5.64]	3.97 – [13.02]	95.7	107 & 108	75.9

[1] Particle Shape: Cylinder (Same as Sensor Fish); Number of Particles Released: 600

[2] The M_V values observed in Howard Hanson Tunnel are significantly lower compared to the laboratory experiments conducted at Pacific Northwest National Laboratory (PNNL).

Table S-3. CFD-particle data summary for the collision lab tests (2025).

Jet Velocity (fps)	Plate Angle (°)	Number of Particles	Percentage of Particles with Severe Events (≥ 95 g_0)	Values of Sensor Fish Particle Strike Metric (M_V)		48-hr Survival Rate Estimated from Sensor Fish Strike Metric (M_V) and Mortal Threshold (4.21 m/s) Calibrated from Collision Tests (Coho salmon experiencing 50 fps-Jet Velocity and 20°-Plate) in 2025	Live Fish – Coho Salmon	
				95th Percentile M_V Collision Events (m/s) –[fps]	Max M_V (m/s) –[fps]		Live Fish Releases (*n*) for Treatment Fish	48-hr Survival Rate (%)
40	20	400	99	3.32 – [11.09]	4.25 – [13.94]	100	30	100
50	20	400	100	4.51 – [14.80]	5.43 – [17.81]	90.74	54	90.7

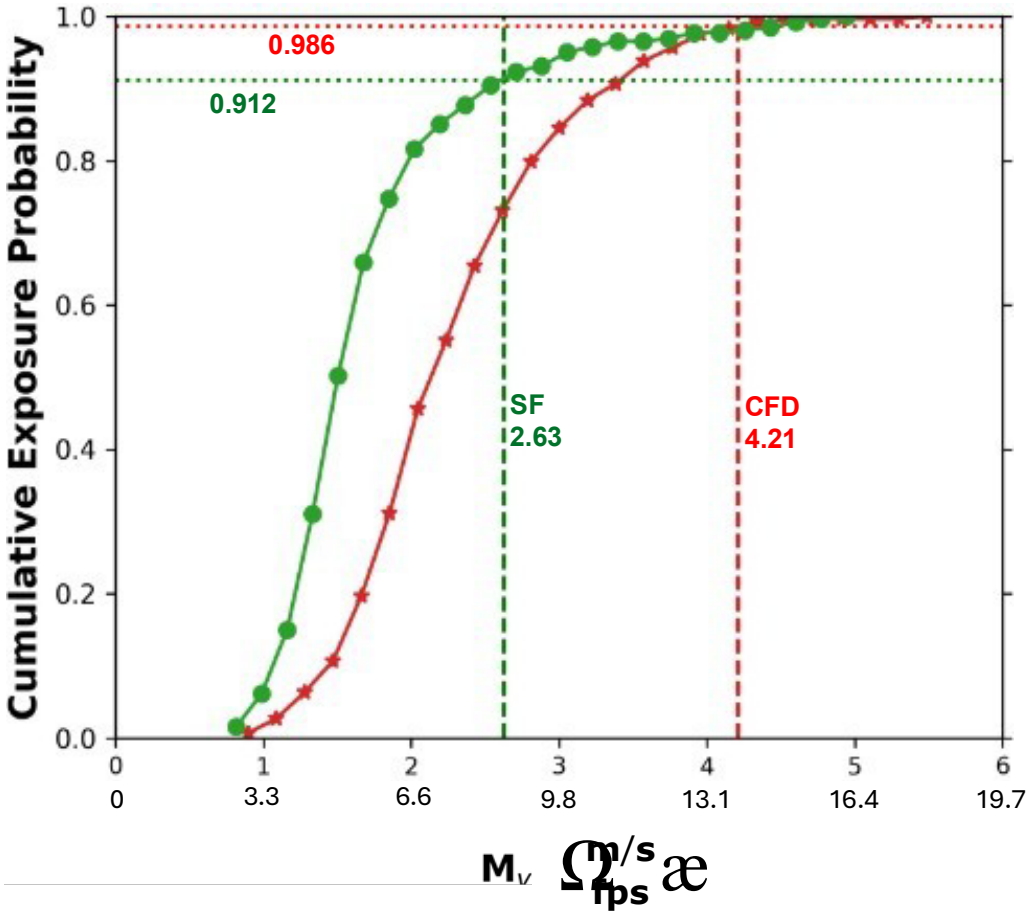

Figure S-1. Comparison of CFD-predicted and Sensor Fish-estimated cumulative exposure probabilities for M_V due to strike at GPR. The vertical green and red dashed lines represent the threshold values of M_V for coho salmon obtained from Sensor Fish experiments and CFD simulations, respectively. The horizontal green and red dotted lines indicate the corresponding survival probability of coho salmon observed in the Sensor Fish experiments and CFD simulations, respectively.

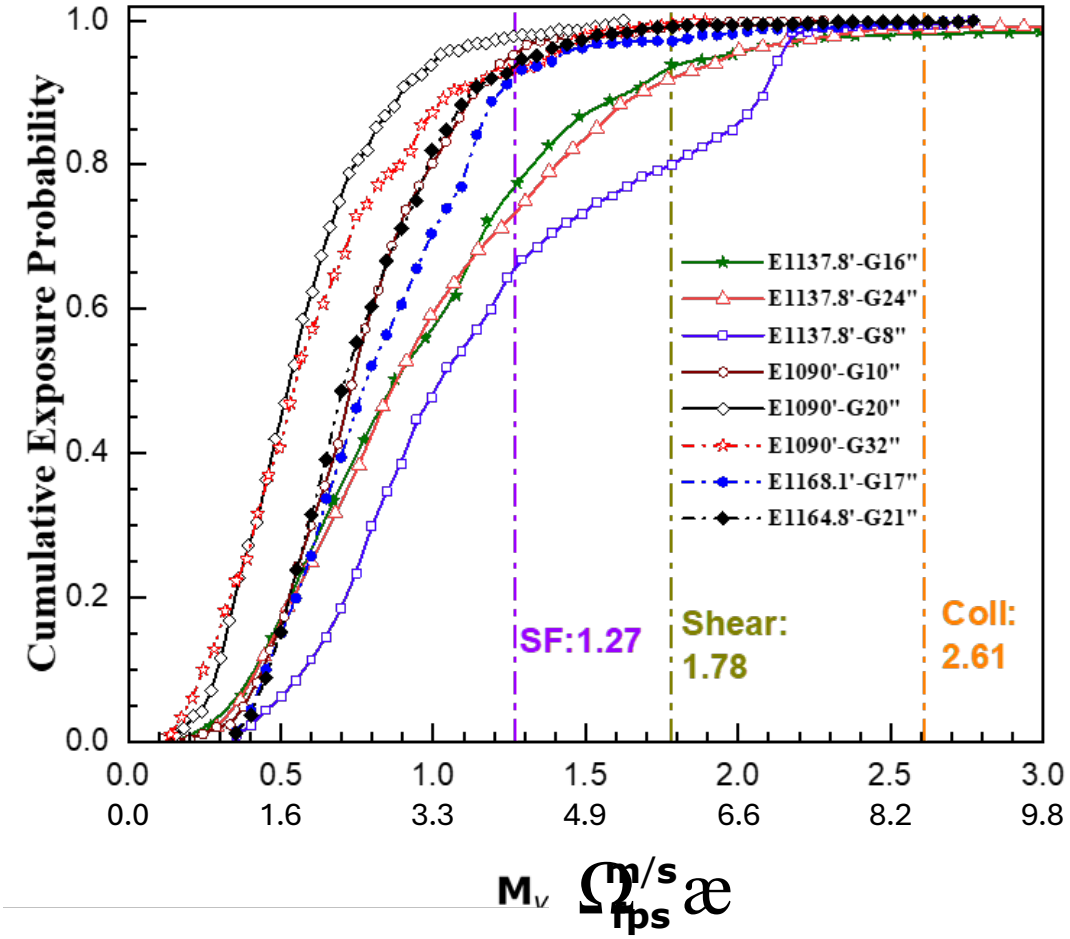

Figure S-2. Cumulative exposure probability of the CFD-predicted M_V under various operating conditions for HAHD fish passage. The three vertical lines denote the calibrated mortality thresholds for Sensor Fish (SF) derived from HAHD, shear, and collision (coll) tests, based on submerged shear lab testing conducted in 2024. The legend is formatted as “E: Forebay Elevation in feet, and G: Gate Opening in inches.

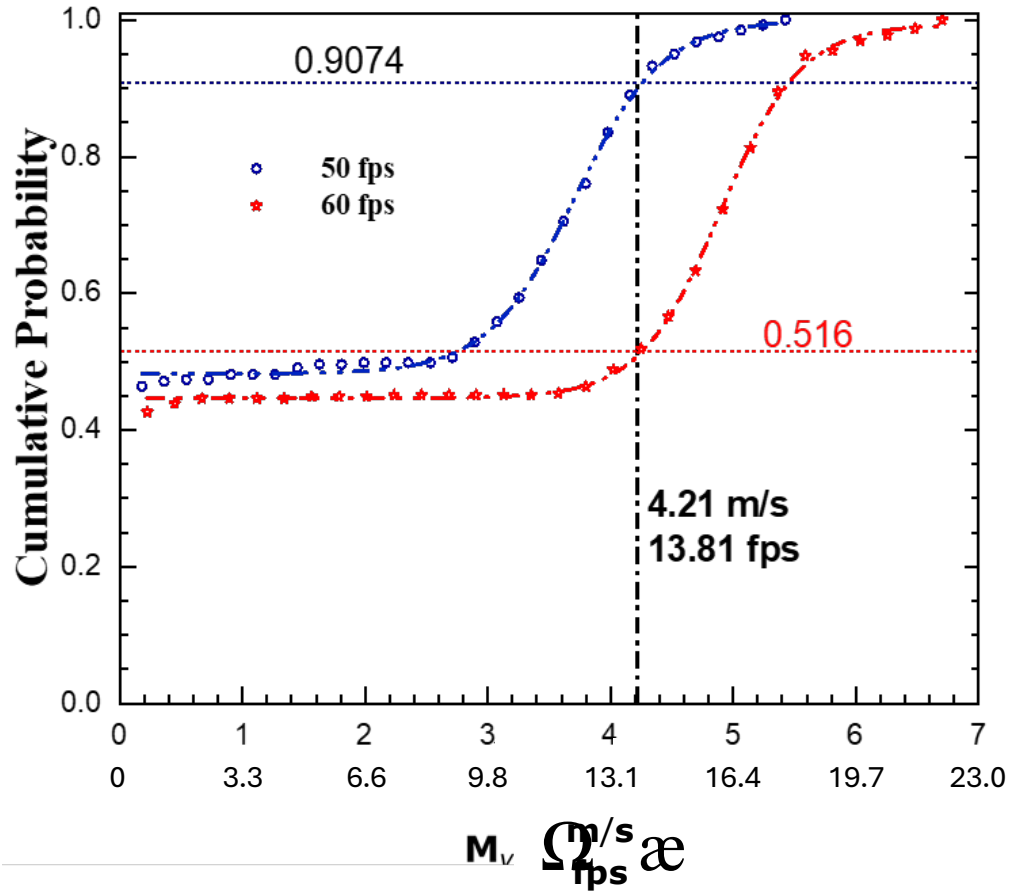

Figure S-3. CFD-predicted cumulative exposure probabilities of M_V values during Collision Testing conducted at PNNL. The top horizontal blue dotted line represents coho salmon survival from laboratory experiments, while the vertical black dash-dot line indicates the CFD-predicted threshold value of M_V. The lower red dotted line represents the predicted survival probability at the jet velocity of 60 fps.

Table S-4. Sensor Fish data summary of severe events and strike metrics, with live fish results from GPR (2023).

Bypass Pipe Elevation (ft)	Gate Opening (%)	Valid Sensor Fish Releases (*n*)	Percentage of Sensor Fish Releases with Severe Events (≥ 95 g_0)		Values of Sensor Fish Strike Metric (M_V) [1]			48-hr Survival Rate Estimated from Sensor Fish Strike Metric (M_V) Mortal Thresholds of 2.63 and 4.25 m/s [1 3 4] [8.63 and 13.94 fps]			Live Fish – Chinook Salmon			
											Live Fish Releases (*n*) for Treatment & Control		48-hr Survival Rate (%) [2]	
			12-in Pipe (%)	24-in Pipe (%)	Average & 95th Percentile M_V for 12-in Pipe (m/s) [fps]	Average & 95th Percentile M_V for 24-in Pipe (m/s) [fps]	Max M_V (m/s) [fps]	12-in Pipe (%)	24-in Pipe (%)	Overall Pipe Region (%)	Fry	Subyearling	Fry	Subyearling
985	100	261	46	100	0.46 & 1.40 [1.51 & 14.59]	1.68 & 3.03 [5.51 & 9.94]	4.95 [16.24]	100 & 100	91.23 & 98.37	91.23 & 98.37	179 & 175	190 & 186	98.8	97.2

[1] There was only one mild shear event (with a duration longer than 7.5 milliseconds and low M_V values) observed in Sensor Fish data for GPR, and it was excluded from the table above.

[2] The live fish survival estimates for GPR may be affected by the unintended stressors due to the severe collisions with the evaluator/collection basin at the end of the bypass passage.

[3] Based on live fish collision laboratory testing conducted in 2025 using juvenile Coho salmon (*Oncorhynchus kisutch*) under a treatment condition of 50 fps jet velocity and a 20° impact plate, the calibrated mortal threshold for the collision-based velocity metric (M_V) was determined to be 2.63 m/s. This threshold is specific to the tested species, size class, and experimental conditions.

[4] Considering the similar flow conditions between the steep pipe flow at GPR and spillway flow, a second mortal threshold for M_V was identified as 4.25 m/s based on combined Sensor Fish and live fish testing with Yearling Chinook salmon (*Oncorhynchus tshawytscha*) conducted at the removable spillway weir of Ice Harbor Dam in 2015 (Duncan et al., 2018). This threshold is specific to the species, size class, and hydraulic conditions evaluated in that study.

Table S-5. Sensor Fish data summary of severe events and strike metrics for HAHD (2024).

Forebay Reservoir Elevation (ft)	Gate Opening (in)	Valid Sensor Fish Releases (*n*)	Percentage of Sensor Fish Releases with Severe Events (≥ 95 g_0)						95th Percentile of Sensor Fish Strike Metric (M_V) [1]					
			Gate Opening Region (%)	Upstream Tunnel Transition (%)	Gate & Upstream Tunnel Transition (%)	Tunnel (%)	Downstream Tunnel Transition (%)	Overall Region (%)	Gate Opening Region (m/s) [fps]	Upstream Tunnel Transition (m/s) [fps]	Gate & Upstream Tunnel Transition (m/s)[3] [fps]	Tunnel (m/s) [fps]	Downstream Tunnel Transition (m/s) [fps]	Overall Region (m/s)
1091.3	9	30	13.3	13.3	26.7	46.7	0	63.3	3.07 [10.07]	1.11 [3.64]	3.07 [10.07]	1.09 [3.58]	0.00 [0.00]	3.07 [10.07]
1089.2	10	29	3.4	34.5	37.9	48.3	0	69	0.00 [0.00]	1.22 [4.00]	1.62 [5.31]	1.06 [3.48]	0.00 [0.00]	1.62 [5.31]
1089.9	20	58	0	25.9	25.9	58.6	0	67.2	0.00 [0.00]	0.95 [3.12]	0.95 [3.12]	1.59 [5.22]	0.00 [0.00]	1.59 [5.22]
1090	32	38	0	23.7	23.7	52.6	5.3	63.2	0.00 [0.00]	1.1 [3.61]	1.10 [3.61]	1.25 [4.10]	0.17 [0.56]	1.50 [4.92]
1145.3	7	28	3.6	67.9	71.4	89.3	0	96.4	0.00 [0.00]	1.45 [4.76]	1.79 [5.87]	1.62 [5.31]	0.00 [0.00]	1.88 [6.17]
1143.4	15	64	4.7	65.6	67.2	62.5	3.1	84.4	0.00 [0.00]	1.79 [5.87]	1.79 [5.87]	1.94 [6.36]	0.00 [0.00]	2.04 [6.69]
1141.5	23	52	0	44.2	44.2	67.3	13.5	76.9	0.00 [0.00]	1.65 [5.41]	1.65 [5.41]	1.31 [4.30]	0.98 [3.22]	1.65 [5.41]
1168.1	17	40	5	67.5	70	57.5	5	80	0.05 [0.16]	1.61 [5.28]	1.67 [5.48]	1.51 [4.95]	0.04 [0.13]	1.90 [6.23]
1164.8	21	110	10	44.5	50.9	27.3	4.5	62.7	1.17 [3.84]	1.56 [5.12]	1.59 [5.22]	1.36 [4.46]	0.00 [0.00]	1.66 [5.45]
Pearson Correlation Coefficient [2]			0.003	-0.74	-0.73	-0.06	-0.58	-0.44	0.34	-0.89	0.07	-0.21		
(p-values)			0.99	0.03	0.03	0.88	0.13	0.27	0.39	0.002	0.86	0.61		

[1] There were only three mild shear events (with a duration longer than 7.5 milliseconds and low M_V values) observed in Sensor Fish data for HAHD, and they were excluded.
[2] Pearson correlation coefficient between Sensor Fish measurements and 48-hr live fish survival rates from HAHD 2023 to 2024. Bolded values indicate a significant correlation.
[3] Gate & Upstream Tunnel Transition region refers to combination of the previous two regions and shows the 95th percentile of the events measured along the two regions.

Table S-6. Sensor Fish data summary of strike metric with live fish survival results for HAHD (2024).

Reservoir Elevation Category	Flow Category	Forebay Reservoir Elevation (ft)	Gate Opening (in)	Valid Sensor Fish Releases (*n*)	48-hr Survival Rate Estimated from Sensor Fish Strike Metric (M_V) Mortal Threshold (1.27 m/s)[3] with the Highest Correlation with HAHD Live Fish Survival Estimates [1]						Live Fish – Coho Salmon	
					Gate Opening (%)	Upstream Tunnel Transition (%)	Gate & Upstream Tunnel Transition (%)	Tunnel (%)	Down-stream Tunnel Transition Region (%)	Overall Tunnel Region (%)	Live Fish Releases (*n*) for Treatment & Control	48-hr Survival Rate (%)
Low	Low	1091.3	9	30	86.67	96.67	83.33	100	100	83.33	48 & 57	92.3
Low	Low	1089.2	10	29	96.55	96.55	93.10	100	100	93.10	….	….
Low	Med	1089.9	20	58	100	100	100	87.93	100	87.93	45 & 55	95.6
Low	High	1090	32	38	100	94.74	94.74	94.74	97.37	86.84	42 & 38	85.7
Med	Low	1145.3	7	28	96.43	82.14	78.57	78.57	100	64.29	50 & 50	80
Med	Med	1143.4	15	64	98.84	76.56	75.00	78.12	100	59.38	66 & 79	80
Med	High	1141.5	23	52	100	84.62	84.62	92.31	98.08	78.85	54 & 63	76.9
High	Med	1168.1	17	40	97.51	85.00	82.50	85.74	97.5	67.5	50 & 50	77.8
High	High	1164.8	21	110	96.36	83.64	80.91	91.82	100	75.45	107 & 108	75.9
Pearson Correlation Coefficient [2]					-0.30	**0.86**	**0.67**	0.36	0.27	**0.65**	/	
(p-values)					0.46	**0.005**	**0.06**	0.37	0.50	**(0.07)**		

[1] There were only three mild shear events (with a duration longer than 7.5 milliseconds and low M_V values) observed in Sensor Fish data for HAHD, and they were excluded. The M_V values observed in Howard Hanson Tunnel are significantly lower compared to the laboratory experiments conducted at Pacific Northwest National Laboratory (PNNL).

[2] Given the uncertainty in live fish results from HAHD 2023, we only focused on the Pearson correlation coefficient between Sensor Fish measurements and 48-hr live fish survival rates from HAHD 2024. Bolded values indicate a significant correlation.

[3] The mortal threshold of 1.27 m/s was calibrated through an iterative evaluation of M_V values and comparison of the resulting survival rate estimates using Pearson correlation coefficients. The value of 1.27 m/s produced the strongest correlation and was therefore selected as the mortal threshold. This threshold should only be applied to the same fish species and size class tested (Coho salmon) and the same or hydraulically similar structures under which it was derived; its applicability may differ for other species, size classes, or hydraulic configurations.

Table S-7. Sensor Fish data summary for shear lab testing with balloon-tagged and non-tagged Sensor Fish.

Jet Velocity (fps) – [m/s]	Balloon-tagged (BT) or Non-tagged (NT)	Sensor Fish releases	Average Value of Sensor Fish Strike Metric M_V (m/s) - [fps]	Max M_V (m/s) – [fps]	Chinook 48-hr Survival Rate (%)	Coho 48-hr Survival Rate (%)
40 [12.2]	BT	9	1.54 - [5.05]	1.62 - [5.31]	95.8	100
40 [12.2]	NT	42	2.18 - [7.14]	3.17 - [10.39]	96.2	70.0
50 [15.2]	BT	27	2.76 - [9.06]	3.51 - [11.52]	100	87.1
50 [15.2]	NT	61	3.28 - [10.77]	3.57 - [11.71]	94.7	100
60 [18.3]	BT	30	4.01 - [13.14]	4.46 - [14.63]	92.9	73.7
60 [18.3]	NT	51	4.69 - [15.38]	5.14 - [16.86]	94.3	66.7
70 [21.3]	BT	19	5.30 - [17.40]	5.92 - [19.42]	73.7	33.3
70 [21.3]	NT	60	6.22 - [20.42]	6.85 - [22.47]	90.0	27.8

Table S-8. Sensor Fish data summary for collision lab testing.

Jet Velocity (fps) – [m/s]	Plate angle	Number of Releases	Average Value of Sensor Fish Strike Metric M_V (m/s) – [fps]	Max M_V (m/s) – [fps]	Estimated Survival Rate from Sensor Fish Strike Metric (%)	Coho 48-hr Survival Rate (%)
40 [12.2]	20°	27	1.21 - [3.98]	2.24 - [7.35]	100	100
50 [15.2]	20°	46	1.80 - [5.92]	3.02 - [9.90]	90.7	91.0

Table S-9. Coefficients and equation, derived from biological response models, used in the BioPA model to determine probability of survival for shear exposure. Exit Orientation: Tail first = 0 and Headfirst = 1. Species: Chinook salmon = 0 and coho salmon = 1. Tag Type: Non-tagged = 0 and Balloon-tagged = 1.

Parameter	Denoted by	β_x	Chinook	Coho
(Intercept)	---	β_0	24.264914	18.824999
Jet Velocity	V_j	β_1	-0.330475	-0.327162
Length	L	β_2	-0.061214	-0.044033
TagType	T_b	β_3	-0.043537	-0.043537
Exit Orientation	E_h	β_4	0.235808	0.246824
Jet Velocity:Length	$V_j \; x \; L$	β_5	0.001074	0.001074
Exit Orientation:Jet Velocity	$E_h \; x \; V_j$	β_6	-0.019297	-0.019297
Exit Orientation:Length	$E_h \; x \; L$	β_7	-0.000216	-0.000216

$$P[y] = \frac{1}{1 + \exp(-\left(\beta_0 + \beta_1 V_j + \beta_2 L + \beta_3 T_b + \beta_4 E_h + \beta_5 \left(V_j \; x \; L\right) + \beta_6 \left(E_h \; x \; V_j\right) + \beta_6 (E_h \; x \; L)\right))}$$

Table S-10. Coefficients and equation, derived from biological response models, used in BioPA model to determine probability of survival for collision exposure. Tag Type: Non-tagged = 0 and Balloon-tagged = 1.

Parameter	Denoted by	β_x	Chinook	Coho
(Intercept)	---	β_0	10.577876	16.629325
Jet Velocity	V_j	β_1	-0.161675	-0.183583
Length	L	β_2	---	-0.080963
TagType	T_b	β_3	---	-0.043537
Jet Velocity:Length	$V_j \; x \; L$	β_4	---	0.000724

$$P[y] = \frac{1}{1 + \exp(-\left(\beta_0 + \beta_1 V_j + \beta_2 L + \beta_3 T_b + \beta_4 \left(V_j \; x \; L\right)\right))}$$

Table S-11. The biological response model for rapid decompression (from Brown et al. 2012) for juvenile Chinook salmon used in the BioPA model for live fish survival estimates.

Coefficient	Definition	Equation
P_M	Probability of Mortality	$P_M = \frac{e^{-5.56+3.85\left(\ln\frac{P_A}{P_N}\right)}}{1+e^{-5.56+3.85\left(\ln\frac{P_A}{P_N}\right)}}$
P_A	Acclimation Pressure	
P_N	Nadir Pressure	

Acknowledgments

This project was a collaborative effort which would not have been possible without the help provided by the U.S. Army Corps of Engineers – Seattle District and Howard A. Hanson Dam Facility Operations staff. These folks were instrumental in study design execution. We would like to acknowledge Nancy Chin for her support and funding, Kevin Heape and Nathan Malmborg for their support of the project, Bill Boyle, Warren Douglas, and staff for accommodations and assistance at the HAHD Facility, and Fenton Khan, Nancy Gleason, Ryan Laughery, and Aaron Litzenberg for study design and implementation collaboration.

We thank the Washington Department of Fish and Wildlife for providing study fish. We also thank the Tacoma Public Utilities, including Tyler Patterson, Jeff Bolam, Nikolas Novotny, Matt Peter, and Tyler Traweek, for performing disinfected equipment inspections and granting PNNL access to their property to hold and tag fish, and deploy autonomous receivers. Finally, we thank several staff at PNNL for their support with permitting, data collection and analysis, and administrative assistance:

Rachel Anguish
Nelly Avila
Brandon Boehnke
Noelani Boise
Jenna Brogdon
David Cancino
Olivia Coleman
Kali Davis
Kate Deters
Bri Friedman
Adrian Garza
Morgan Gilligan
James Graff
Adam Hall
Kris Hand
Joe Hawkins
Chris Henderson
Aidan Henson
Jill Janak
Greg Kondyukov
Huidong Li
Yachen Li
Toby Lidov
Micah Little
Kailan Mackereth
Emily Martin
Jayson Martinez
Brian Mason
Sophia McKever
Bob Mueller
Emily Newbould
Faridhe Puente
Sandy Rech
Rodrigo Ruiz
Jason Serkowski
Cassy Shaffer
John Stephenson
Scott Titzler
Lupita Torgeson
Josh Torgeson
Ben Vaage
Miguel Valdes
Dana Vesty
Alex Walters
Maddie Wilson
Natalie Wilson
Shon Zimmerman
Erin McCann Zionce
Heather Howell
Taylor Oxman
And many more

PNNL's Institutional Animal Care and Use Committee approved the protocol governing the care and use of fish for this study (protocol numbers 2023-03 [HAHD & GPR 2023], 2023-11 [Shear 2023], 2024-02 [HAHD 2024], 2024-11 [Shear 2024]).

All equipment deployed in the HAHD Reservoir was sterilized per Tacoma Public Utilities – Tacoma Water's "Requirements for Protection of Water Supply in the Green River Watershed, Appendix D: Decontamination of Equipment and Supplies" (Appendix A).

Acronyms and Abbreviations

|a|	absolute value of acceleration
AFF	Adult Fish Facility
AIC	Akaike Information Criterion
AICc	Second-order Akaike Information Criterion
ARL	Aquatic Research Laboratory
AUC	area under curve
BiOp	Biological Opinion
BioPA	Biological Performance Assessment Toolset
°C	degree(s) Celsius
CFD	Computational Fluid Dynamics
cfs	cubic (foot) feet per second
Corps	U.S. Army Corps of Engineers
DEM	discrete element method
DO	dissolved oxygen
el.	Elevation
ε	Turbulence dissipation rate
FL	fork length
fmsl	feet above mean sea level
FPF	Fish Passage Facility
fps	feet per second
ft	foot (feet)
g_0	standard gravity
g	gram(s)
GLM	generalized linear model
GPR	Green Peter Dam
HAHD	Howard A. Hanson Dam
HBET	Hydropower Biological Evaluation Tools
HF	headfirst
hr	hour(s)
HS video	High speed video
Hz	hertz
in	inch
k	Turbulent kinetic energy
L_f	fish length
L	Liter
mg	milligram(s)-

mL	milliliter(s)
mm	millimeter(s)
m/s	meters per second
MS-222	Tricaine methanesulfonate
M_V	velocity-based strike metric
n	number (sample size)
N	number (population size)
NCR	coefficient of the normal restitution
NGVD 29	National Geodetic Vertical Datum of 1929
NOAA	National Oceanic and Atmospheric Administration
ODFW	Oregon Department of Fish and Wildlife
PIT	Passive Integrated Transponder
PNNL	Pacific Northwest National Laboratory
PS	Puget Sound
PSI	pound per square inch
psia	pound per square inch absolute
r	Pearson correlation coefficient
ROC	receiver operating characteristic
s or sec	second(s)
SE	standard error
Δt	change in time
TF	tail first
TPU	Tacoma Public Utilities
V_j	jet velocity
VFD	variable frequency drive
VOF	Volume of Fluid method
WDFW	Washington Department of Fish and Wildlife
$\bar{x}$	sample mean

Contents

Figures

Tables

1.0 Introduction

Howard A. Hanson Dam (HAHD), owned and operated by the U.S. Army Corps of Engineers – Seattle District (Corps), is located on the Green River in western Washington State (Figure 1-1). HAHD is primarily a flood risk management project and serves secondary purposes for water supply to the City of Tacoma and flow augmentation during the summer months for fisheries downstream.

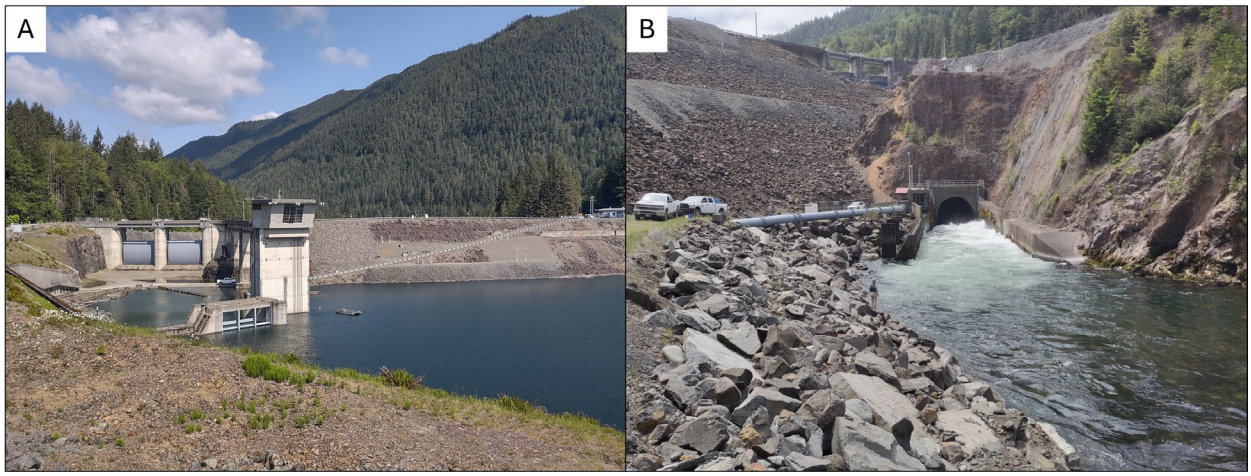

Figure 1-1. Howard A. Hanson Dam viewed from (A) the reservoir and (B) the tailrace.

Currently, information about fish passage and survival at HAHD is lacking. Endangered Species Act listed Puget Sound Chinook salmon (*Oncorhynchus tshawytscha*), and steelhead (*O. mykiss*) were historically present in the area and there is a renewed interest to reintroduce them; thus, there is a need to understand existing fish passage conditions at HAHD. Understanding current conditions can provide data to inform engineering design updates to improve fish passage.

In accordance with the Biological Opinion (BiOp) issued by the National Marine Fisheries Service (NOAA 2019), the Corps is designing a new fish passage project at HAHD, with construction to be completed by 2030. The purpose for the new fish passage facility (FPF) is to provide safe, timely, and effective downstream fish passage throughout the range of operating and reservoir conditions likely to occur during the annual fry and smolt outmigration. The current concept of the FPF design includes a multi-port collector on the forebay face of the dam (i.e., stacked vertical fish horns) and a steep slope bypass on the downstream side of the dam. The new FPF must meet the fish passage performance criteria as required by Reasonable and Prudent Alternatives outlined in the BiOp (NOAA 2019). These criteria include:

1. An overall juvenile fish project passage survival rate of 75%, from entry into the HAHD Reservoir (Eagle Gorge Reservoir) to release points downstream of HAHD.
2. 95% collection of fish attracted to the FPF.
3. 98% survival of all fish passing through the FPF to release downstream of HAHD.

This report describes four of the six tasks associated with the Evaluation of Howard A. Hanson Dam Juvenile Fish Passage and Survival Study:

1. Evaluating and comparing direct live fish injury and survival, associated hydraulic conditions (Sensor Fish), and Computational Fluid Dynamics (CFD) modeling performed under laboratory conditions (shear tank testing; Section 2.0)

2. Performing a direct live fish injury and survival and associated hydraulic conditions (Sensor Fish) study at Green Peter Dam (GPR; Section 3.0)
3. Performing a direct live fish injury and survival and associated hydraulic conditions (Sensor Fish) study at HAHD (Section 4.0)
4. CFD modeling of GPR and HAHD for Biological Performance Assessment toolset (BioPA; Sections 2.0, 3.0, and 4.0)

The ultimate goal of these tasks was to gather biological and simulation baseline information about the current and potential passage conditions and survival of juvenile salmon at HAHD. Results from these tasks will be used by biologists, engineers, resource managers, and regional decision-makers to inform baseline conditions under current operations and the engineering design of the new FPF at HAHD.

The subsequent sections of this report are separated by task (Sections 2.0, 3.0, 4.0). Each section is comprised of the objectives, methods, and results for the task. A dedicated section (Section 5.0) incorporating the findings from the four tasks into the BioPA toolset is also included. At the end, a conclusion section (Section 6.0) synthesizes survival estimates across all four tasks. Appendices A–I are located under a separate cover to minimize file size. The appendices provide detailed information supporting the four tasks.

1.1 Howard A. Hanson Dam Outlet Works Overview

The HAHD outlet works are used to pass flows and regulate the release of impounded water. The outlet works are comprised of a 19-foot (ft) wide, 900-ft long horseshoe-shaped concrete outflow tunnel controlled by two 10-ft wide by 12-ft tall tainter gates, a 700-ft long spillway chute controlled by two 45-ft wide by 30-ft tall radial arm gates, a 48-inch (in) diameter steel bypass pipe regulated with a slide gate near its outlet, and a smaller 36-in diameter steel bypass pipe. During flood and spring refill seasons, the 19-ft outflow tunnel is primarily used to pass outflows. The 48-in steel bypass pipe has some outflows passed through it, typically during the low flow season, and is solely used when regulated outflows are at or below 500 cubic feet per second (cfs). The spillway may be used only during exceptionally high flow-flood events. The 36-in bypass pipe is only used during some maintenance activities. Total outflows from HAHD range from 200 cfs in the summer months to as much as 8,500 cfs during the flood season (October–February). Typical March–July outflows are in the 200–6,000 cfs range, with few exceptions of higher flows.

2.0 Laboratory Testing and Correlation

The objective of the laboratory testing was to evaluate live fish, Sensor Fish and CFD-particle exposed to shear and impact (collision) events at varying jet velocities and impact angles using the PNNL water flume (i.e., shear tank). Designed to be performed under controlled conditions, this task developed new biological response models for fish response to varying shear and collision exposure which were applied from HAHD and GPR field testing. To develop the response models three tasks were performed:

1. Injury and survival of live fish (balloon-tagged and non-tagged) were evaluated.
2. Hydraulic conditions of the shear tank were assessed using Sensor Fish.
3. The shear tank was modeled and analyzed using Computational Fluid Dynamics (CFD).

The critical survival factors assessed through this testing were shear stressors and collisions. Shear is experienced by fish or sensor fish while transitioning through regions of differing velocities in a flow field. In the laboratory, this was modeled using a jet to create a region of high velocity in stationary water. Collisions are impacts experienced by fish or sensor fish against stationary objects. In the HAHD assessment impacts can occur with walls or with the floor of the passage. This was modeled using a jet to deflect flow off a plate in the laboratory.

Test results from this task were used to correlate live fish injury and survival (tagged with and without balloon tags) and develop biological response models based on Sensor Fish measurements of shear and impact (collision) information. Further, the computed values for shear and collision produced from the CFD analyses were compared to the corresponding measured values of Sensor Fish data. The results of the overall injury and survival of live fish to the flow shear and collisions with structures were used in the validation of the CFD modeling method and could inform future modeling of fish passage at HAHD.

2.1 Shear and Collision Laboratory Testing Methods

Laboratory testing of live fish and Sensor Fish occurred from fall 2024 through spring 2025 (October–April). The live fish component examined juvenile coho (*Oncorhynchus kisutch*) and Chinook (*O. tshawytscha*) salmon to determine how shear and collision events affect injury rates and survival.

2.1.1 Testing Facility

Laboratory evaluations were conducted in the shear tank at PNNL's Aquatic Research Laboratory (ARL). The shear tank measures 30 ft × 4 ft × 4 ft (length × width × height) and simulates various water velocities using an underwater jet nozzle (Figure 2-1). To facilitate controlled releases of live fish and Sensor Fish, the tank was equipped with a lock system positioned above the main pipe, upstream of the jet terminus (Figure 2-2). This system consisted of three valves with an intervening pipe section, allowing fish to be injected into the flow just before the jet (Neitzel et al., 2000). The middle valve restricted movement of smaller fish and was typically left open, while an extended handle on the lower valve aided operation. High-speed video cameras were installed on the side and below the shear tank to capture the nozzle and jet region and record physical and behavioral responses of fish during an exposure event.

The testing apparatus was modified with an aluminum plate installed adjacent to the jet nozzle. The aluminum plate was mounted to a frame built of 80/20 aluminum T-Slot Framing system, which was attached to bracketry located on the top of the shear tank to minimize the amount of

added structure within the tank (Figure 2-1). For shear testing, the aluminum plate was mounted parallel to the flow coming from the jet to create a boundary layer shearing exposure to fish (0° plate angle). For collision testing, the plate was rotated into the flow of the jet by 10°, 20°, and 30° to create various collision exposures and impact angles. Shear testing was operated with the jet submerged, while collision testing was first conducted with the jet submerged (Appendix B) and then with the jet above the water line.

Figure 2-1. (A) Side view of the PNNL shear tank showing the pump motor, and (B) a view from the interior of the shear tank facing the jet nozzle.

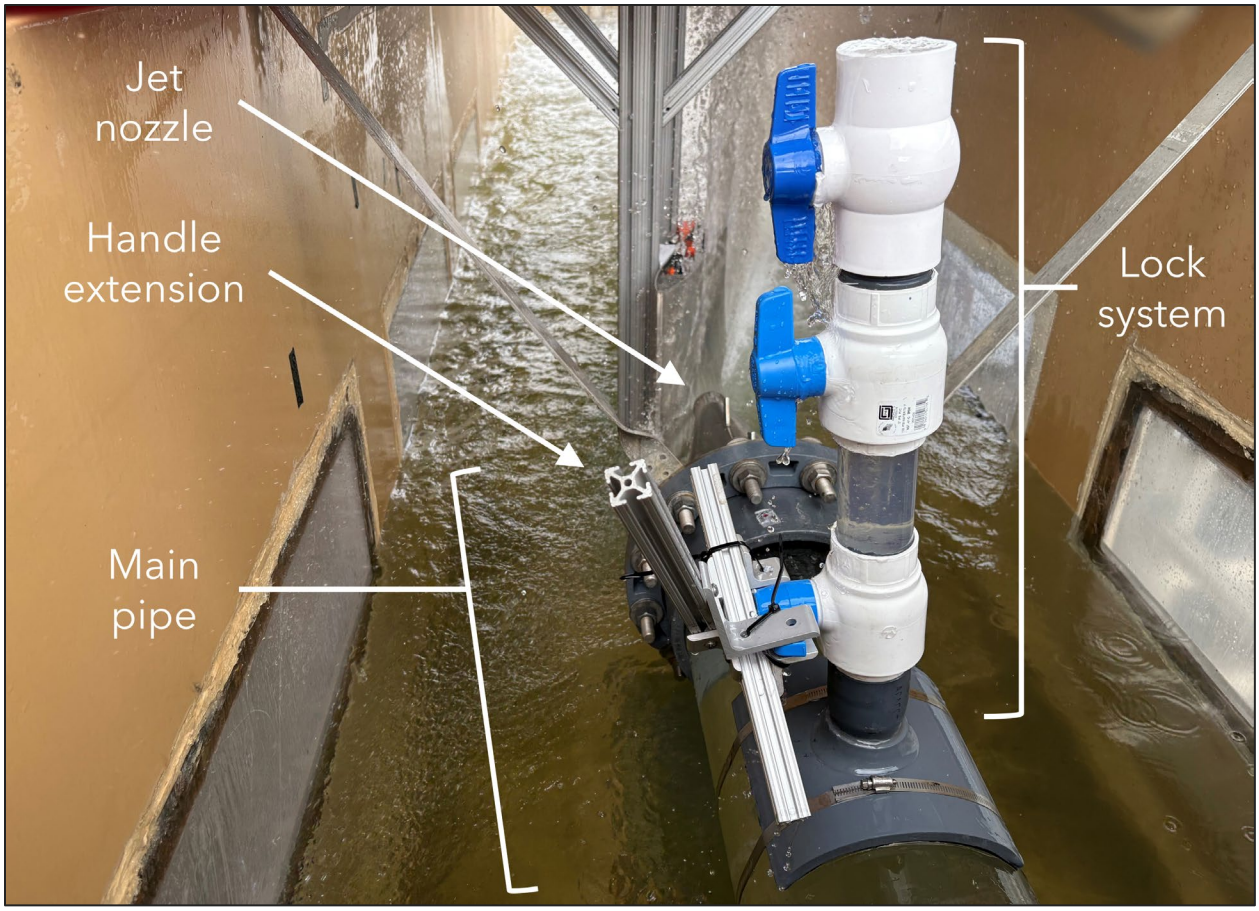

Figure 2-2. Release lock system used for shear and collision testing. A handle extension was added to the lowest valve, which was used to induct Sensor Fish and live fish into the main pipe, to allow for easier releases. The setup pictured was for collision testing with the jet unsubmerged and the aluminum plate at a 20° angle.

2.1.2 Sensor Fish

The Sensor Fish (Figure 2-3) is a nearly neutrally buoyant cylindrical device designed to measure hydrodynamic forces experienced by fish during passage through hydraulic structures. Each unit is approximately one inch in diameter and 3.5 inches in length and weighs 1.5 ounces (oz). They are equipped with sensors that record linear acceleration in three dimensions, rotational velocity in three dimensions, absolute pressure and temperature. The Sensor Fish have a sampling rate of 2,048 samples per second (2,048 Hz), providing high-resolution time-series suitable for capturing short-duration events such as gate passage, shear exposure, and impacts. Each device was calibrated prior to testing following PNNL's standard Sensor Fish operating procedures. Moreover, the Sensor Fish is designed for field deployment equipped with an onboard radio-frequency transmitter, LED beacon and detachable ballast for recovery in the field.

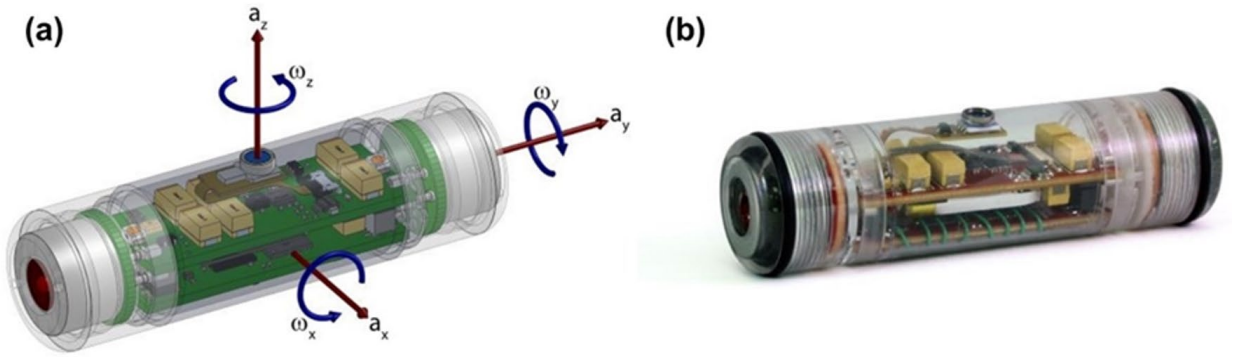

Figure 2-3. Sensor Fish device. (a) CAD rendering illustrating the orientation of linear acceleration and rotational velocity measurement axes. (b) Photograph of the assembled Sensor Fish unit.

2.1.3 Shear Testing

Shear testing took place from October to December 2024. During shear testing, the effects of shear flow at seven jet velocities (10 to 70 fps, at intervals of 10 fps) were examined in live fish and Sensor Fish. Both live fish and Sensor Fish were tested with and without balloon tags. High-speed (HS) video was recorded for both live fish and Sensor Fish releases to examine fish behavioral responses to shear and record collisions with the interior of the jet nozzle or plate (Appendix C). Live fish and Sensor Fish that collided with the interior of the jet nozzle or plate during testing were excluded from the shear analyses.

2.1.3.1 Balloon Tags

Balloon tags are self-inflating balloons attached externally to live fish and Sensor Fish. Each balloon contained two vegetable glycerin capsules with oxalic acid and sodium bicarbonate, which allowed for time delayed inflation, sealed with a silicone stopper (Figure 2-4A; Salalila et al. 2023). The silicone stopper served as an anchor point for braided fishing line that was tied onto the stopper, which was used as a tether for connection to the live fish or Sensor Fish. For laboratory testing, dummy balloon tags were used that had 3D printed fake capsules matching the same size and weight as the standard capsule so that the tags could be reused; all other specifications remained the same.

To activate the balloon tag and facilitate the time delayed inflation, water was injected through the stopper into the balloon, which dissolved the glycerin to interact with the chemical mixture and form carbon dioxide gas, thereby inflating the balloon (Figure 2-4B; Salalila et al. 2023). The additional buoyancy created by the inflated balloon floats the released live fish or Sensor Fish to the water surface, allowing for recapture.

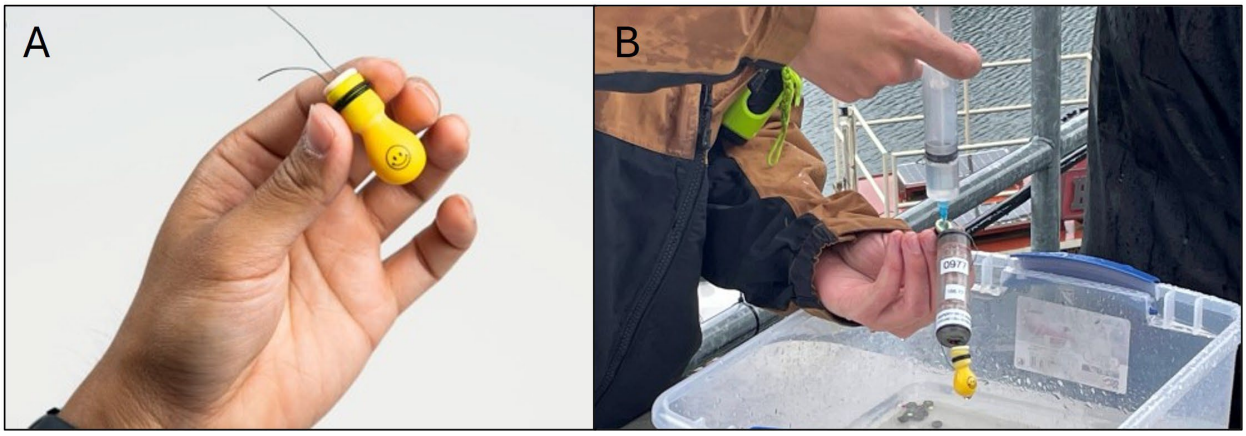

Figure 2-4. (A) A completely assembled balloon tag and (B) preparing a Sensor Fish for release at HAHD. Sensor Fish are prepared for release by injecting water into the balloons tied to the caps on either end using a syringe and needle.

2.1.3.2 Shear: Live Fish

Live fish shear testing utilized juvenile coho salmon obtained from the Washington Department of Fish and Wildlife (WDFW) Soos Creek Hatchery in Auburn, Washington, which were the same stock of fish that were sampled in the field at HAHD in 2024 (Section 4.0). However, because lab testing was conducted several months after the field tests, the coho salmon had grown significantly and were larger than the field-tested coho salmon. To better account for a potential size effect in shear exposure, juvenile Chinook salmon from the ARL of similar size to the coho salmon tested in the field (i.e., 91–139 mm FL) were included in the lab experiments.

Before initiating live fish laboratory experiments, a preliminary study was conducted to identify the most effective surgical techniques for attaching balloon tags and ensuring optimal tag retention. The tagging methods evaluated, and the results of that study, are presented in Appendix D. Based on those findings, the horizontal mattress suturing technique attaching the tag below the dorsal fin using a laminated disc on both sides was identified as the most effective method (Appendix D.3, Table 0-15 [Method 2]).

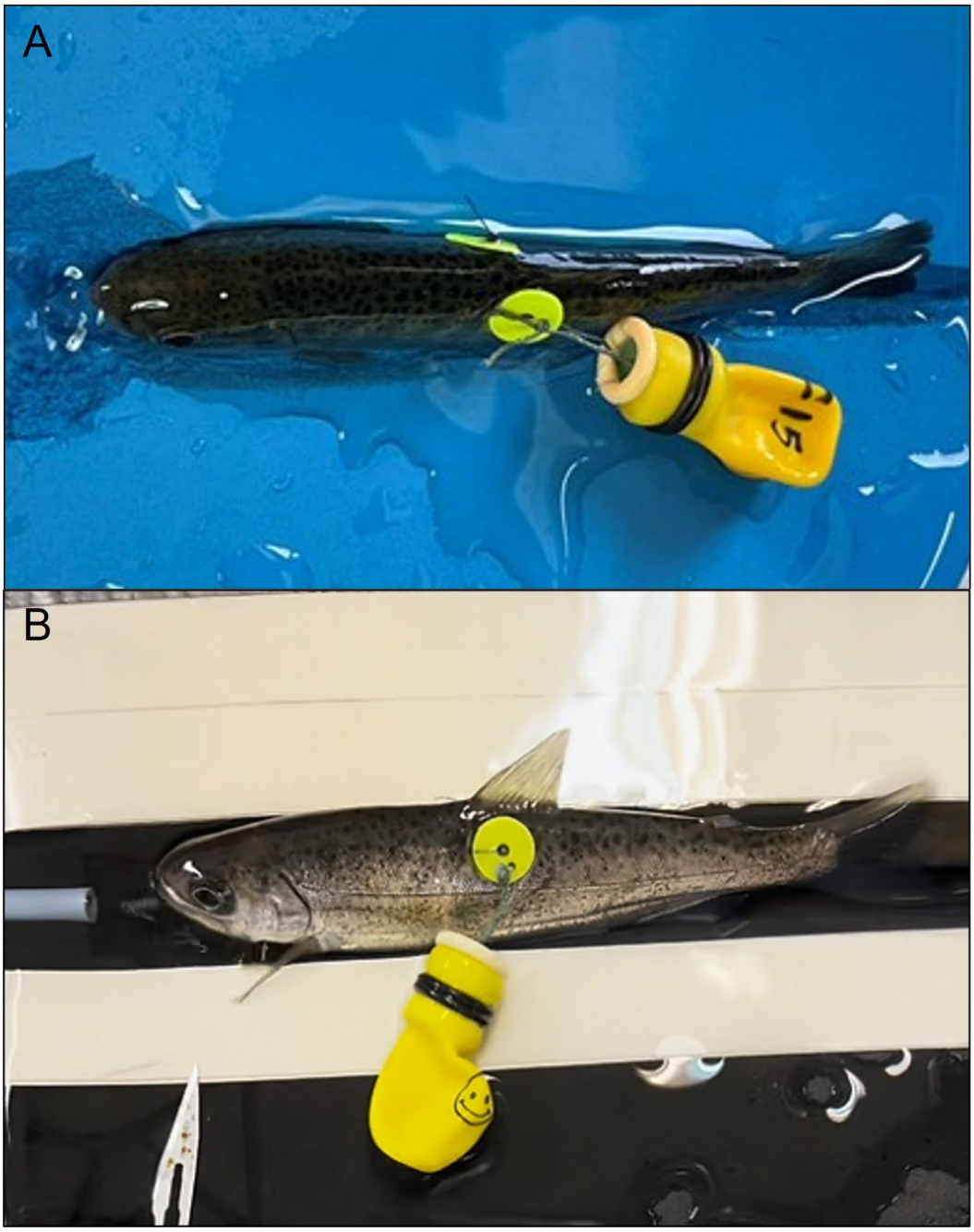

Figure 2-5. Juvenile coho salmon balloon-tagged using a horizontal mattress suture method below the dorsal fin, shown from the (A) top and (B) side.

To begin the tagging process for the live fish laboratory experiments, fish were anesthetized to sedation (80 mg/L tricaine methanesulfonate [MS-222] buffered with 80 mg/L of sodium bicarbonate). Fish weight (g), fork length (mm) and condition for each fish were then recorded. Condition was assessed using the same criteria described in Appendix E, identifying any minor preexisting conditions (i.e. minor descaling, fin fray etc.). Fish with significant preexisting conditions were excluded from the study. Each fish received a PIT tag (8 mm, Biomark [Merck], Rahway, NJ) for identification over the 48-hr evaluation period. The PIT tag was surgically implanted into the fish via a small sutureless incision made between the pectoral and pelvic fins,

just off the linea alba. Fish were randomly assigned to a balloon-tagged or non-tagged group. Fish that were assigned to be tagged were fitted with balloon tags. After tagging, fish recovered in perforated buckets (maximum of 3 fish per bucket) placed in a circular tank with flow-through water. Fish were allowed to recover from sedation and tagging for at least 30 minutes before being exposed to shear forces.

Following the recovery period, the buckets of fish were brought to the shear tank and prepped for testing. The release lock system was primed, and a fish was loaded into the top of the lock system with the lower valve closed. If the fish was tagged it went through the balloon tag activation process immediately prior to being loaded into the lock to avoid any prolonged disruption of normal swimming activity. Once a fish was loaded and facing headfirst towards the main pipe, the top valve was closed, and the shear tank pump was turned on to the appropriate velocity. Each fish was randomly assigned to one of the seven testing velocities (10 to 70 fps, in 10 fps increments). Once flows stabilized, the lower valve was opened, and the fish entered the main pipe and passed out of the jet. After the fish was visually observed exiting the jet terminus, the pump was shut off. Any auditory indications of collision (either with the jet or plate) heard as the fish exited the jet were noted and confirmed with HS video data, if possible. In addition to confirming collision events, HS video also documented fish exit orientation (i.e., headfirst, tail first, sideways; Appendix C).

To ensure data integrity and isolate the effects of shear, fish experiencing atypical testing conditions or handling issues were excluded from analyses. Atypical testing conditions included observed collisions with the nozzle or plate, fish that exited the jet sideways, fish that were not immediately entrained and swam against the flow within the pipe, and any fish subjected to handling issues (e.g., pinched by the release valve, dropped, or not exposed to the full treatment).

A detailed description of the HS video review process – including collision classification, detection of mechanical interactions, and determination of fish exit orientation – is provided in Appendix C. In brief, HS video was systematically reviewed to identify jet and plate collisions and to determine fish orientation upon exiting the nozzle. Because the nozzle diameter (64 mm) was smaller than the lengths of the fish tested, individuals exiting sideways were assumed to have contacted the nozzle. Consistent with criteria established from the HS video review (Appendix C), fish experiencing a collision or exhibiting sideways or unknown exit orientation were excluded from statistical analysis to ensure that only the effects of shear were assessed.

After their release, the fish's behavior (lethargy, loss of equilibrium, erratic swimming, etc.) was quickly assessed within the shear tank and then the fish were netted and returned to their bucket, where their condition was briefly assessed for apparent signs of distress. Obvious injuries (hemorrhage, enucleation, lacerations, etc.), abnormal behavior (loss of equilibrium, lethargy, burst swimming, etc.), balloon detachment or failure (i.e., broken balloon or rubber stopper came loose), morbidity, and mortality were recorded. Once all three fish within a bucket had been exposed and recovered, they were brought to the post-assessment station where a more detailed condition assessment was conducted.

At the post-assessment station, fish were again anesthetized (buffered 80 mg/L MS-222) until loss of equilibrium. Balloons and sutures were removed from balloon-tagged fish, and a picture was taken of both sides of each fish. A full examination of each fish's condition was performed, as described in Appendix E. Following their assessment, live fish were transferred to a circular tank with flow-through water and held for 48-hours (hr) to be monitored for delayed mortality. Any fish that were moribund at this time were euthanized immediately following their post-assessment. Any fish that died during the 48-hr holding period were recorded as a mortality and removed from the holding tanks. Fish that had a handling event during the 48-hr holding period (i.e., jumped

from the holding tank) were removed from analyses. After the 48-hr holding period, another assessment was performed following the same methods and then the fish was euthanized.

Statistical Analyses

Live fish injury rates were generated by counting the number of new injuries (i.e., descaling, abrasion, laceration, fin fraying/tears, etc.; Appendix E, Table 0-16) present on each fish during post-assessments. Immediate survival (binary variable, 0 for mortality and 1 for survival) was determined within 1-hr after exposure, while overall survival was assessed within 48-hr after exposure. Testing conditions (i.e., jet velocity, tag type [balloon-tagged or non-tagged]) and fish characteristics (i.e., fork length, exit orientation, species) were evaluated for their effect on injury rates and survival probability. Jet velocity was treated as a continuous variable to allow injury rates and probability of survival to be examined and predicted across a range of flows.

The influence of these variables (i.e., testing conditions and fish characteristics; x_k) on injury rates ($\mathrm{E}[\mathrm{y}]$) and both immediate and overall survival probability ($P[y]$) was evaluated using generalized linear models (GLM) in R programming (R version 4.5.0). Injury analysis was performed using a negative binomial GLM with a log link function to account for overdispersion in injury rates:

$$\mathrm{E}[\mathrm{y}] = \exp(\beta_0 + \beta_1 x_1 \ldots \beta_k x_k)$$

Survival analyses (both immediate and overall) were performed with a binomial GLM using a logit link function:

$$P[y] = \frac{1}{1 + \exp(-(\beta_0 + \beta_1 x_1 \ldots \beta_k x_k))}$$

All main effects and possible two-way interactions were assessed for inclusion in the injury and survival models. Various combinations of the full models were run to identify interactions that had little to no influence on injury rates or survival. Model selection was performed using model averaging (MuMIn package in R) based on AIC weights. Models within two AIC units of the lowest AIC-valued model were included in a best-models subset to create the final model average.

Predictive performance of both survival models was evaluated using the area under the receiver operating characteristic (ROC) curve (AUC; Hosmer and Lemeshow 2000). Once the final model average was fitted for immediate and overall survival, survival predictions were generated using full average coefficients and a new dataset consisting of the tested fish lengths across all levels of the categorical variables (exit orientation, species, tag type) and a full range of jet velocities (10 to 70 fps, by intervals of 1 fps).

2.1.3.3 Shear: Sensor Fish

During shear testing, Sensor Fish were released in conjunction with live fish and exposed to identical conditions (jet velocity, balloon-tagged vs. non-tagged). Non-tagged Sensor Fish were released immediately following a non-tagged live fish release and were exposed to the same velocity. However, to release balloon-tagged Sensor Fish, the release lock system had to be altered slightly. As a result, balloon-tagged Sensor Fish were tested at one time, after all other live fish releases for shear testing were completed.

Prior to release, each Sensor Fish was activated using a magnet, which initiated a five-second delay indicated by five LED blinks. After this delay, the Sensor Fish began recording data. Each unit was then tapped three times on the shear tank to generate three distinct acceleration

magnitude signals, which served as a marker indicating that the Sensor Fish was about to be released into tank. The Sensor Fish was then loaded into the release lock system and released into the jet. Non-tagged and balloon-tagged Sensor Fish were tested at the same seven velocities used during live fish testing. Similar to live fish releases, any plate/jet collisions and balloon detachments or failures were recorded for Sensor Fish releases. The record time of each Sensor Fish release was set as one minute, and the contraction and nozzle regions corresponded to the pressure drop (shown in the Sensor Fish data).

2.1.3.4 Sensor Fish Data Analyses

Severe Acceleration Events

The analysis of Sensor Fish data involves a comprehensive investigation of time histories from all Sensor Fish datasets using the Hydropower Biological Evaluation Tools (HBET). This software enables the detection and identification of critical events such as strikes, collisions, or shear occurrences (Hou et al. 2018). These events are recognizable as high-amplitude impulses within the acceleration time histories. To be considered a severe event, an acceleration impulse with high amplitude (measured in g-force) must exhibit a peak value ≥ 95 g_0 (Deng et al. 2007). A severe event is categorized as a strike when 70% of its maximum amplitude (0.7 |a|) is less than 0.0075 seconds (s). Conversely, if 70% of the maximum amplitude of the event lasts longer than 0.0075 s, it is classified as shear (Figure 2-6). Accordingly, the percentages of Sensor Fish releases with acceleration events exceeding a 95 g_0 reference value were analyzed during the fish passage.

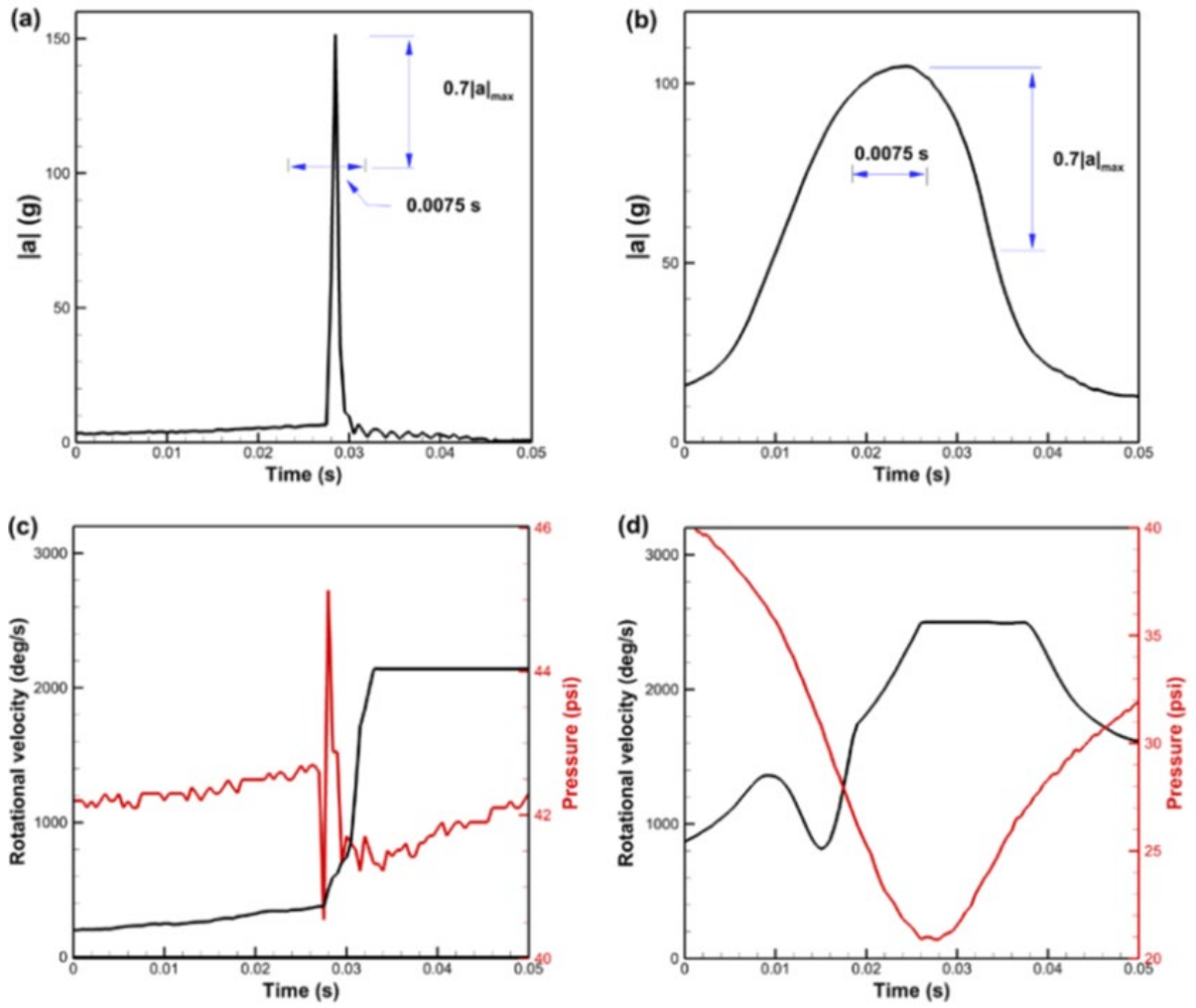

Figure 2-6. Shear and collision signatures. (a) Duration of acceleration within 70% of the peak value is less than 0.0075 s for a collision event; (b) Duration of acceleration within 70% of the peak value is greater than 0.0075 s for a shear event. Pressure and rotation increase more dramatically during (c) a collision event than during (d) a shear event (Deng et al. 2007).

Velocity-based Strike Metric

The severity of strike events between fish and hydraulic structures is further characterized by considering both acceleration peak magnitudes and event durations. Specifically, a velocity-based strike metric was employed to estimate the survival rate of passage-passed fish at a population scale (Huang et al. 2025). The velocity-based strike metric, denoted as M_V, is designed to capture the change in velocity and hence the strike force exerted on a fish during a strike event. It is centered at the peak acceleration with index *n*=0 and three sample points to the left and right of the center to cover the duration of a collision event.

$$M_V := \Delta t \left\| \sum_{n=-3}^{3} (a_x[n], a_y[n], a_z[n])^T \right\|$$

where ||·|| is the Euclidean norm of the acceleration vector and Δt = 1⁄2048 s as the sampling rate of Sensor Fish is 2048 Hz (Deng et al. 2014).

For clarity, this formulation is equivalently expressed in component form as

$$M_V = \Delta t \sqrt{\left(\sum_{n=-3}^{3} a_x[n]\right)^2 + \left(\sum_{n=-3}^{3} a_y[n]\right)^2 + \left(\sum_{n=-3}^{3} a_z[n]\right)^2}$$

which explicitly shows that the acceleration components are first summed component-wise over the duration of the event, and the Euclidean norm is then applied to the resulting vector. This ensures that M_V represents the magnitude of the net change in velocity during the collision.

To estimate the survival rate of fish passing through the passage structure, M_V must first be computed for each Sensor Fish release. Each Sensor Fish release produces a time series of acceleration magnitude across the complete passage from the starting region of the fish passage to the ending region. The procedure is described as follows:

1. Compute M_V for each severe exposure event ($\| a \| \geq 95\ g_0$) that the Sensor Fish experiences.
2. Retain the maximum value of M_V across all severe exposure events for the given Sensor Fish release and discard all other values.
3. If there are no severe exposure events, then set M_V=0.

Steps 1–3 thus produce a single measurement of M_V for each Sensor Fish release. In other words, if there are *N* Sensor Fish releases, then *N* measurements of M_V are obtained. The mortal threshold for M_V was calibrated by determining the percentile of M_V that corresponds with the 48-hr survival rate (%) from the live fish experiments. Thus, fish experiencing M_V values above the established threshold are not likely to survive passage, whereas fish experiencing M_V values below the threshold are more likely to survive passage.

2.1.4 Collision Testing

Collision testing took place from January to April 2025. To determine the best setup for collision testing, several pilot tests were performed using various velocities, plate angles, and water levels (submerged or unsubmerged jet; Appendix B). When pilot testing was performed with a submerged jet, it was found that the Sensor Fish had the potential to be exposed to both shear and collision, making it difficult to differentiate between the two stressors. During CFD modeling, discussed later in this report, CFD modeled particles confirmed this behavior.

Results of the pilot tests helped identify a final collision testing plan, which was:

1. Test Sensor Fish with an unsubmerged jet and a 30° plate angle at 50 fps.

2. Test live fish and Sensor Fish with an unsubmerged jet at a 20° angle at 50 fps first, then at velocities above and below 50 fps to define a survival range.

This testing plan was designed to efficiently determine a mortality range for fish that experience collision events. Final collision testing took place over the course of two days in April 2025.

2.1.4.1 Collision: Live Fish

Live fish used in collision testing were not tagged and were evaluated only for obvious injuries, as well as immediate and delayed mortality. Yearling coho salmon (90–133 mm FL [$\bar{x}$ = 111 mm], 7.4–24.8 g [$\bar{x}$ = 16.0 g]), obtained by the WDFW Soos Creek Hatchery were used as the study fish for collision testing.

Prior to their release, each fish was briefly assessed for any obvious injuries or abnormalities. Fish were loaded into the release lock system using the same method described in Section 2.1.3.2. To operate the pump with the jet unsubmerged, the pump had to be run for a few minutes each time it was turned on to purge any air in the system before a release. However, because the jet was unsubmerged, the water level within the shear tank was low enough to remain minimally disturbed while the pump was running. Therefore, to maximize the number of fish tested each day, fish were released one at a time in small batches, while the pump was kept running. After approximately ten fish were released, the pump was shut off, and all fish were recovered from the shear tank.

Live fish were only tested at a 20° plate angle due to the expectation of a major secondary event (i.e., collision with the shear tank wall) occurring at a 30° angle. First, 60 fish were released at 50 fps, and subsequent velocities and sample sizes were determined based on estimates of mortality from preliminary Sensor Fish results obtained during final collision testing.

Following their recovery from the shear tank, each fish was again briefly assessed for any new injuries or abnormal swimming behavior, and a tally of fish exhibiting these conditions was recorded. Any mortalities were noted, and moribund fish were counted and euthanized. All surviving fish were brought to a circular holding tank, where they were held and monitored for 48-hr for delayed mortality. Following the 48-hr holding period, all fish were euthanized. At this time, fish fork lengths (mm) and weights (g) were recorded. A fish with handling events during the 48-hr holding period (i.e., jumped from the holding tank) were removed from analysis.

The effect of jet velocity (V_j) and fish length (L_f) on immediate (within 1-hr after exposure) and overall (within 48-hr after exposure) survival probabilities ($P[y]$) were evaluated using Firth's bias reduced model. Firth's bias reduced model is a binary logistic regression model that uses a penalized maximum likelihood estimate to allow the model to converge when small sample sizes were used or when data exhibits complete separation, making it an appropriate test for live fish collision data where few jet velocities were tested and mortalities were expected at some velocities but not all.

To apply the survival predictions to a distribution of M_V values (measured by Sensor Fish or quantified by CFD modeling), a model was generated with jet velocity included as a continuous variable. The model included an interaction between jet velocity and fish length:

$$P[y] = \frac{1}{1 + exp(-(\beta 0 + \beta 1 V_j + \beta 2 L_f + \beta 3 V_j L_f))}$$

Once the model was fitted, it was used to generate predicted immediate and delayed survival probability over the range of fish lengths and jet velocities tested during collision testing.

2.1.4.2 Collision: Sensor Fish

All Sensor Fish used during the collision testing were deployed without attached balloons. To maximize data collection over the two-day testing period, Sensor Fish were released in batches, similar to the procedure used in live fish collision tests. Prior to release, each Sensor Fish was

activated using a magnet, which initiated a five-second delay indicated by five LED blinks. After this delay, Sensor Fish began recording data. Each unit was then tapped three times on the shear tank to generate three distinct acceleration magnitude signals, which served as a marker indicating that the Sensor Fish was about to be released into tank. The Sensor Fish was then loaded into the release lock system and released into the jet. All prepared Sensor Fish were released consecutively while the pump remained running. After each batch, the devices were recovered from the tank and their data downloaded. Each release was set to record for one minute. The contraction and nozzle regions are corresponding to the pressure drop (shown in the Sensor Fish data).

To validate Computational Fluid Dynamics (CFD) modeling results, a total of 50 Sensor Fish were tested at a 30° plate angle with a velocity of 50 fps. After these tests, the aluminum plate was adjusted to a 20° angle for the remainder of the trials. At this configuration, 50 Sensor Fish were released at 50 fps, and an additional 30 Sensor Fish were tested at both 40 and 60 fps. Single and double collisions (including secondary impacts) detected during the releases were documented. The analysis methods for these collision tests are consistent with those described in Section 2.1.3.4. To isolate plate collision effects, any Sensor Fish data associated with potential jet collisions were excluded from further analysis.

2.1.5 Computational Fluid Dynamics Modeling

Computational Fluid Dynamics (CFD) investigations for understanding the hydrodynamics and flow field within the shear tank were conducted. These hydrodynamic conditions are critical in characterizing the stressors that a fish may encounter during turbulent shear flow. Further, CFD-particle flow simulations were conducted to investigate the exposure probability due to the shear and collision events that may be responsible for fish injury/mortality in the existing HAHD and GPR fish passage. By integrating CFD results with Sensor Fish data and live-fish observations, the study validates that the CFD model accurately predicts the magnitude and distribution of key stressors affecting fish survival. Once validated, CFD enables designers to evaluate how design changes influence fish survival in a fully digital environment, reducing the need to construct physical hydraulic models for each modification and limiting reliance on repeated live-fish testing. This supports faster, more efficient, and less resource-intensive design and modification. A full description of how the CFD modeling was conducted, and the tunnel validation of the CFD results for jet velocity measurement are outlined in Appendix F.

2.1.5.1 CFD Modeling for Shear Testing

Shear testing was conducted using a submerged jet that expanded in water. As mentioned earlier, the laboratory setup included an aluminum plate installed adjacent to the jet nozzle to replicate the shear conditions that fish may encounter in field environments. The computational model of the flow domain of the shear tank was developed using SolidWorks (Dassault Systems. 2022), a commercial CAD software, based on the as-constructed drawings (The design and dimensions of the shear tank were already presented in Section 2.1.1). Further modifications were made based on input from the Corps. These modifications included extending the plexiglass pipe upstream of the converging nozzle and adding an adjacent aluminum plate to create fluid shear (see Figure 2-7(b) for the final three dimensional model of flow domain).

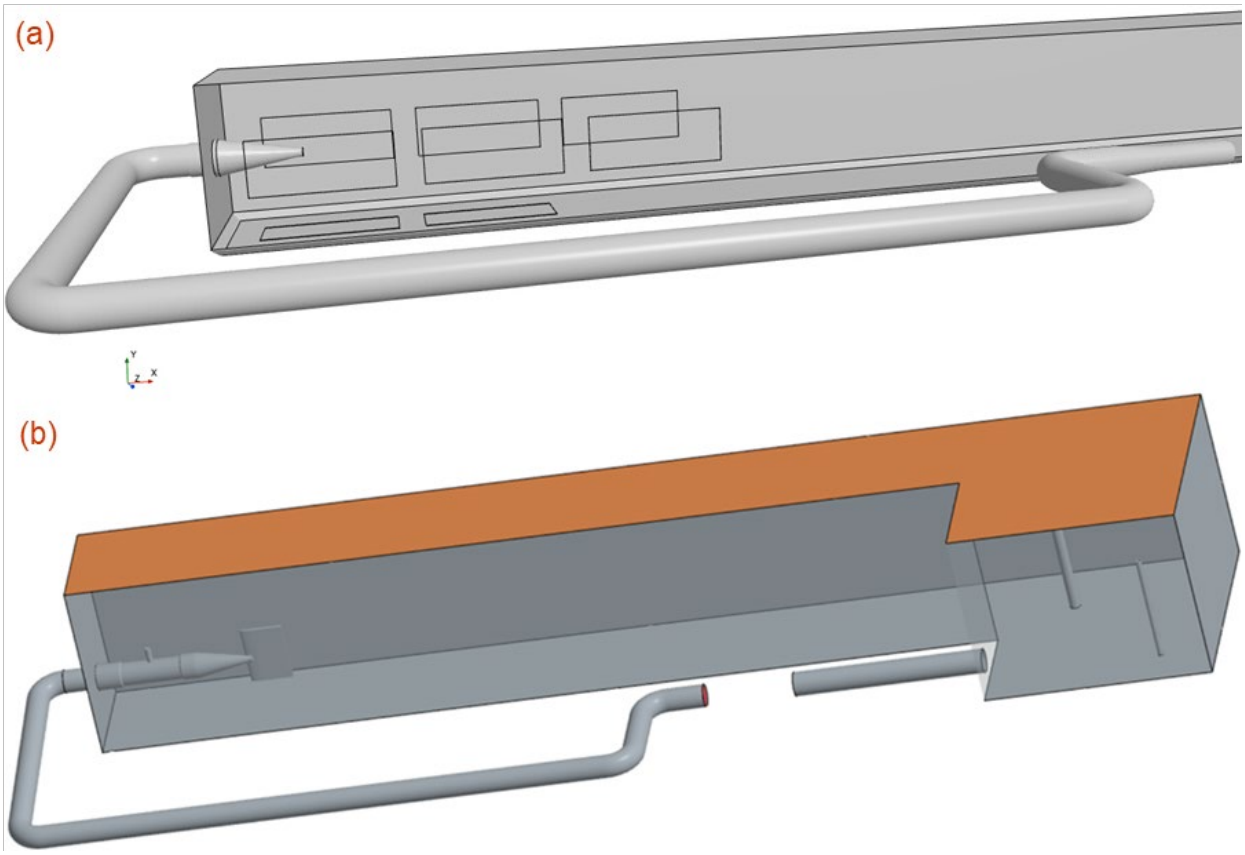

Figure 2-7. Three dimensional model of the computational flow domain of the shear tank with the (a) original design and (b) modified design. The shear tank was extended in the vertical direction to specify the atmospheric condition (shown in the brown color).

The developed CAD model was subsequently exported to STAR-CCM+ (Siemens DIS, 2022), a commercial CFD software, for meshing and flow simulations. In CFD, meshing is the process of dividing the fluid region into small discreet volume for analysis. A non-uniform meshing strategy was employed to accurately and efficiently capture the flow physics. Prizm layer meshing, similar to the boundary layer meshing, was used near the wall to capture the steep velocity gradient (Figure 2-8). Additionally, the flow region near the plate was meshed with a very fine mesh to accurately capture the flow shear. Initially the mesh in the free surface region was also created with very fine mesh resolution. Note that the dynamic free surface wave appears with flow progress, therefore, the dynamic mesh adaptation mesh scheme based on free surface interface criteria was used to capture the physics of free surface flow.

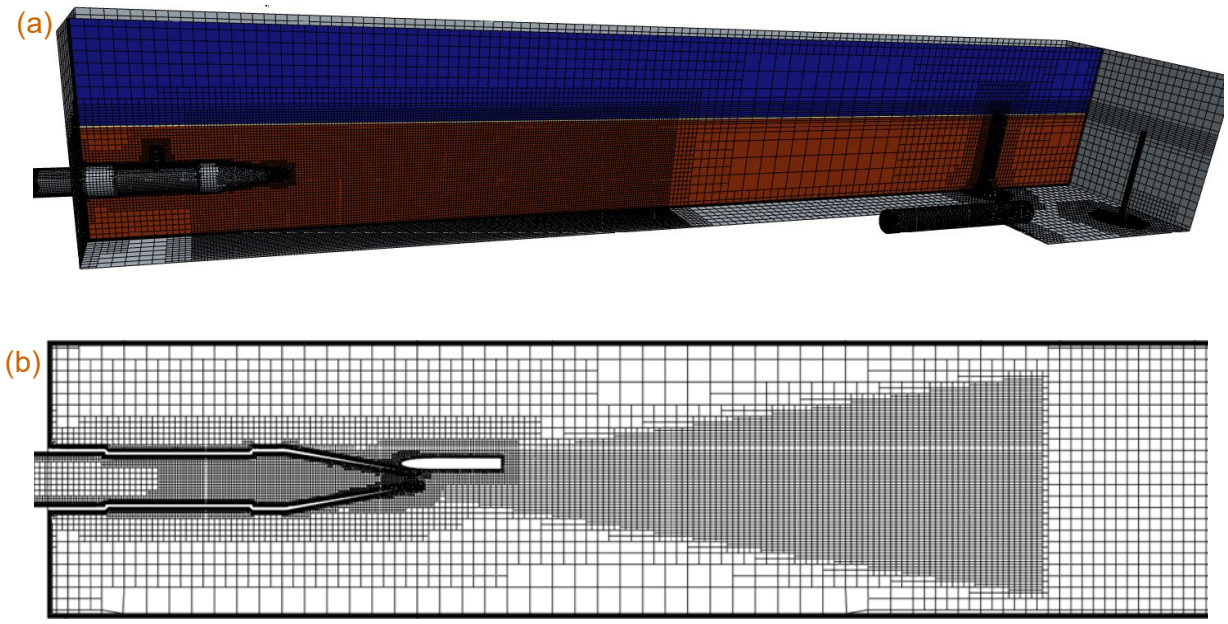

Figure 2-8. Meshing scheme used in the two-phase flow simulation for shear test shows very fine mesh used to accurately and efficiently capture the flow characteristics. (a) 3D meshing shows the non-uniform meshing in a flow domain. Bule and red color show the air and water in two phase flow simulation respectively. (b) Meshing at the horizontal plane through the center of the Nozzle shows the boundary layer mesh near the solid wall and a refined mesh in the region where expansion of the submerged water jet is expected.

As discussed in Appendix B, the collision testing was for performed for a submerged as well as an unsubmerged jet. Initially, collision testing was performed for a submerged jet (Appendix B). In this case, plates were placed 10° and 20° inclined to the to the axis of the nozzle (Figure 2-9).

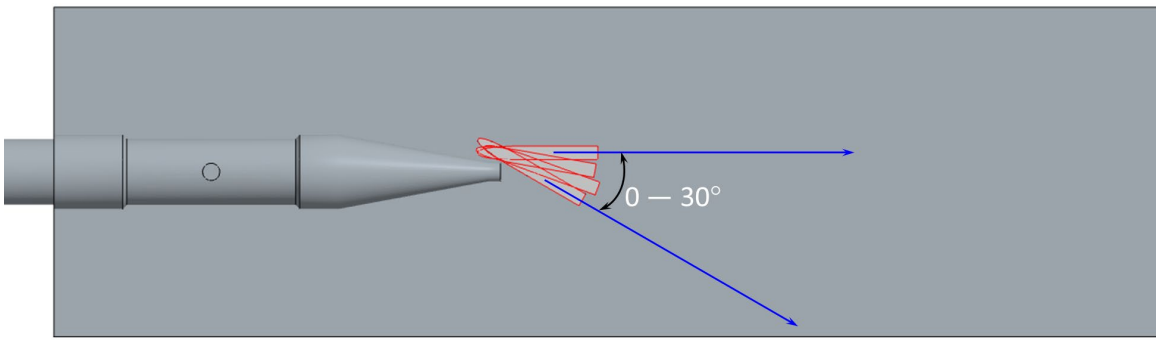

Figure 2-9. Top view of the shear tank showing the orientation of the plate for collision testing. The plate was inclined to 0 – 30° with 10° increment. The experiment was conducted up to 20°.

It is worth noting that the flow and particles were deflected after striking the plate. Therefore, grid refinement was also conducted to capture the flow physics of the deflected water outside of the fine meshed regions. The mesh was refined in the diverging conical region, whose axis coincides

with axis of the plate. In addition, regions near to the plate and nozzle were also meshed with very fine region, where one can expect a very steep gradient of the flow (Figure 2-10, dark region).

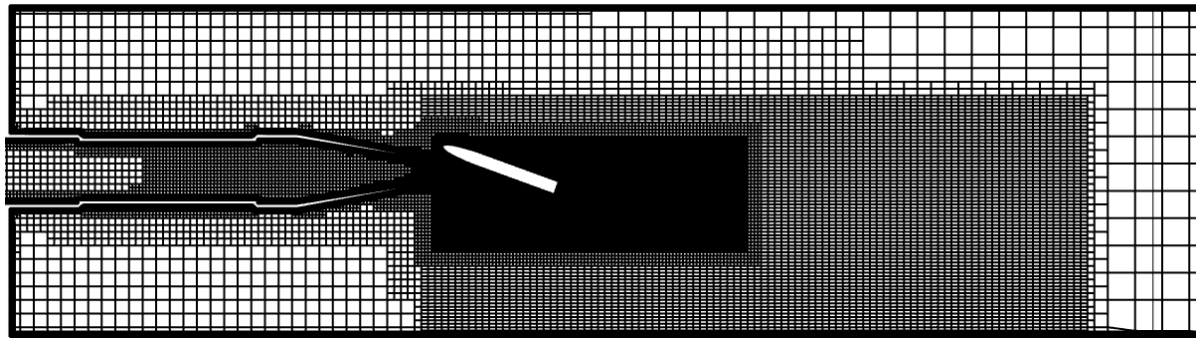

Figure 2-10. Top view of the mesh in a horizontal plane showing the meshing scheme used in the two-phase flow simulation for submerged collision test. A very fine mesh used to accurately and efficiently capture the flow characteristics. The rest of the region was meshed with coarse mesh for efficient simulations.

After the generation of a mesh for the flow domain, turbulent multiphase flow simulations were performed using the Volume of Fluid (VOF) method at different velocities for the unsubmerged jet (Table 2-1). Because the free surface of water within the shear tank was not fixed, the VOF method was chosen due to its suitability for modeling open-channel flow scenarios. A uniform velocity profile was specified at the extended pipe inlet, with the magnitude of the inlet velocity back calculated based on the jet exit velocity and ramping behavior observed in experimental studies.

Table 2-1. Velocity and ramping time used as boundary conditions in the flow simulations.

Inlet Velocity (fps)	Jet Velocity (fps)	Ramp Time(sec)
1.511	20	2.23
2.248	30	2.85
2.985	40	3.85
3.798	50	4.48
4.557	60	5.60
5.317	70	6.18

2.1.5.2 CFD Modeling for Collision Testing

Because the particles and Sensor Fish had the potential to be exposed to both shear and collision with a submerged jet (as discussed in Appendix B), collision testing with the jet was performed above the water line in which the jet would strike the plate in the air. In the unsubmerged jet testing, the breakup of the water jet, the water splash at the plate, and the water droplet formation takes place. In this case, a very fine mesh to resolve the associated flow morphology at these length scales in the flow simulation is required. The conic region coinciding with the axis of the plate was more refined (Figure 2-11) as the field moves away from the plate. Further, dynamic mesh adaptation scheme was used to capture the droplet, slander jet, etc.

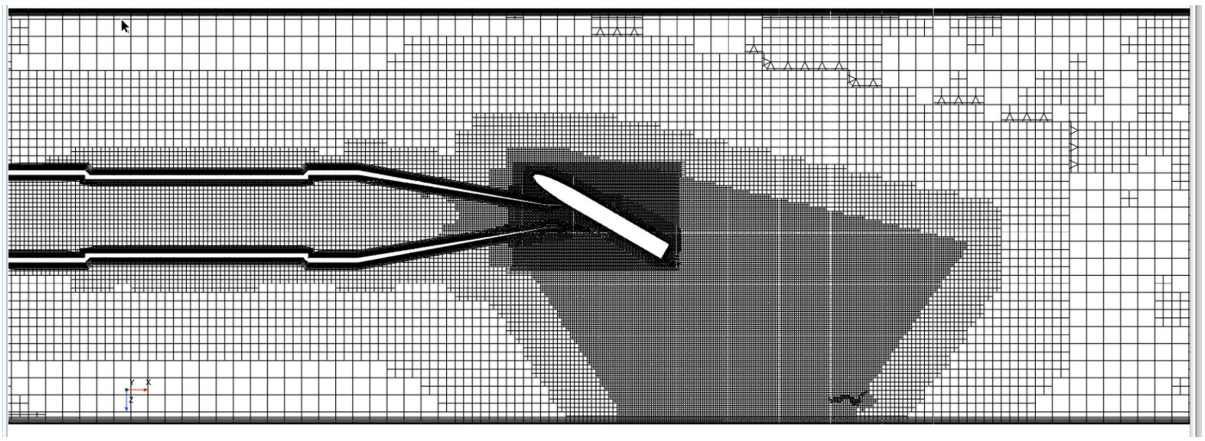

Figure 2-11. Top view of the mesh in a horizontal plane showing the meshing scheme used in the two-phase flow simulation for submerged collision test. Very fine mesh in the conical region was used to capture the splash.

After the generation of a mesh for the flow domain, turbulent multiphase flow simulations were performed using the VOF method at the three velocities for the unsubmerged jet (40, 50 and 60 fps). In addition, the water level in the tank was kept 12-in below the nozzle. Because the free surface of water within the shear tank was not fixed, the VOF method was chosen due to its suitability for modeling open-channel flow scenarios. A uniform velocity profile was specified at the extended pipe inlet, with the magnitude of the inlet velocity calculated based on the jet velocity.

In contrast to submerged jet simulations that used the realizable $k-\epsilon$ model of turbulence closure, the Detached Eddy Simulation (DES) approach, a hybrid turbulence modeling technique, was employed for unsubmerged jet simulations. DES demonstrates significant advantages in accurately predicting complex phenomena such as atomization, jet breakup, and liquid splashing upon impact with solid surfaces. This approach requires the use of exceptionally fine meshes, with adaptive meshing techniques leading to an extensive computational grid containing roughly 25 million cells. The need for such high-resolution meshes stems from dynamic mesh adaptation designed to capture the intricate behaviors of droplets, splashes, and high waves within the flow domain. As a result, these simulations demand substantial computational resources due to the combination of exceedingly small time-step requirements and the massive number of mesh cells involved.

2.1.5.3 CFD Modeling for Particle Flow

Flow simulations were conducted to ensure that flow achieved a pseudo-steady state (i.e., when flow variables such as velocity and pressure do not vary significantly). Time to achieve the pseudo-steady state depends on the velocity and ramping time. Furthermore, the CFD-particle simulations were conducted for sampling the stressors that a fish may experience. CFD-particle simulation approach has been extensively explained earlier (Singh et al, 2022), therefore, it is not presented here for the sake of brevity. Particle-flow simulation was conducted using the Discrete Element Method (DEM) particles that were analogous to Sensor Fish studies at all velocities prescribed in Table 2-1. Cylindrical particles with dimensions identical to those of Sensor Fish were used in the simulations. A total of 300 cylindrical particles were released from a circular plane located beneath the vertical introduction tube. The center of the injection plane coincided with the axis of the horizontal nozzle. The particle injection rate was kept low to prevent interparticle collisions and varied with jet velocity, specifically a very low injection rate (5 particles/sec) at a jet velocity of 20 fps. DEM particle simulations were conducted for a sufficient

duration to ensure that all particles passed through the region of interest. As a result, flow simulation time depends on the particle injection rate, jet velocity, Figure 2-12 shows a snapshot of the velocity and dispersion of cylindrical particles in the shear tank.

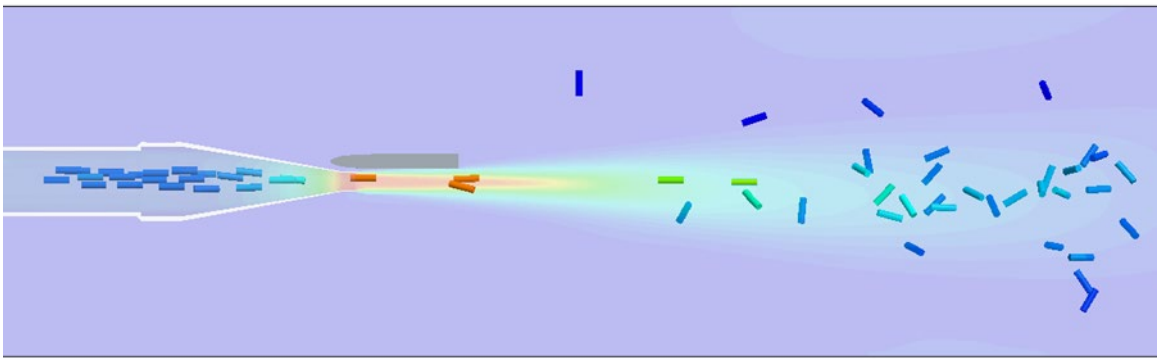

Figure 2-12. The snapshot shows the velocity field and dispersion of cylindrical particles, representative of Sensor Fish, within the shear tank. The filled color contour represents the velocity field at a horizontal plane that passes through the centerline of the nozzle.

2.2 Shear and Collision Laboratory Testing Results

2.2.1 Shear Laboratory Results

2.2.1.1 Shear: Live Fish

Fish size differed between Coho and Chinook salmon tested for shear exposure, with coho salmon generally being larger than Chinook salmon. Chinook salmon (n = 500) fork length ranged from 90 to 139 mm ($\bar{x}$ = 116 mm), and their weight ranged from 9.1 to 36.5 g ($\bar{x}$ = 20.7 g). Coho salmon (n = 400) fork length ranged from 118 to 210 mm ($\bar{x}$ = 167 mm), and their weight ranged from 17.8 to 108.2 g ($\bar{x}$ = 54.5 g). Throughout the entirety of shear testing, temperatures remained relatively consistent for both the shear tank (14.8–16.3 °C) and the holding tanks (13.0–17.6 °C).

Collision occurred in about twenty-eight percent of live fish deployments during shear testing with the submerged jet (Appendix C). Approximately 1% of Chinook salmon (n = 52) and coho salmon (n = 52) exited sideways or had an unknown exit orientation (Appendix C). Final samples sizes and survival rates for Chinook and coho salmon used in injury and mortality analysis are in Table 2-2 and Table 2-3, respectively.

Table 2-2. Final Chinook salmon sample sizes. Sample sizes for non-tagged fish, balloon-tagged fish (and combined total) show the number of mortalities (Mort), and the survival rates for each velocity both immediately after testing (Immediate Survival, top) and 48-hr after testing (Overall Survival, bottom).

Chinook Salmon: Immediate Survival									
Jet Velocity (fps)	**Non-Tagged**			**Balloon-Tagged**			**Combined Total**		
	n	**Mort**	**Survival**	***n***	**Mort**	**Survival**	***n***	**Mort**	**Survival**
10	7	0	1.000	5	0	1.000	12	0	1.000
20	5	0	1.000	8	0	1.000	13	0	1.000
30	5	0	1.000	8	0	1.000	13	0	1.000
40	27	0	1.000	27	0	1.000	54	0	1.000
50	40	0	1.000	36	0	1.000	76	0	1.000
60	36	0	1.000	42	1	0.976	78	1	0.987
70	32	2	0.938	39	6	0.846	71	8	0.887
Total	**152**	**2**	**0.987**	**165**	**7**	**0.958**	**317**	**9**	**0.971**
Chinook Salmon: Overall Survival									
Jet Velocity (fps)	**Non-Tagged**			**Balloon-Tagged**			**Combined Total**		
	***n*[1]**	**Mort**	**Survival**	***n*[1]**	**Mort**	**Survival**	***n*[1]**	**Mort**	**Survival**
10	7	0	1.000	5	1	0.800	12	1	0.917
20	5	0	1.000	7	0	1.000	12	0	1.000
30	4	1	0.750	7	0	1.000	11	1	0.909
40	26	1	0.962	24	1	0.958	50	2	0.960
50	38	2	0.947	32	0	1.000	70	2	0.971
60	35	2	0.943	42	3	0.929	77	5	0.935
70	30	3	0.900	38	10	0.737	68	13	0.808
Total	**145**	**9**	**0.938**	**155**	**15**	**0.903**	**300**	**24**	**0.920**

[1]Fish with handling events (i.e. jumped out of the holding tanks) were rejected from the 48-hr analysis.

Table 2-3. Final coho salmon sample sizes. Sample sizes for non-tagged fish, balloon-tagged fish (and combined total) show the number of mortalities (Mort), and the survival rates for each velocity both immediately after testing (Immediate Survival, top) and 48-hr after testing (Overall Survival, bottom).

Coho Salmon: Immediate Survival									
Jet Velocity (fps)	Non-Tagged			Balloon-Tagged			Combined Total		
	n	Mort	Survival	*n*	Mort	Survival	*n*	Mort	Survival
10	3	0	1.000	2	0	1.000	5	0	1.000
20	3	0	1.000	6	0	1.000	9	0	1.000
30	6	0	1.000	5	0	1.000	11	0	1.000
40	10	1	0.900	12	0	1.000	22	1	0.954
50	16	0	1.000	31	2	0.935	47	2	0.957
60	24	3	0.875	19	2	0.895	43	5	0.883
70	19	11	0.421	24	14	0.417	43	25	0.419
Total	**81**	**15**	**0.815**	**99**	**18**	**0.818**	**180**	**33**	**0.817**
Coho Salmon: Overall Survival									
Jet Velocity (fps)	**Non-Tagged**			**Balloon-Tagged**			**Combined Total**		
	***n*[1]**	**Mort**	**Survival**	***n*[1]**	**Mort**	**Survival**	***n*[1]**	**Mort**	**Survival**
10	3	1	0.667	2	0	1.000	5	1	0.800
20	3	0	1.000	6	1	0.833	9	1	0.889
30	6	1	0.833	5	0	1.000	11	1	0.909
40	10	3	0.700	11	0	1.000	21	3	0.857
50	15	0	1.000	31	4	0.871	46	4	0.913
60	24	8	0.667	19	5	0.737	43	13	0.697
70	18	13	0.278	24	16	0.333	42	29	0.309
Total	**79**	**26**	**0.671**	**98**	**26**	**0.735**	**177**	**52**	**0.706**

[1]Fish with handling events (i.e. jumped out of the holding tanks) were rejected from the 48-hr analysis.

Out of the 497 fish assessed immediately after testing, 97% of fish (Chinook salmon *n* = 304 [of 317], coho salmon *n* = 177 [of 180]) were found to have new injuries. The most common injuries seen were an increase in descaling (Chinook salmon *n* = 42, coho salmon *n* = 98, loss of >10% of scales on either side of the body; Appendix E.1 Figure 0-5). Other common injuries included bruising, eye hemorrhages, operculum folding/abrasions, and fin damage. Severe injuries observed during testing were usually caused by balloon tags damaging the dorsal fin or musculature. Additional information on injury results and analysis are provided in Appendix E.

A total of 1,450 models (binomial GLM; Section 2.1.3.2) were calculated for consideration in immediate and overall survival model averages. For the best-models subset (within 2 AICc units of the lowest AICc model), a total of 14 models were retained for immediate survival and 9 models for overall survival. Model discrimination was excellent for both immediate and overall survival

model averages – the model generated for immediate survival had AUC value of 0.92, while the AUC value for the overall survival model was slightly lower at 0.81 (Hosmer and Lemeshow 2000).

In addition to the main effects of all variables, both immediate and overall survival model averages included interactions between exit orientation and jet velocity, exit orientation and length, exit orientation and species, jet velocity and length, and jet velocity and species. The immediate survival model average also included an interaction between length and species, which was not included in the model average for overall survival (Table 2-4).

Table 2-4. Coefficients and associated standard errors from the averaged (full) model generated to predict the probability of immediate and overall live fish survival. Exit Orientation: Tail first = 0 and Headfirst = 1. Species: Chinook salmon = 0 and coho salmon = 1. Tag Type: Non-tagged = 0 and Balloon-tagged = 1.

Parameter	Immediate (1-hr)			Overall (48-hr)		
	Coefficient	SE	p-value	Coefficient	SE	p-value
Intercept	24.2649	13.1329	0.07	7.8258	4.5728	0.09
Exit Orientation	0.2358	2.9668	0.94	5.1117	2.0789	**0.01***
Jet Velocity	-0.3305	0.1842	0.07	-0.1071	0.0832	0.20
Length	-0.0612	0.0923	0.51	-0.0328	0.0404	0.42
Species	-5.4399	4.3100	0.21	0.5672	2.4968	0.82
Tag Type	-0.0435	0.1986	0.83	0.0106	0.0908	0.91
Exit Orientation:Jet Velocity	-0.0193	0.0446	0.67	-0.0884	0.0304	**0.004***
Jet Velocity:Length	0.0011	0.0013	0.39	0.0007	0.0007	0.33
Jet Velocity:Species	0.0033	0.0279	0.91	-0.0382	0.0454	0.40
Exit Orientation:Length	-0.0002	0.0036	0.95	-0.0011	0.0049	0.83
Exit Orientation:Species	0.0110	0.2069	0.96	-0.4635	0.6651	0.49
Length:Species	0.0172	0.0336	0.61	-	-	

* Indicates a p-value < 0.05.

For both immediate and overall models, higher jet velocities were found to substantially lower survival probabilities (Table 2-2, Table 2-3, Table 2-4). Predicted immediate survival probability decreased dramatically around 50 fps for coho salmon and 60 fps for Chinook salmon (Figure 2-13). During shear testing, observed immediate survival rates for Chinook salmon were 100% for all jet velocities below 60 fps, and coho salmon similarly had high immediate survival (>95%) up until 50 fps (Table 2-2, Table 2-3). This general trend was also observed in predicted overall survival probabilities, although the downward slope of the line was more gradual and negative effects seemed to appear at lower velocities when compared to immediate survival probabilities (Figure 2-14). The main effect of jet velocity had a weaker influence on overall survival than immediate survival, while interactions between jet velocity and exit orientation and species gained strength (Table 2-4).

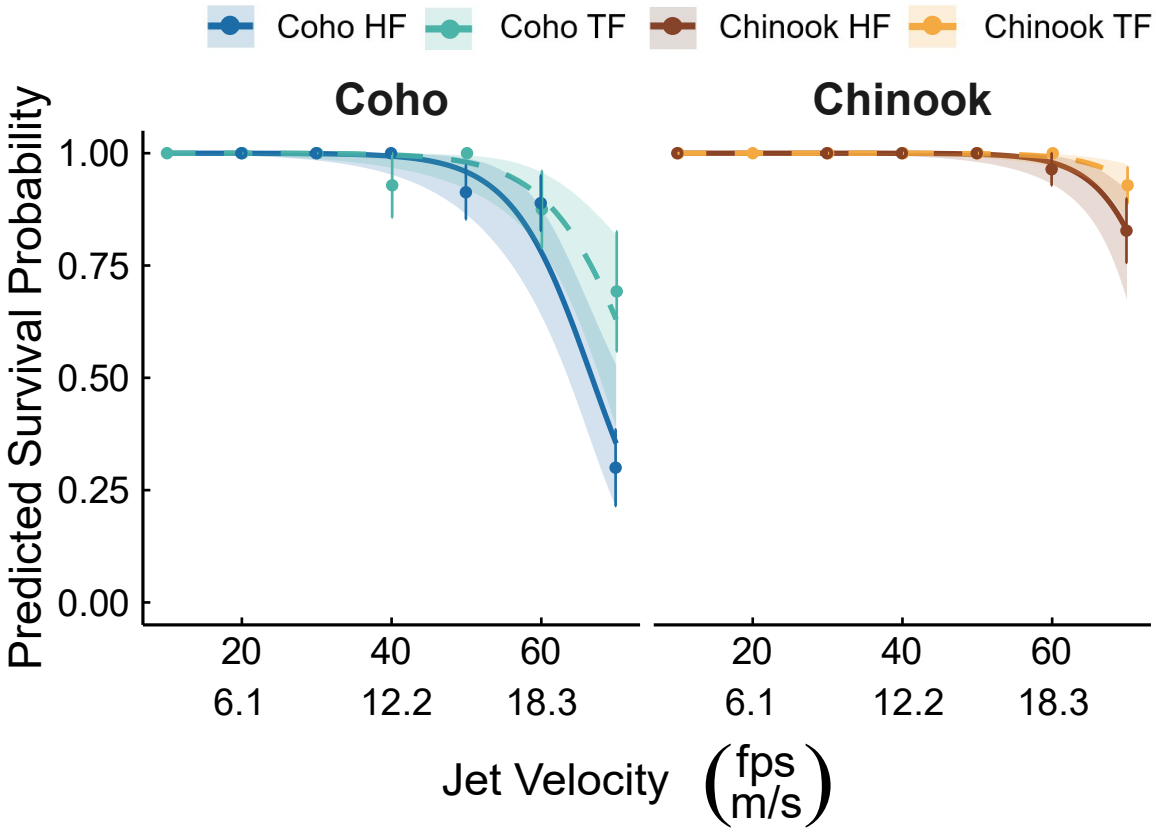

Figure 2-13. Relationship between jet velocity and immediate survival probability, shown for each exit orientation (HF = headfirst, TF = tail first) and each species. Other variables (tag type, length) were held constant at the species-specific mean lengths and an equal proportion of non-tagged and balloon-tagged fish. Shaded regions show the 95% confidence intervals. Observed survival rates for each group are overlayed as points with SE shown (bars).

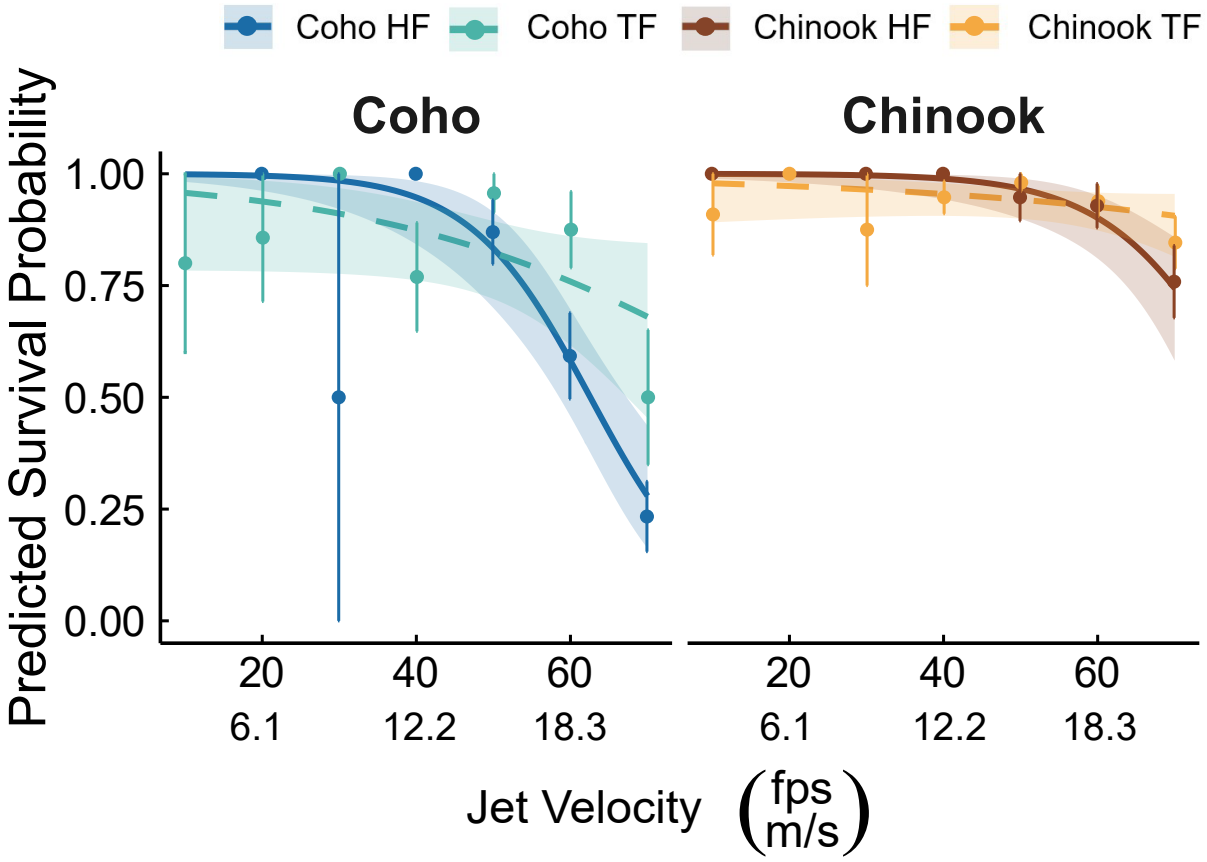

Figure 2-14. Relationship between jet velocity and overall survival probability, shown for each exit orientation (HF = headfirst, TF = tail first) and each species. Other variables (tag type, length) were held constant at the species-specific mean lengths and an equal proportion of non-tagged and balloon-tagged fish. Shaded regions show the 95% confidence intervals. Observed survival rates for each group are overlayed as points with SE shown (bars). Only 2 coho salmon tested at 30 fps that exited headfirst were retained for overall survival analysis – one fish survived while the other did not, causing the large SE seen at this jet velocity for observed survival.

Species-specific effects on survival were present in both survival models but were particularly strong for immediate survival. In model predictions, coho salmon generally had lower survival probabilities, both immediate (Figure 2-13, Figure 2-15) and overall (Figure 2-14, Figure 2-16). This trend was reflected in observed survival rates, with Chinook salmon showing 97% immediate survival and 92% overall survival, while coho salmon immediate survival was 82% and overall survival 71% (Table 2-2, Table 2-3).

The effect of species on survival became more apparent as jet velocity increased. Both Chinook and coho salmon had relatively high immediate predicted survival probabilities (Figure 2-13, Figure 2-15) and observed immediate survival rates (Chinook salmon = 100%; coho salmon = 95%) when tested between 10 and 50 fps. Above 50 fps, immediate survival probability of coho salmon dropped drastically, and while Chinook salmon immediate survival probability also decreased over 50 fps, it was a milder decline (Figure 2-13, Figure 2-15). For observed immediate

survival rates, less than 94% of Chinook salmon and 65% of coho salmon survived at flows over 50 fps. Coho salmon immediate survival at 70 fps was particularly low at 42%, compared to 89% for Chinook salmon (Table 2-2, Table 2-3). The main effect of species was less pronounced in overall predicted survival probabilities than in immediate; therefore, the lower overall predicted survival of coho salmon may be controlled more by interactions between species and exit orientation and/or jet velocity (Table 2-4).

Fish orientation when exiting the jet nozzle considerably affected immediate survival for both Chinook and coho salmon. In general, a tail first (TF) orientation was associated with higher survival in both species. Immediate predicted survival probabilities for headfirst (HF) and TF exit orientations did not diverge until higher jet velocities were reached (Figure 2-13). Immediate survival probability dropped for both HF and TF exit orientations at velocities over 50 fps for coho salmon and 60 fps for Chinook salmon, but the rate of this decline was more severe for HF orientations in both species (Figure 2-13). The negative effect of exiting HF at high jet velocities appears especially strong for coho salmon (Figure 2-15).

The overall survival probability was also predicted to decrease as jet velocity increased for both HF and TF exit orientations (Figure 2-14). Exit orientation (main effect) and its interaction with jet velocity were significant terms in the overall survival model average (Table 2-4). The decline in predicted survival was more gradual for a TF exit orientation, and at jet velocities below approximately 50 fps for coho salmon and 60 fps for Chinook salmon, TF predicted survival was lower than predicted survival for a HF exit orientation (Figure 2-14).

Relationship trends between exit orientation and modeled survival accurately described observed exit orientations and survival rates. Both coho and Chinook salmon had higher immediate mortality when exiting HF (coho salmon = 28%, Chinook salmon = 12%) compared to TF (coho salmon = 8%, Chinook salmon = 1%). Additionally, HF exit orientations were observed more frequently at higher jet velocities (Appendix C).

In general, longer fish appeared to have higher predicted immediate and overall survival than shorter fish. This was true for both coho and Chinook salmon (Figure 2-15, Figure 2-16). This trend was more dramatic in coho salmon survival predictions than in Chinook salmon survival. Larger fish typically have a greater swimming ability and these differences in survival may be attributed to how the fish exited the jet, as this greater swimming ability likely increases the likelihood that fish exit tail first which was also shown to increase survival. Additionally, it must be considered that subyearling Chinook and yearling coho were the only life stages that were examined, and applying this trend to other life stages may not be appropriate.

Tag type had a minimal effect on survival probabilities for both Chinook and coho salmon. For immediate survival, balloon-tagged fish were predicted to have a slightly lower probability of survival compared to non-tagged, but this effect disappeared when examining overall survival (Table 2-4). No interactions between tag type and any other variables were included in either of the final survival model averages (Table 2-4). During testing, balloon-tagged Chinook salmon (immediate = 96%, overall = 90%) were observed to have lower survival rates than non-tagged Chinook salmon (immediate = 99%, overall = 94%), although this trend was not seen in coho salmon (Table 2-2, Table 2-3).

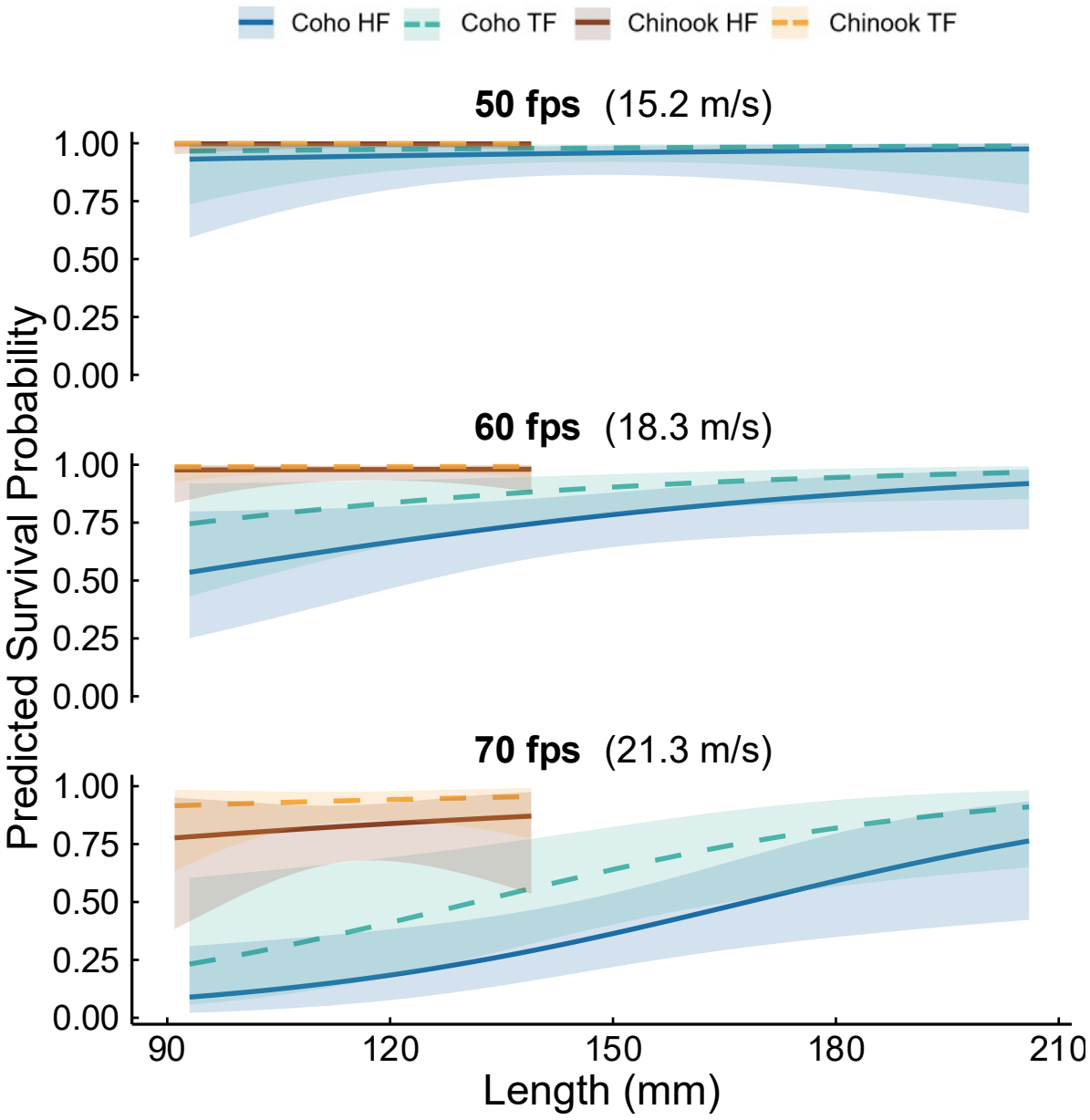

Figure 2-15. Relationship between fish lengths (mm) and immediate survival probability. The relationship is shown for each species, exit orientation (HF = headfirst, TF = tail first), and jet velocity over 50 fps. The remaining variable, tag type, was held constant at an equal proportion of non-tagged and balloon-tagged fish. Shaded regions show the 95% confidence intervals.

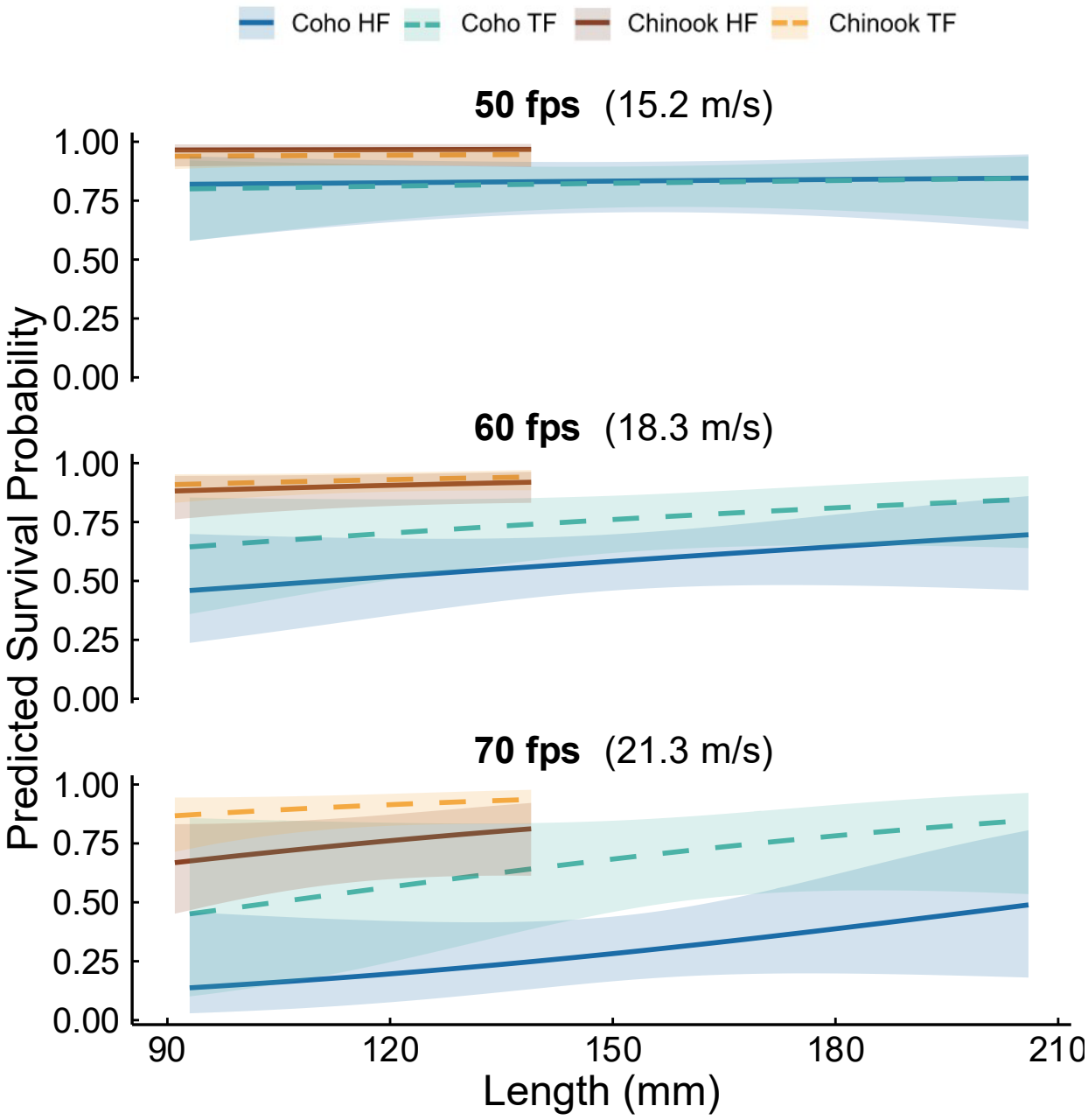

Figure 2-16. Relationship between fish lengths (mm) and overall survival probability. The relationship is shown for each species, exit orientation (HF = headfirst, TF = tail first), and jet velocity over 50 fps. The remaining variable, tag type, was held constant at an equal proportion of non-tagged and balloon-tagged fish. Shaded regions show the 95% confidence intervals.

2.2.1.2 Shear: Sensor Fish

This section summarizes the data and results of the Sensor Fish (Salalila et al., 2019) shear testing conducted from October to December 2024 in the shear tank. The Sensor Fish devices were used to characterize the physical conditions that live fish may experience during exposure

to shear events. Sensor Fish Mini tests were also conducted, and their results are summarized in Appendix G.

Treatments and Sample Sizes

From October to December 2024, 11 treatments (combinations of jet velocity and balloon tag presence) of Sensor Fish shear tests were performed at different jet velocities under submerged jet flow conditions, for balloon-tagged or non-tagged Sensor Fish (Table 2-5). There were 336 valid Sensor Fish datasets collected. A valid dataset requires recovery of the Sensor Fish devices, successful downloading of the data, acquisition of complete data from the introduction tube to when the Sensor Fish devices exited the jet nozzle into the downstream tank, and no potential collisions with any rigid objects in the shear tank.

Table 2-5. Treatments and sample sizes for the Sensor Fish datasets.

Treatments		Valid Sensor Fish Releases (*n*)
Jet Velocity (fps) [m/s]	**Balloon-Tagged (Yes/No)**	
10 [3.0]	No	19
20 [6.1]	No	6
30 [9.1]	No	13
40 [12.2]	No	42
40 [12.2]	Yes	9
50 [15.2]	No	61
50 [15.2]	Yes	27
60 [18.3]	No	50
60 [18.3]	Yes	30
70 [21.3]	No	60
70 [21.3]	Yes	19

Timing Marks

According to the analysis of the time-series pressure data, different regions of the hydraulic passage can be divided to identify the approximate locations where shear events occurred. The Sensor Fish was released from the upstream vertical introduction tube into the horizontal jet nozzle and then recovered manually from the downstream tank. Based on the comparison with the simulation results from computational fluid dynamics, three regions of Sensor Fish data for the shear tank were delineated and described as follows. An example of the Sensor Fish dataset with four timing marks (T0-T3) is shown in Figure 2-17.

- Introduction Tube (T0-T1): From the start point to the endpoint of the pressure bump, the peak pressure of which increases with the jet velocity.
- Contraction and Nozzle Region (T1-T2): From the endpoint of the pressure bump to the end of the pressure drop that is close to the atmospheric pressure (14.7 psia). This region

typically includes the nadir pressure and the highest acceleration peak, and the duration is within 0.05 s.

- Region Outside of Nozzle (T2-T3): Approximately five seconds after the end of the pressure drop.

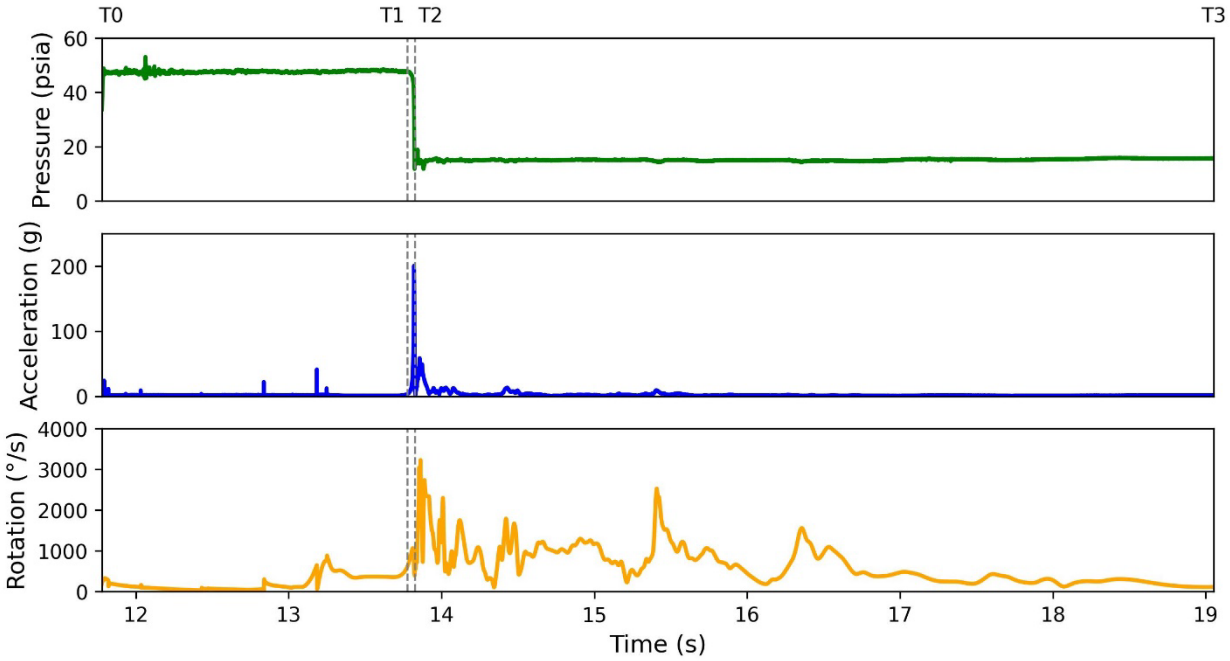

(a) T0-T3.

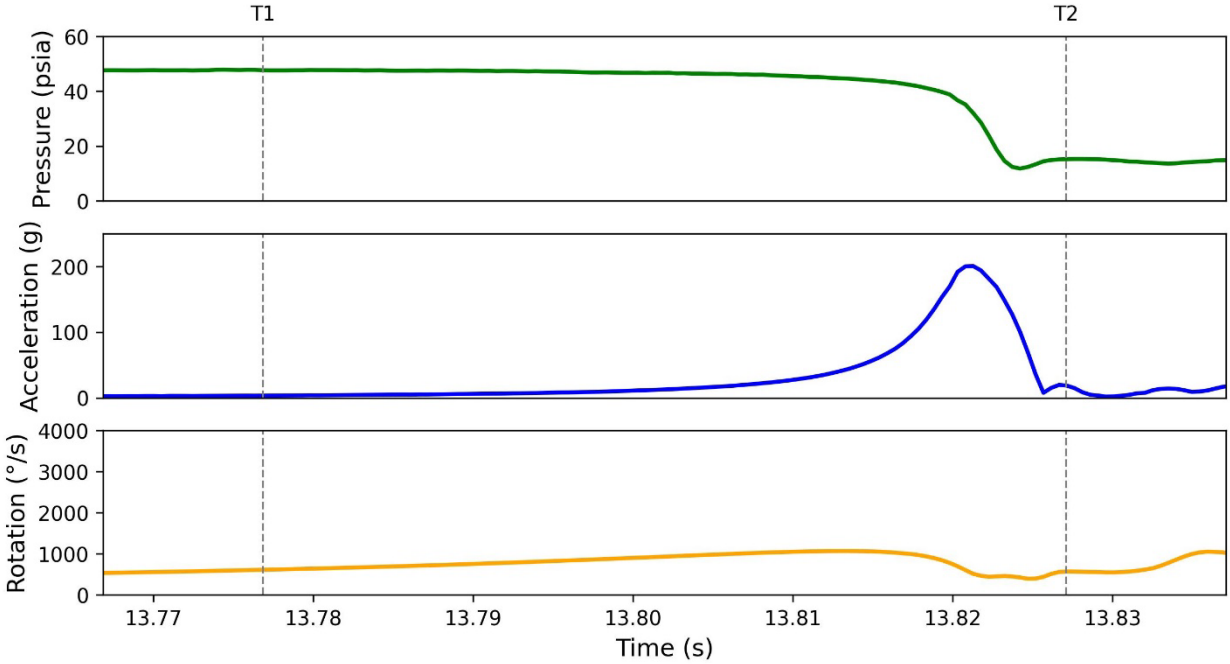

(b) T1-T2.

Figure 2-17. Typical Sensor Fish dataset example with timing marks showing (a) all four timing marks (T0-T3), and (b) the contraction and nozzle region timing marks (T1-T2).

Acceleration Events

The peak accelerations of Sensor Fish are presented in Figure 2-18, Figure 2-19, and in Table 2-6. The results indicate that the mean values of peak acceleration increased with jet velocity. Moreover, the presence of a balloon tag introduced extra resistance for the accelerating process of Sensor Fish when passing through the contraction and nozzle region. Thus, the peak accelerations of tagged Sensor Fish were lower than those of non-tagged Sensor Fish. The balloon tag effect on the Sensor Fish peak accelerations was significant ($p < 0.01$; *t*-test), which may be due to the small size of the jet nozzle. Consistent with these findings, the highest shear events were observed in the contraction and nozzle region.

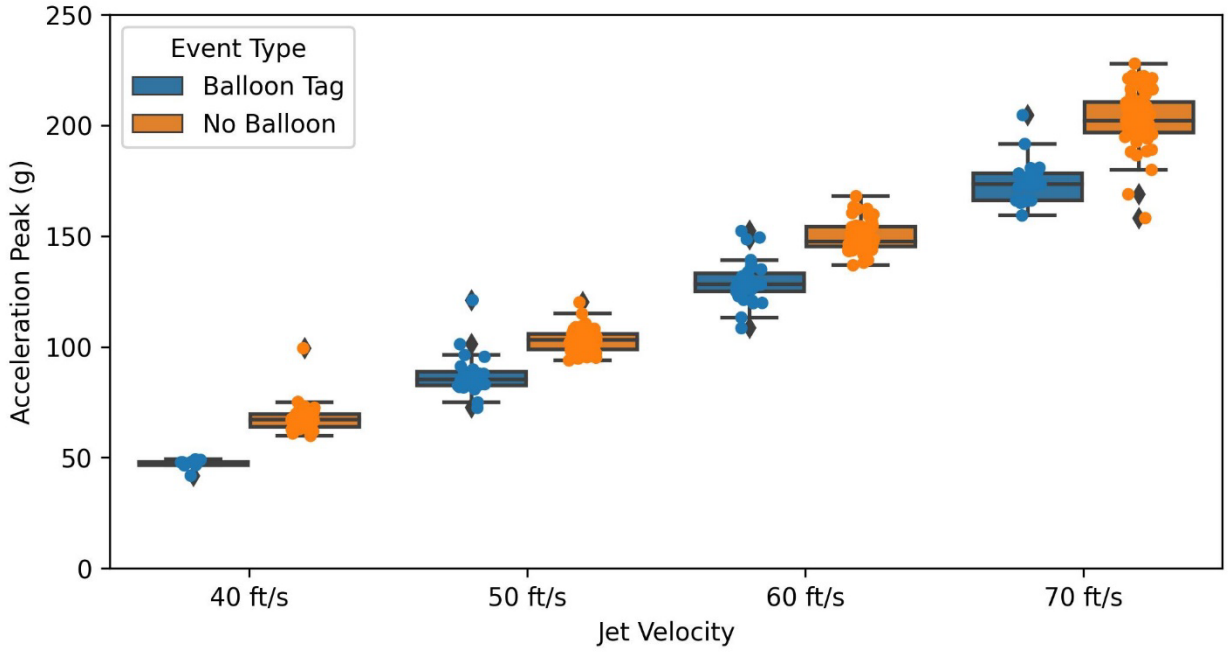

Figure 2-18. Comparison of Sensor Fish peak acceleration during contraction and nozzle region (T1-T2).

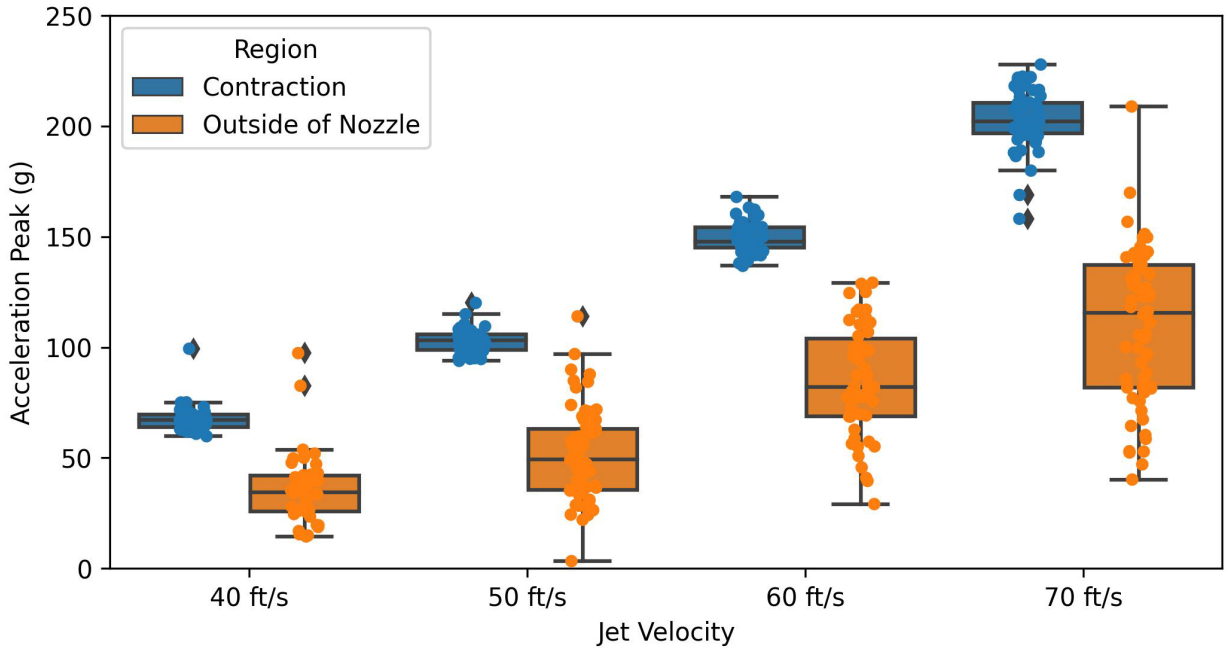

Figure 2-19. Comparison of non-tagged Sensor Fish peak acceleration for inside (T1-T2) and outside (T2-T3) of the nozzle regions.

Table 2-6. Mean peak values of Sensor Fish and Sensor Fish mini acceleration events.

Treatments		Sensor Fish	
Jet Velocity (fps) [m/s]	Balloon-Tagged (Yes/No)	Mean Values of Maximum Accelerations Inside Nozzle (g_0)	Mean Values of Maximum Accelerations Outside Nozzle (g_0)
10 [3.0]	No	7	4
20 [6.1]	No	19	14
30 [9.1]	No	37	21
40 [12.2]	No	68	36
40 [12.2]	Yes	47	31
50 [15.2]	No	103	51
50 [15.2]	Yes	87	42
60 [18.3]	No	150	85
60 [18.3]	Yes	129	69
70 [21.3]	No	203	110
70 [21.3]	Yes	175	97

Estimated Survival Rates

As described in the Methods Section 2.1.2, the velocity-based strike metric M_V was developed to characterize the severity of strike events between fish and hydraulic structures. To investigate the applicability of M_V to a shear event, one to five sample points to the left and right of the peak acceleration were employed to quantify the severity of a shear event observed in the contraction region of the shear tank. CFD results confirmed that the maximum M_V values for both CFD particles and Sensor Fish consistently occurred within the nozzle and contraction region, indicating that the CFD and Sensor Fish analyses are directly comparable despite differences in spatial domains. Table 2-7 and Table 2-8 show that the Pearson correlation coefficients between mean M_V values and the raw live fish 48-hr survival rates under the jet velocities greater than 40 fps were not sensitive to the number of data points in calculating M_V values. Thus, to keep the definition of the shear metric consistent with the strike metric, three sample points before and after the peak were also used for further analysis.

Table 2-7. Pearson correlation coefficients between mean shear M_V values and raw live fish 48-hr survival rates in shear testing.

Number of Sample Points before and after the Peak Acceleration used in Shear M_V	Correlation Coefficients for Chinook Salmon	Correlation Coefficients for Coho Salmon
1	0.63	0.86
2	0.62	0.85
3 (default for Strike M_V)	0.61	0.85
4	0.61	0.85
5	0.60	0.84

Table 2-8. Mean shear M_V (default definition with seven sample points in total) values and raw live fish 48-hr survival rates in shear testing.

Treatment	Sensor Fish Mean Shear M_V (m/s) – [fps]	Raw Chinook Salmon 48-hr Survival Rate (%)	Raw Coho Salmon 48-hr Survival Rate (%)
40 fps without Balloons [12.2 m/s]	2.17 - [7.12]	96.2	70.0
40 fps with Balloons [12.2 m/s]	1.54 - [5.05]	95.8	100
50 fps without Balloons [15.3 m/s]	3.28 - [10.76]	94.7	100
50 fps with Balloons [15.3 m/s]	2.76 - [9.06]	100	87.1
60 fps without Balloons [18.3 m/s]	4.69 - [15.39]	94.3	66.7
60 fps with Balloons [18.3 m/s]	4.01 - [13.16]	92.9	73.7
70 fps without Balloons [21.3 m/s]	6.22 - [20.41]	90.0	27.8
70 fps with Balloons [21.3 m/s]	5.30 - [17.39]	73.7	33.3
	Pearson correlation coefficient	0.61	0.85
	p-value	0.11	**0.01**

Following the same definition of the strike metric, the cumulative distribution function curves of shear M_V for different treatments are shown in Figure 2-20, Figure 2-21, Figure 2-22 and Figure 2-23. Based on the raw live fish survival rates at the highest jet velocity of 70 fps, the calibrated mortal thresholds of M_V were found to be 5.48 m/s for tagged Sensor Fish and tagged Chinook salmon, 6.61 m/s for non-tagged Sensor Fish and non-tagged Chinook salmon, 5.17 m/s for tagged Sensor Fish and tagged coho salmon, and 6.08 m/s for non-tagged Sensor Fish and non-tagged coho salmon. Thus, the fish experiencing the shear M_V values above the specific mortal threshold are likely to be killed during the passage, otherwise the fish are likely to survive through the passage.

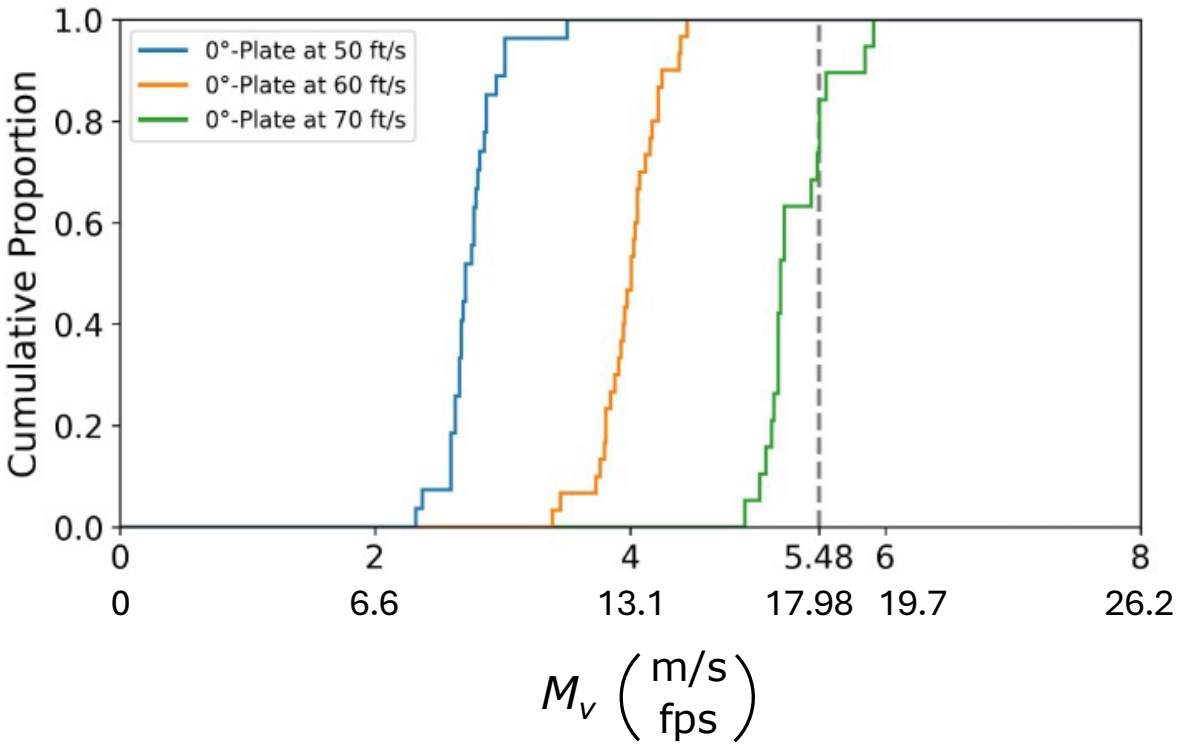

Figure 2-20. Cumulative distribution function curves of shear M_V of tagged Sensor Fish and tagged Chinook salmon. The vertical dashed gray line indicates the M_V (5.48 m/s).

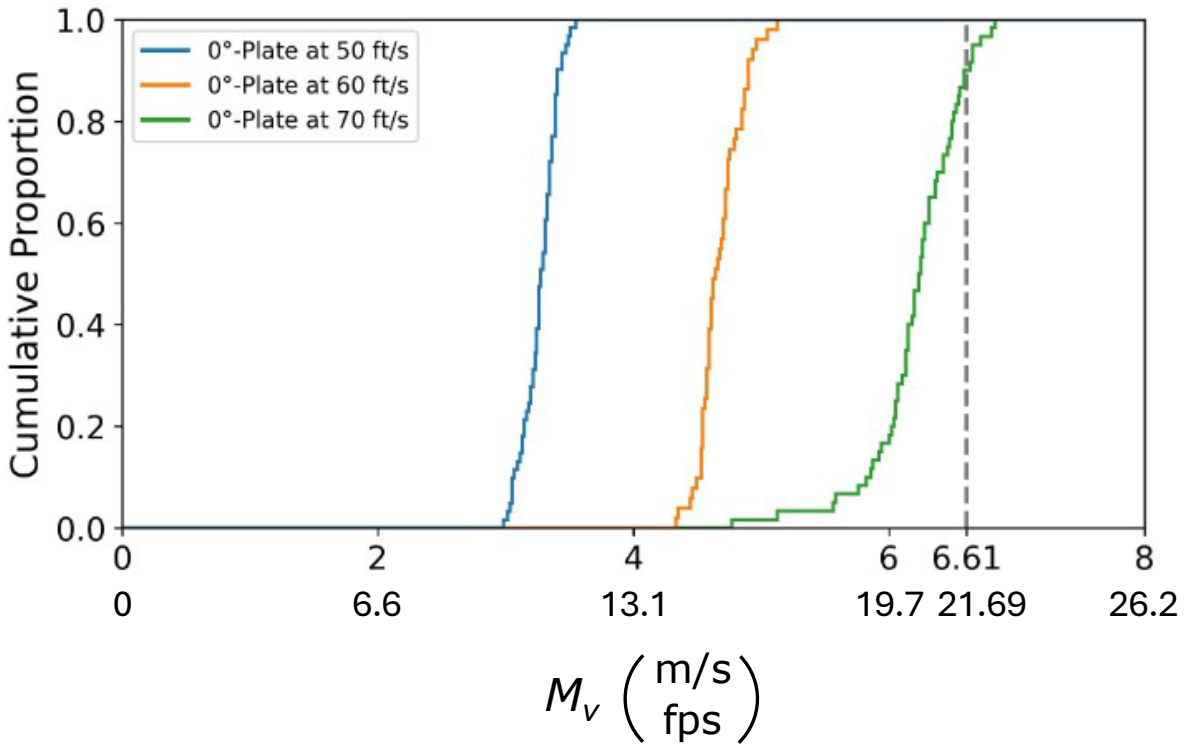

Figure 2-21. Cumulative distribution function curves of shear M_V of non-tagged Sensor Fish and non-tagged Chinook salmon. The vertical dashed gray line indicates the M_V (6.61 m/s).

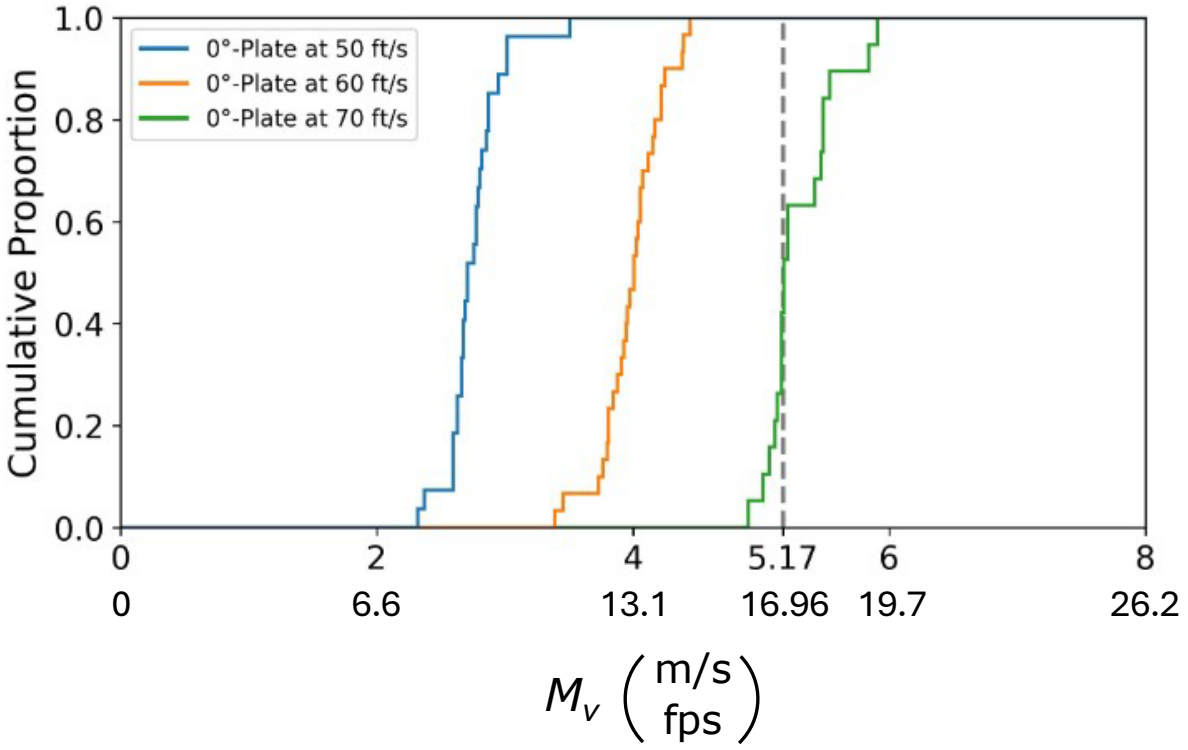

Figure 2-22. Cumulative distribution function curves of shear M_V of tagged Sensor Fish and tagged coho salmon. The vertical dashed gray line indicates the M_V (5.17 m/s).

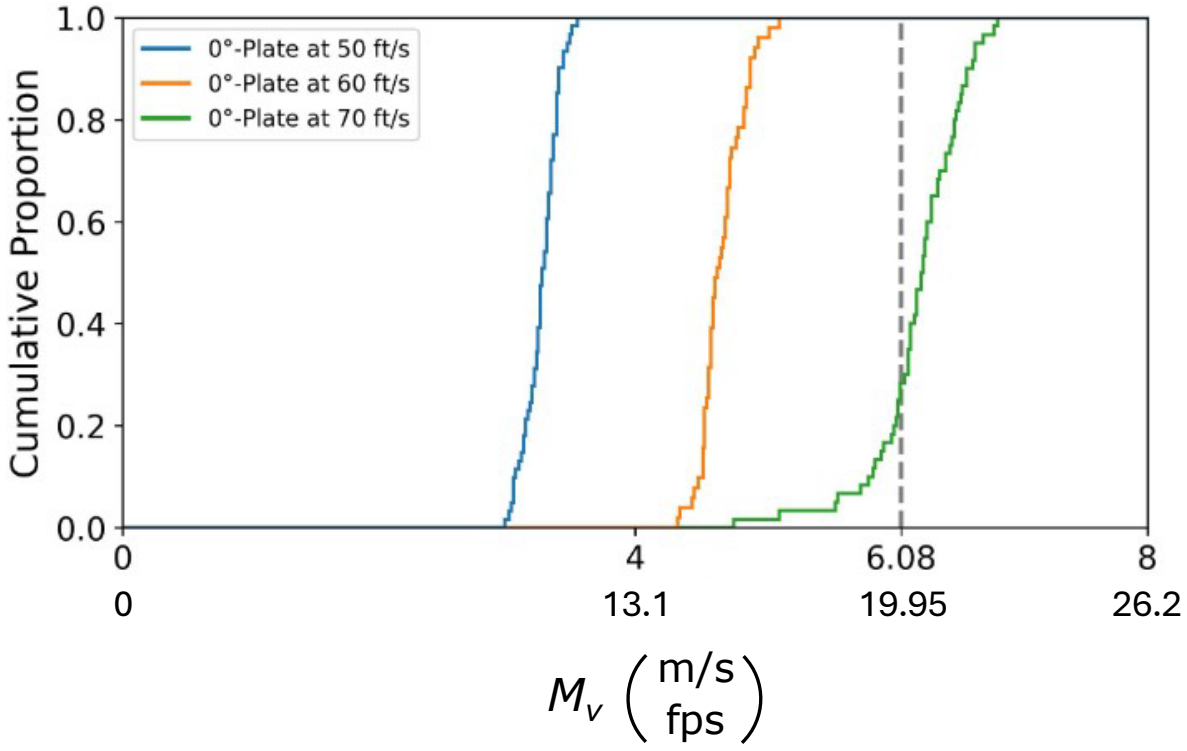

Figure 2-23. Cumulative distribution function curves of shear M_V of non-tagged Sensor Fish and non-tagged coho salmon. The vertical dashed gray line indicates the M_V (6.08 m/s).

2.2.1.3 Shear: CFD Modeling

This section summarizes the results of the coupled CFD-particle simulations performed for shear testing. The predicted results from these simulations were subsequently compared with experimental observations obtained from live fish tests and Sensor Fish data obtained from shear testing. Similar to the computational approach applied in HAHD and GPR tasks involving multiphase simulations with a coupled CFD-DEM framework, cylindrical DEM particles with identical sizes and physical properties of Sensor Fish were used. These particles were used to model and characterize the hydraulic conditions that live fish are likely to encounter during exposure to shear events.

Comparison of CFD-predicted Results with Sensor Fish Studies

The coupled CFD-particle simulations were conducted once the flow in the submerged jet reached pseudo-steady-state conditions. A total of 400 cylindrical particles, matching the dimensions of the Sensor Fish, were injected randomly over a time interval of 10–20 seconds. The injection duration varied with jet velocity, and particles were periodically injected at specific time intervals to minimize inter-particle collisions. Longer injection durations were strategically chosen at lower jet velocities to further reduce the likelihood of collisions. The flow simulation was terminated once all particles exited the region of interest, i.e. wall of shear tank and zone away from plate. Subsequently, trajectory data from the simulations were analyzed to predict the mortal threshold value and severe acceleration.

The results were further analyzed to estimate the shear event, particle acceleration analogous to the Sensor Fish and pressure variation within the shear tank. The domain of interest falls within nozzle and the adjacent plate region, where higher value of shear is expected. It is important to note that live fish also encounter shear within the nozzle. Therefore, shear inside the nozzle cannot be excluded when comparing results related to injury and mortality rates in live fish. The domain of interest of this study is the nozzle and plate region, where higher shear is expected. Figure 2-24 shows the variation of absolute pressure (in psia) and normalized acceleration (in g_0 = a/9.81, where *a* denotes particle acceleration) for a cylindrical particle subjected to a nozzle velocity of 70 fps. The vertically dotted lines indicate key transition points: the start and end of the converged section (associated with contraction region in Sensor Fish studies) within the nozzle, as well as the exit from the extended cylindrical section. As previously described, the green plot highlights the occurrence of two distinct shear events: the first shear due to flow acceleration inside the nozzle and the second shear located near the plate. Flow acceleration leads to a drop in pressure below atmospheric levels—referred to as nadir pressure—within the cylindrical extension, as indicated by the red plot.

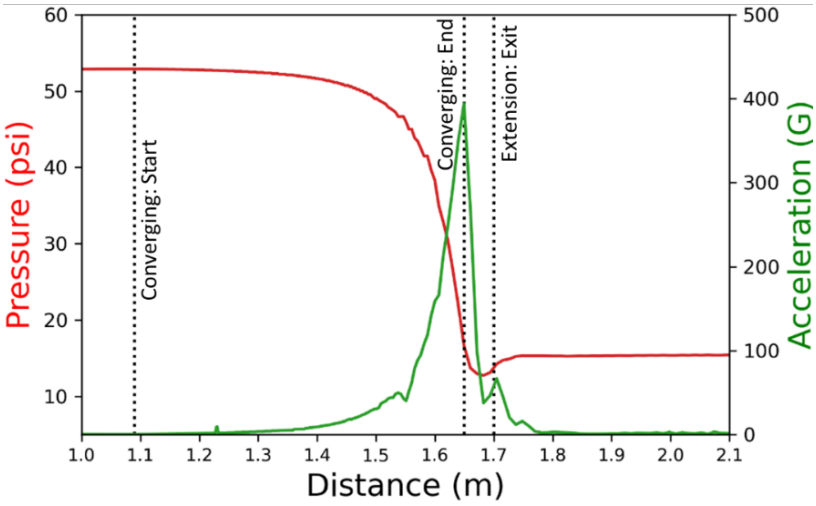

Figure 2-24. Variation of the absolute pressure and particle acceleration inside and in the region that is proximate to the exit of nozzle at a velocity of 70 fps.

Figure 2-25 presents a comparison between CFD-predicted results for particle acceleration and absolute pressure at a nozzle velocity of 70 fps and Sensor Fish data. Both the CFD predictions and the Sensor Fish measurements demonstrate similar trends in the variation of these stressor variables. Although the CFD-predicted values for particle acceleration were slightly higher than those observed in Sensor Fish data, the predicted pressure values closely aligned with experimental findings under similar conditions. This consistency indicates that the CFD model successfully captures the accurate flow dynamics influencing particle acceleration and pressure within the shear tank during experimental testing.

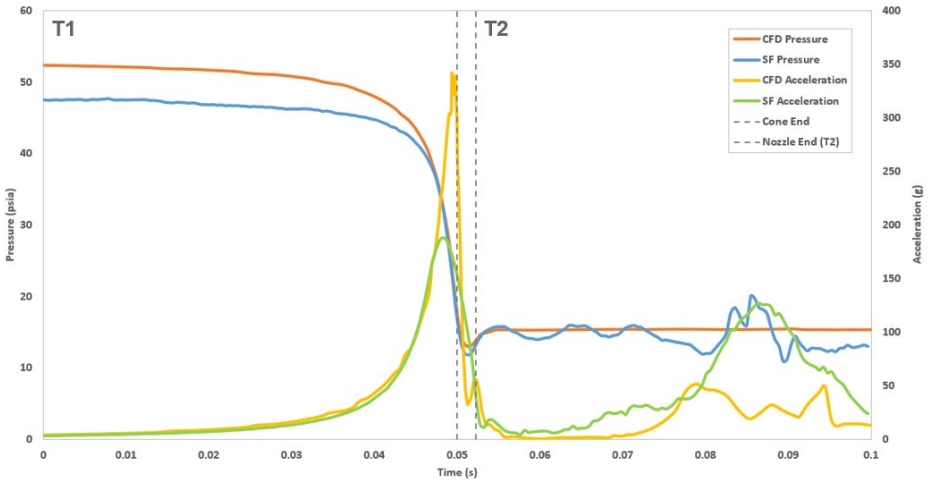

Figure 2-25. Comparison of the predicted pressure and particle acceleration in converging and extended section of nozzle with sensor fish studies.

Acceleration Events

The CFD-predicted accelerations and corresponding results obtained from Sensor Fish studies are presented in Figure 2-26 and in Table 2-9. As expected, both results show similar trends – increasing value of the acceleration with increased jet velocity. Moreover, the peak accelerations of Sensor Fish were lower than those predicted from the CFD studies. Overall, the 95% cumulative exposure probability of acceleration event from both methods correlates well for the range of jet velocity included in the shear test ($p < 0.01$; *t*-test).

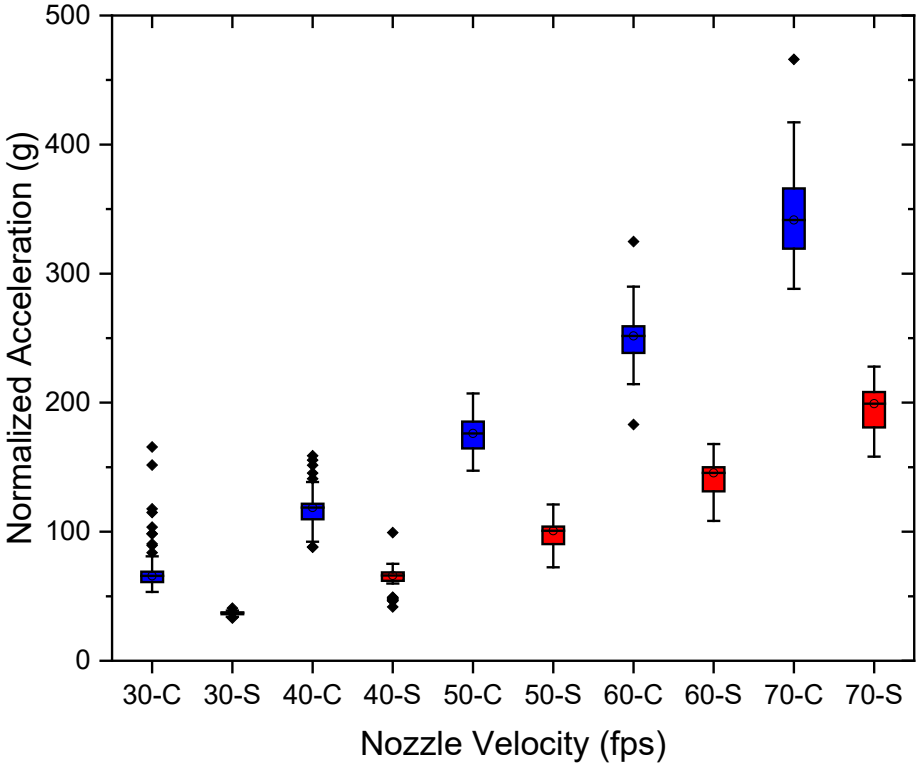

Figure 2-26. Box plot shows the comparison of the CFD predicted acceleration with the Sensor Fish acceleration for the full CFD domain. C and S in the X-axis denote CFD simulation and Sensor Fish respectively. Number (30–70) shows the magnitude of jet velocity in fps.

Table 2-9. Comparison of CFD-predicted severe event (0° plate angle) due to shear with corresponding one for Sensor Fish studies at 95% cumulative exposure probability.

Plate Angle (°)	Jet Velocity (fps) – [m/s]	Percentage Collison With Plate	Maximum Acceleration (g_0)		M_V Value (m/s) – [fps]	
			CFD	SF	CFD	SF
00	20 [6.1]	0.67	69	19	0.98 - [3.22]	
00	30 [9.1]	1.33	77	41	1.90 - [6.23]	
00	40 [12.2]	2.65	124	99	3.06 - [10.04]	2.36 - [7.74]
00	50 [15.2]	2.66	198	121	4.45 - [14.60]	3.48 - [11.42]
00	60 [18.3]	3.99	283	168	5.75 - [18.86]	4.96 - [16.27]
00	70 [21.3]	4.32	386	228	6.75 - [22.15]	6.67 - [21.88]
		Correlation Coefficient	0.99		0.987	
		p-value	0.0077		0.0131	

Survival Rates Predictions

Consistent with the Sensor Fish studies, the velocity-based strike metric, M_V, was calculated to characterize the severity of shear events within the shear tank. The methodology for computing M_V is described in the methods section of Sensor Fish studies (2.1.3.4); therefore, it is not reiterated here. For each particle, M_V values were computed using three sample points before and after the peak acceleration. Table 2-9 presents the CFD-predicted 95% cumulative exposure probability of M_V alongside the corresponding values from Sensor Fish data. As shown in Table 2-9, the M_V values calculated using both methods exhibit strong correlation across the range of jet velocities tested (p ~ 0.01; t-test). Figure 2-27 presents the cumulative exposure probability of M_V values of particles at various jet velocities. Based on raw live fish survival rates observed at the highest jet velocity of 70 fps, calibrated mortality thresholds for M_V were determined to be 5.88 m/s for coho salmon and 6.92 m/s for Chinook salmon, respectively. These thresholds indicate that fish of the species and lengths in our study exposed to shear M_V values exceeding the species-specific mortality thresholds are not likely to survive during passage, while fish of the species and lengths in our study experiencing lower M_V values are likely to survive.

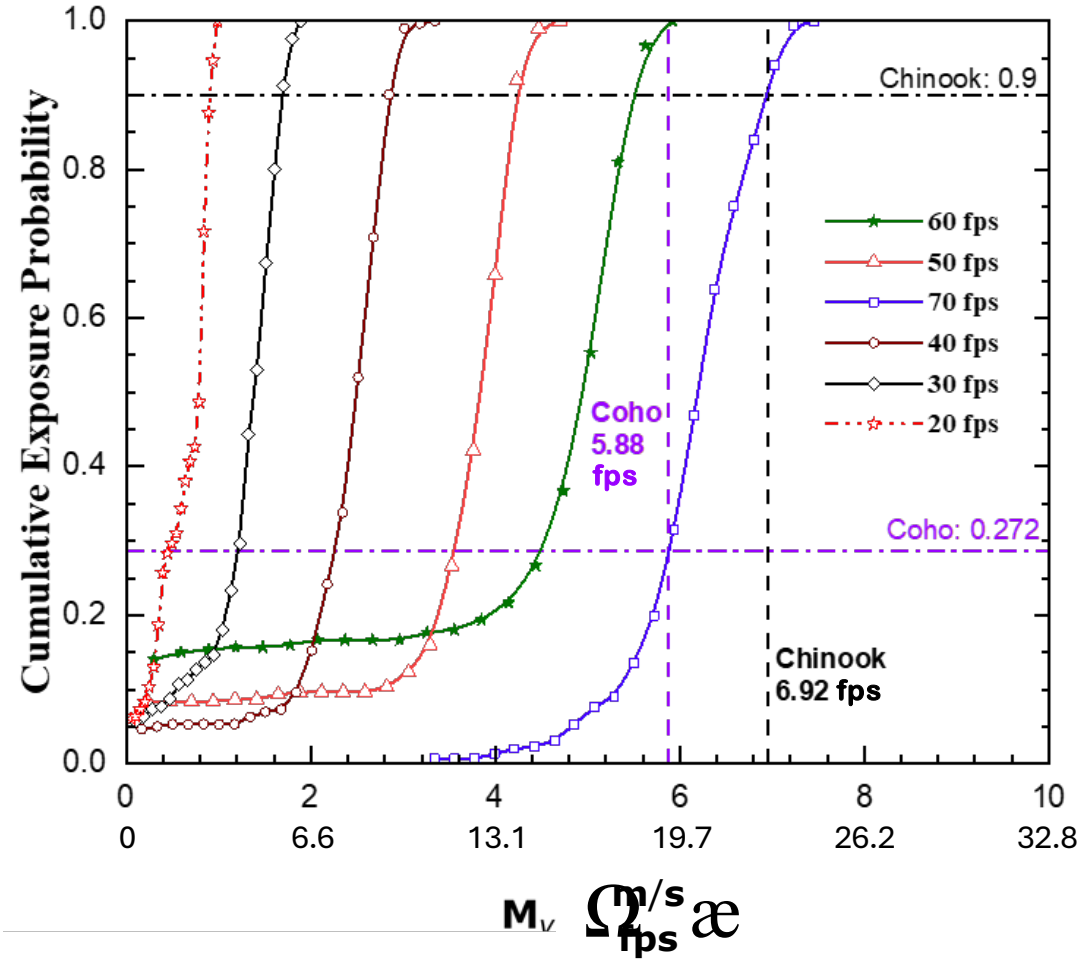

Figure 2-27. The cumulative distribution probability of M_V for submerged jet simulations during shear tests under varying jet velocities. The vertical violet and black dashed lines denote the threshold M_V values for coho and Chinook salmon, respectively. The horizontal violet and black dashed-dot lines indicate the survival rates of Coho and Chinook salmon observed during live fish testing conducted in the shear tank.

The CFD-predicted exposure probability has been compared with the corresponding data calculated from Sensor Fish studies, as shown in Figure 2-28, at four jet velocities. Both methods exhibit similar trends in the variation of exposure probability, with the cumulative exposure probability of M_V values increasing alongside rising jet velocity. However, the CFD-predicted M_V values are consistently higher across all four jet velocities. This observation aligns with the variation in normalized acceleration with jet velocity, as shown in Figure 2-26. According to Huang et al. (Huang et al., 2025), computed M_V accounts for the peak acceleration experienced by the Sensor Fish as it passes through the hydro passage.

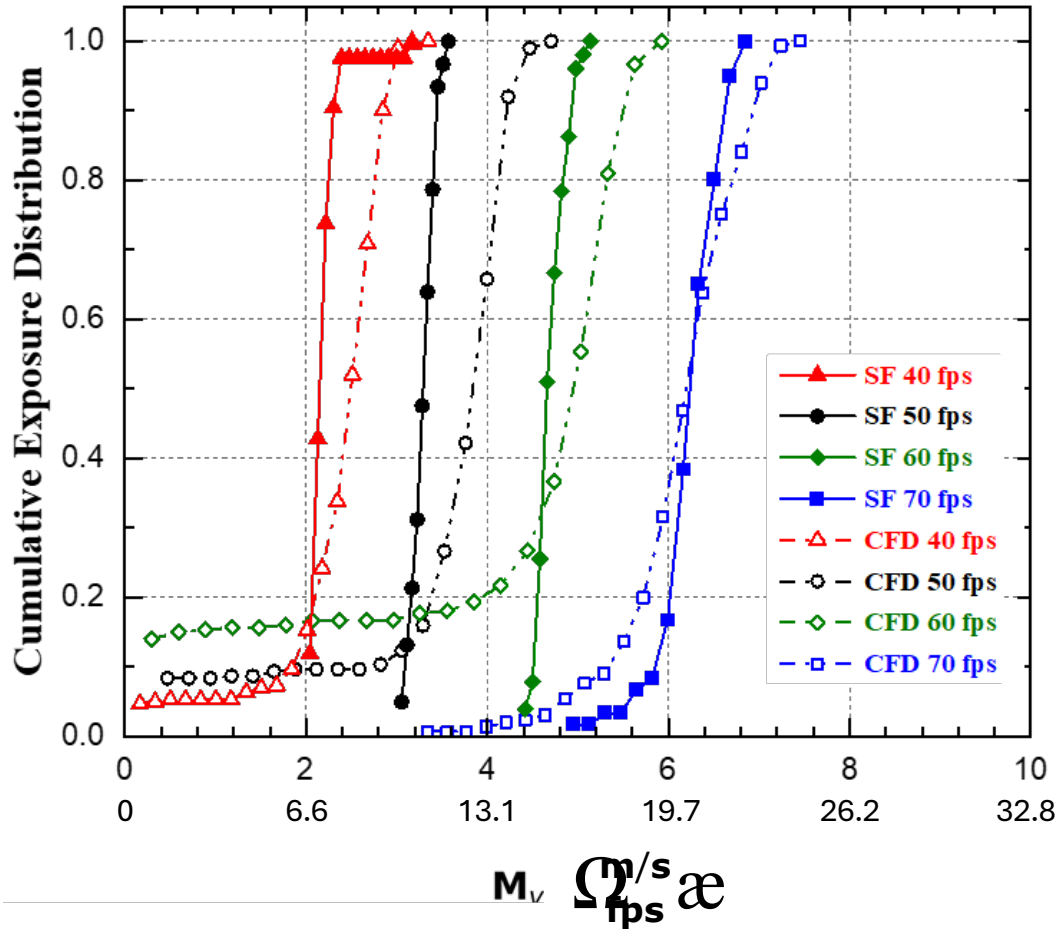

Figure 2-28. Comparison of CFD-predicted cumulative exposure distribution of M_V for shear tests with Sensor Fish studies at four jet velocities. CFD-predicted M_V values are consistently higher than those observed in Sensor Fish studies across all four jet velocities.

In addition to determining M_V as a mortality threshold in Sensor Fish studies, CFD-particle simulations can directly compute shear stressor as the modulus of the strain rate tensor. Shear data was recorded at each time step in CFD-particle simulations, and the maximum shear value for each particle was extracted. Subsequently, the cumulative exposure probability of shear at various jet velocities was computed. Figure 2-29 shows the cumulative exposure probability of shear values for particles at different jet velocities. Based on raw live fish survival rates observed at the highest jet velocity of 70 fps, calibrated mortality thresholds for extreme shear events were estimated to be $399\,1/sec$ for coho salmon and $888\,1/sec$ for Chinook salmon. The CFD-predicted shear threshold for Chinook salmon ($888\,1/sec$) lies within the range of historical data ($800 - 950\ 1/sec$) for fish mortality. However, a significantly lower shear threshold was observed for coho salmon compared to historical values ($1100 - 1200\ 1/sec$) of fish mortality (Neitzel et. al. 2000). This discrepancy suggests that additional stressors, such as collisions, might have influenced live fish testing due to the larger size of fish used (approximate length ~200 mm). These threshold values indicate that fish of the species and lengths in our study exposed to shear levels exceeding species-specific mortality thresholds are likely to die during passage, while those experiencing shear levels below the thresholds are likely to either survive or sustain only minor injuries.

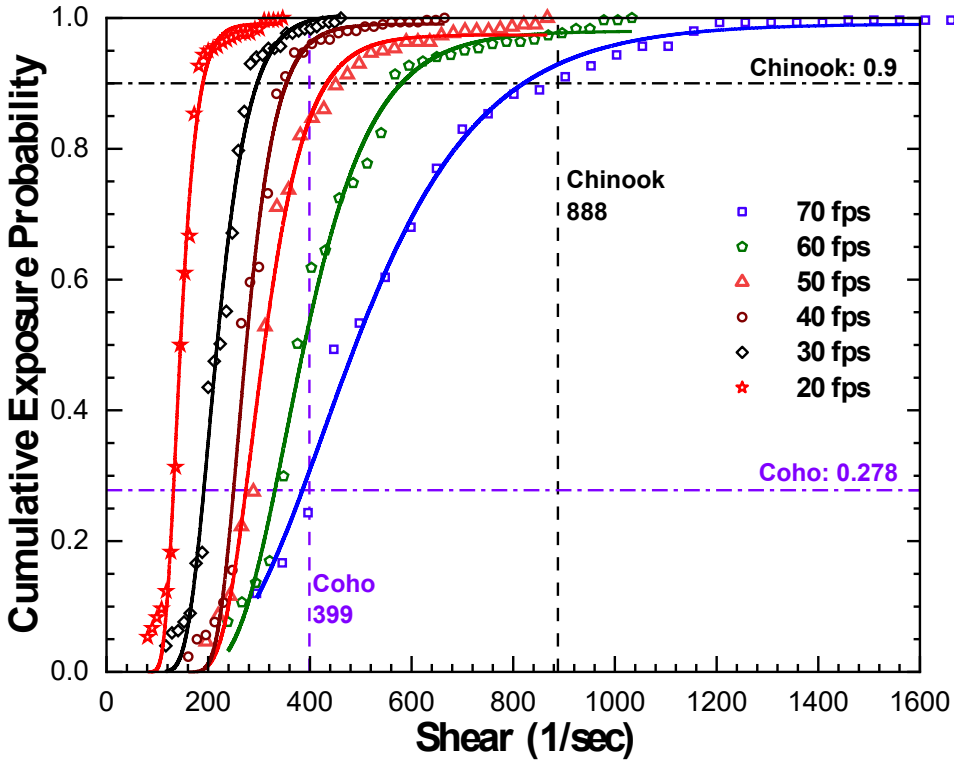

Figure 2-29. The cumulative distribution probability of the shear value for submerged jet simulations during shear tests under varying jet velocities. The vertical violet and black dashed lines denote the threshold Shear values for coho and Chinook salmon, respectively. The horizontal violet and black dashed-dot lines indicate the survival rates of coho and Chinook salmon observed during live fish testing conducted in the shear tank.

Using the mortality threshold values for shear, the survival probability of Chinook salmon and Coho salmon was predicted and subsequently compared with raw survival rate obtained from live fish studies, as presented in Table 2-10. The Pearson correlation coefficients also provided in Table 2-10. The analysis reveals that the Pearson correlation coefficients between the CFD-predicted survival and raw live fish 48-hr survival rates under various jet velocities were consistently strong for coho salmon. Notably, the highest correlation was observed for coho salmon, with Pearson's r = 0.86 and p = 0.03.

Table 2-10. Comparison of the CFD-predicted survival rate with experimental observation of the live survival based on raw live fish 48-hr survival rates.

Jet Velocity (fps) [m/s]	Chinook Salmon		Coho Salmon	
	Predicted Survival Rate (%)	Raw 48-hr Survival Rate (%)	Predicted Survival Rate (%)	Raw 48-hr Survival Rate (%)
20 [6.1]	100	100	100	100
30 [9.1]	100	75.0	98.53	83.3
40 [12.2]	100	96.2	95.9	70.0
50 [15.2]	100	94.7	84.0	100
60 [18.3]	100	94.3	61.7	66.7
70 [21.3]	90.0	90.0	27.8	27.8
	Pearson correlation coefficient		0.86	
	p-value		**0.03**	

2.2.2 Collision Laboratory Results

The following sections describe the results from the collision laboratory testing for the live fish injury assessments, Sensor Fish, and CFD modeling.

2.2.2.1 Collision: Live Fish

All live fish collision testing was conducted at a 20° plate angle due to the expectation of a major secondary collision event occurring at a 30° angle. The secondary collision was observed using sensor fish and validated in the CFD model. An initial 60 coho salmon (90–133 mm FL [$\bar{x}$ = 112 mm]; 7.4–22.1 g [$\bar{x}$ = 16.1 g]) were tested at 50 fps. Immediate mortality was low (*n* = 4), and no major injuries were observed in surviving fish (Table 2-11). Bruising and eye hemorrhages were occasionally observed on fish tested at 50 fps (bruising *n* = 5, eye hemorrhage *n* = 3), with fish that did not survive testing exhibiting more extreme versions of these injuries (Figure 2-30). To establish thresholds for mortality during collision events, fish were expected to be released at 60 fps and 40 fps. Preliminary results from Sensor Fish released at a 20° plate angle and 60 fps estimated a mortality rate of 20% for live fish exposed to identical conditions. Due to this high estimate, live fish were tested at 40 fps instead of 60 fps to establish a lower threshold for mortality. A total of 30 live fish (96–128 mm FL [$\bar{x}$ = 111 mm]; 9.9–24.8 g [$\bar{x}$ = 15.6 g]) were released at 40 fps (Table 2-11). No immediate or delayed mortality (i.e., 100% overall survival), or major injuries, were observed in fish tested at this velocity.

Table 2-11. Sample sizes, mortality counts and survival rates (immediate, delayed and overall) for coho salmon during collision testing.

Collision Testing: Observed Survival							
Jet Velocity (fps) [m/s]	N	Immediate (1-hr)			Overall (48-hr)		
		n[1]	Mort	Survival Prop.	*n*[1]	Mort	Survival Prop.
40 [12.2]	30	30	0	1.00	30	0	1.00
50 [15.2]	60	58	4	0.93	54	5	0.91
Total	**90**	**88**	**4**	**0.95**	**84**	**5**	**0.94**

[1]Any fish that had a handling event (dropped, jumped from holding tank, etc.) or other unintended stressor were removed from the analysis and are not included in this sample size.

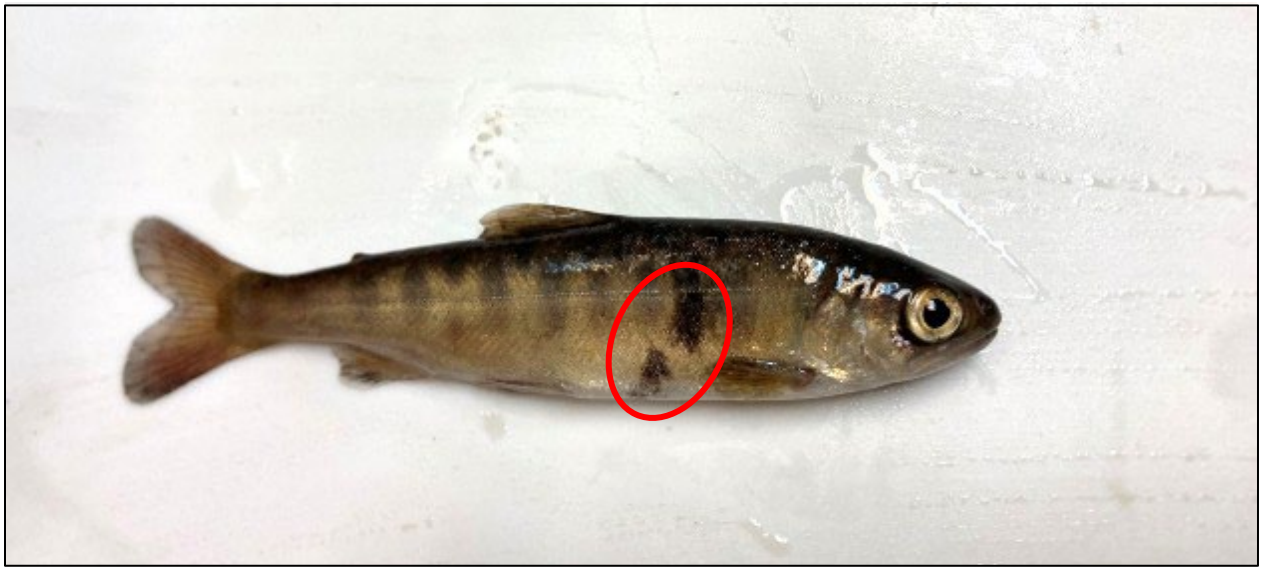

Figure 2-30. Injuries (bruising) seen on a coho salmon that did not survive exposure to a 20° plate angle at 50 fps.

Model discrimination was acceptable to excellent for both immediate and overall collision survival models (Firth's bias reduced model, Section 2.1.4.1). The model generated for immediate survival had an AUC value of 0.76, while the AUC value for the overall survival model was slightly higher at 0.81 (Hosmer and Lemeshow 2000). However, given the small sample size and low number of jet velocities used during collision testing, standard error (SE) for both immediate and overall models was large (Table 2-12, Table 2-13). For this reason, model results and model-generated predictions should be interpreted and used with caution.

Table 2-12. Coefficients and associated standard errors from Firth's bias reduced models generated to predict the probability of immediate and overall live fish survival. For this model, jet velocity was used as a categorical variable (cat.). Jet Velocity: 40 fps = 0 and 50 fps = 1.

Parameter	Immediate (1-hr)			Overall (48-hr)		
	Coefficient	SE	p-value	Coefficient	SE	p-value
Intercept	9.2860	13.7000	0.6803	9.2860	13.7000	0.6803
Jet Velocity (cat.)	-1.8358	15.3305	0.9338	2.3152	15.9389	0.9168
Length	-0.0520	0.1196	0.7864	-0.0520	0.1196	0.7864
Jet Velocity (cat.):Length	0.0072	0.1339	0.9700	-0.0324	0.1394	0.8656

Table 2-13. Coefficients and associated standard errors from Firth's bias reduced models generated to predict the probability of immediate and overall live fish survival.For this model, jet velocity was used as a continuous variable (cont.).

Parameter	Immediate (1-hr)			Overall (48-hr)		
	Coefficient	SE	p-value	Coefficient	SE	p-value
Intercept	16.6293	73.8215	0.8792	0.0254	75.8551	0.9998
Jet Velocity (cont.)	-0.1836	1.5331	0.9338	0.2315	1.5939	0.9168
Length	-0.0810	0.6447	0.9320	0.0777	0.6630	0.9340
Jet Velocity (cont.): Length	0.0007	0.0134	0.9700	-0.0032	0.0139	0.8656

Little difference between immediate and overall predicted survival probabilities was seen (Figure 2-31), reflecting trends during testing in observed survival rates (immediate = 94%, overall = 95%; Table 2-11). Overall predicted survival probability was slightly lower than immediate at 50 fps (Figure 2-31), which was the only jet velocity where mortality was observed during final collision testing (Table 2-11).

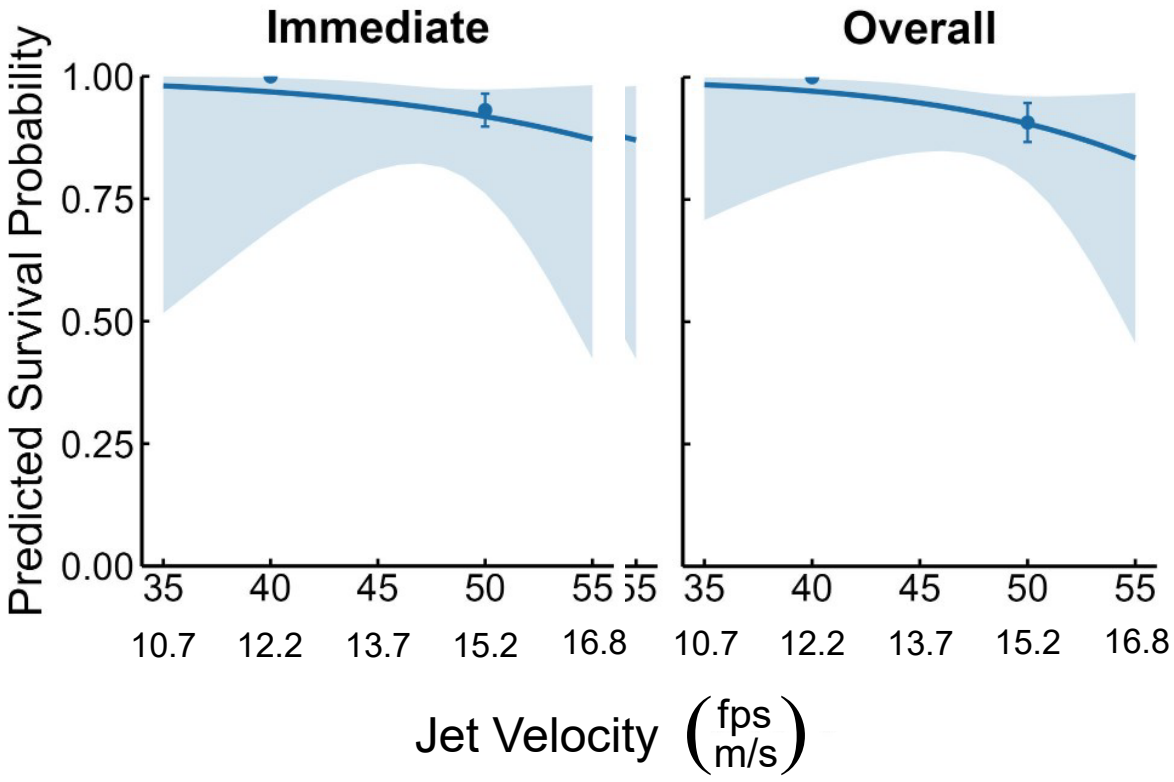

Figure 2-31. Relationships between jet velocity (fps) and predicted immediate and overall survival probability. These relationships were generated using jet velocity modeled as a continuous variable and the mean length ($\bar{x}$ = 111 mm) of fish used in testing. Shaded regions indicate 95% confidence intervals, which were large at flows beyond those at which testing occurred. Observed survival rates are overlayed as points with SE shown (bars).

As expected, predicted survival probability decreased as jet velocity increased for both immediate and overall models (Figure 2-31, Figure 2-32, Figure 2-33). However, given the uniformly high survival rates at 40 fps and 50 fps, predictive confidence is limited at the lower (40 fps) and untested higher velocities (Figure 2-31).

Fish length showed a weak negative effect on predicted survival, largely driven by a small number of mortalities among larger individuals (*n* = 5; 109–119 mm FL), all of which were exposed to 50 fps. Additionally, several larger fish (*n* = 4; 115–133 mm FL) were excluded from the overall survival analysis due to non-treatment related handling events. Consequently, survival estimates at greater lengths should be interpreted cautiously due to limited data rather than indicating a strong size-based effect.

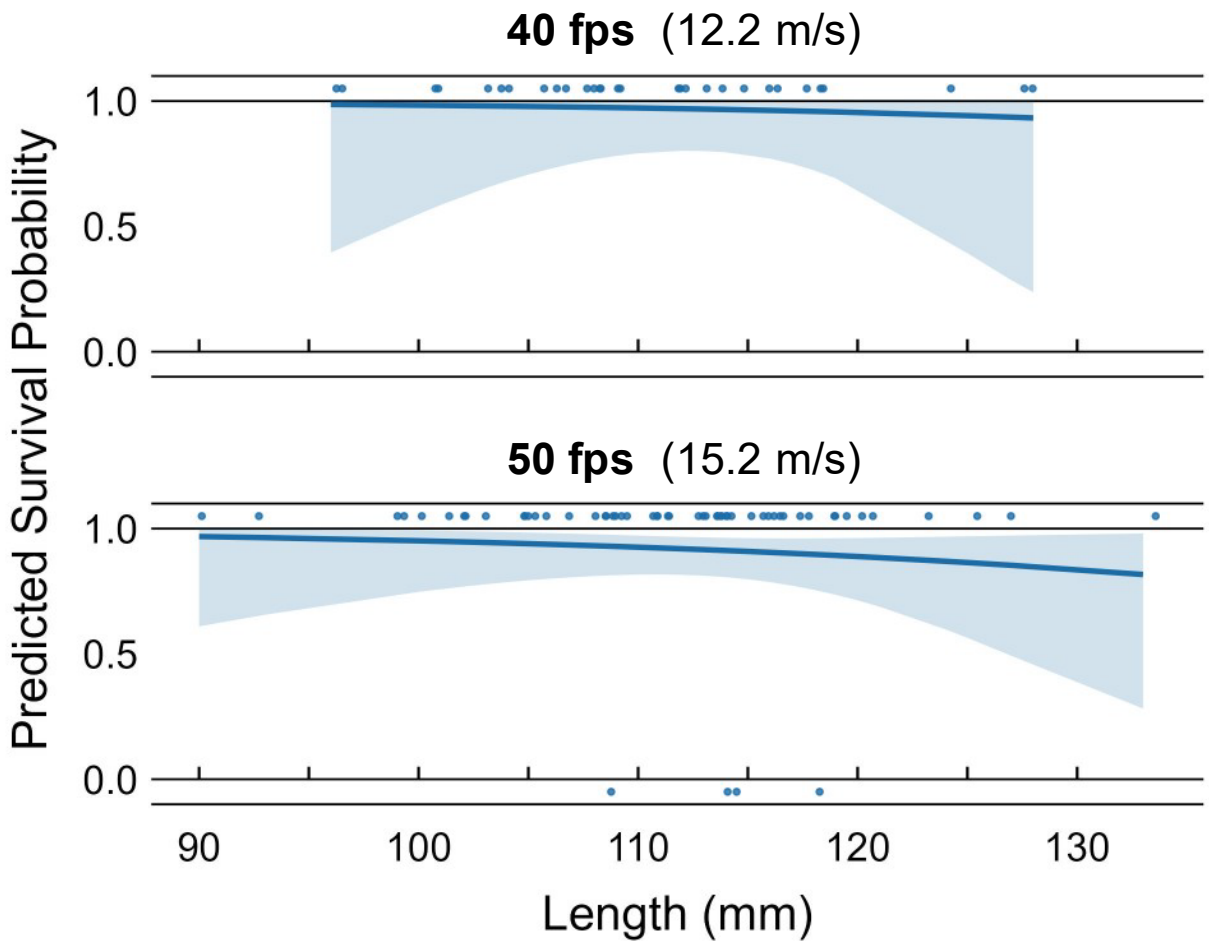

Figure 2-32. Relationship between fish fork length (mm) and predicted immediate survival probability, for both jet velocities used during live fish collision testing (40 and 50 fps). Shaded regions are 95% confidence intervals. Rug plots show the distribution of lengths used for testing at each jet velocity, as well as the observed survival of fish at those lengths. Rug points on the top of the plot indicate the fish of that length survived, while points on the bottom indicate immediate mortality, at respective jet velocities.

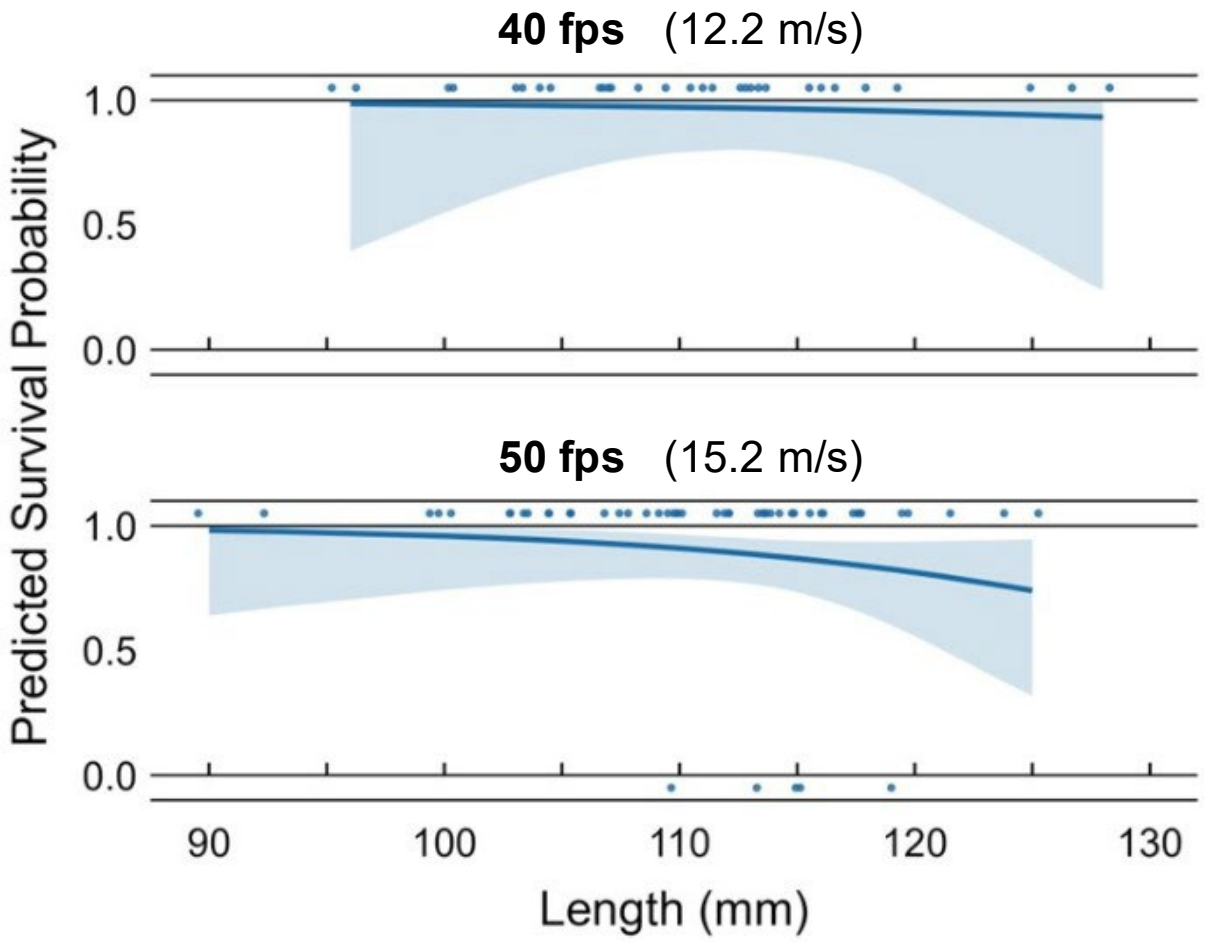

Figure 2-33. Relationship between fish fork length (mm) and predicted overall survival probability, for both jet velocities used during live fish collision testing (40 and 50 fps). Shaded regions are 95% confidence intervals. Rug plots show the distribution of lengths used for testing at each jet velocity, as well as the observed overall survival of fish at those lengths. Rug points on the top of the plot indicate the fish of that length survived, while points on the bottom indicate mortality, at respective jet velocities.

2.2.2.2 Collision: Sensor Fish

This section summarizes the data and results of the Sensor Fish collision testing conducted in April 2025 in the shear tank. The Sensor Fish devices were used to characterize the physical conditions that live fish may experience during exposure to collision events under the non-submerged jet flow condition.

Treatments and Sample Sizes

In April 2025, four treatments of Sensor Fish collision tests with different velocities and plate angles were conducted under non-submerged jet flow conditions in the shear tank, and 135 valid Sensor Fish datasets were collected as presented in Table 2-14. A valid release requires recovery

of the Sensor Fish devices, successful downloading of the data, acquisition of complete data from the introduction tube to when the Sensor Fish devices exited the jet nozzle into the downstream tank, and no potential collisions with the nozzle.

Table 2-14. Treatments and sample sizes for the Sensor Fish datasets.

Treatments (Non-submerged Flow)		Valid Sensor Fish Releases (*n*)
Jet Velocity (fps) [m/s]	Plate Angle (°)	
50 [15.2]	30	42
60 [18.3]	20	20
50 [15.2]	20	46
40 [12.2]	20	27

Timing Marks

According to the analysis of the time-series pressure data, different regions of the hydraulic passage can be divided to identify the approximate locations where collision events occurred. The Sensor Fish was released from the upstream vertical introduction tube into the horizontal jet nozzle and then recovered manually from the downstream tank. Based on the comparison with the simulation results from computational fluid dynamics, three regions of Sensor Fish data for the shear tank were delineated and described as follows. An example of the Sensor Fish dataset with five timing marks (T0-T4) is shown in Figure 2-34.

- Introduction Tube (T0-T1): From the start point to the endpoint of the pressure bump, the peak pressure of which increases with the jet velocity.
- Contraction and Nozzle Region (T1-T2): From the endpoint of the pressure bump to the end of the pressure drop that is close to the atmospheric pressure (14.7 psia). This region typically includes the nadir pressure and an acceleration peak, and the duration is within 0.05 s.
- Region of Plate Collisions (T2-T3): This region ranges approximately 0.05 s after the end of the pressure drop, and typically includes multiple acceleration peaks (i.e., primary collisions with the plate).
- Region of Tank Collisions (T3-T4): This region ranges approximately 0.1 ~ 0.2 s after the primary collisions with the plate, and the acceleration peaks (i.e., secondary collisions with the tank side wall) are not necessarily observed in each Sensor Fish release.

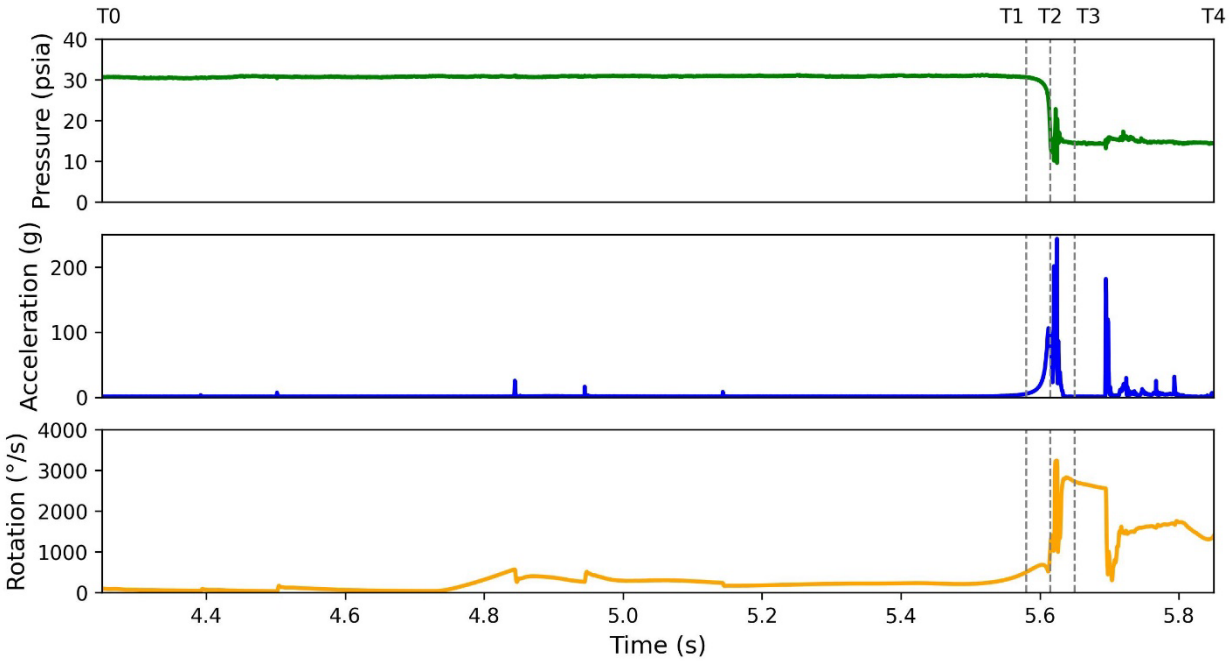

(a) T0-T4.

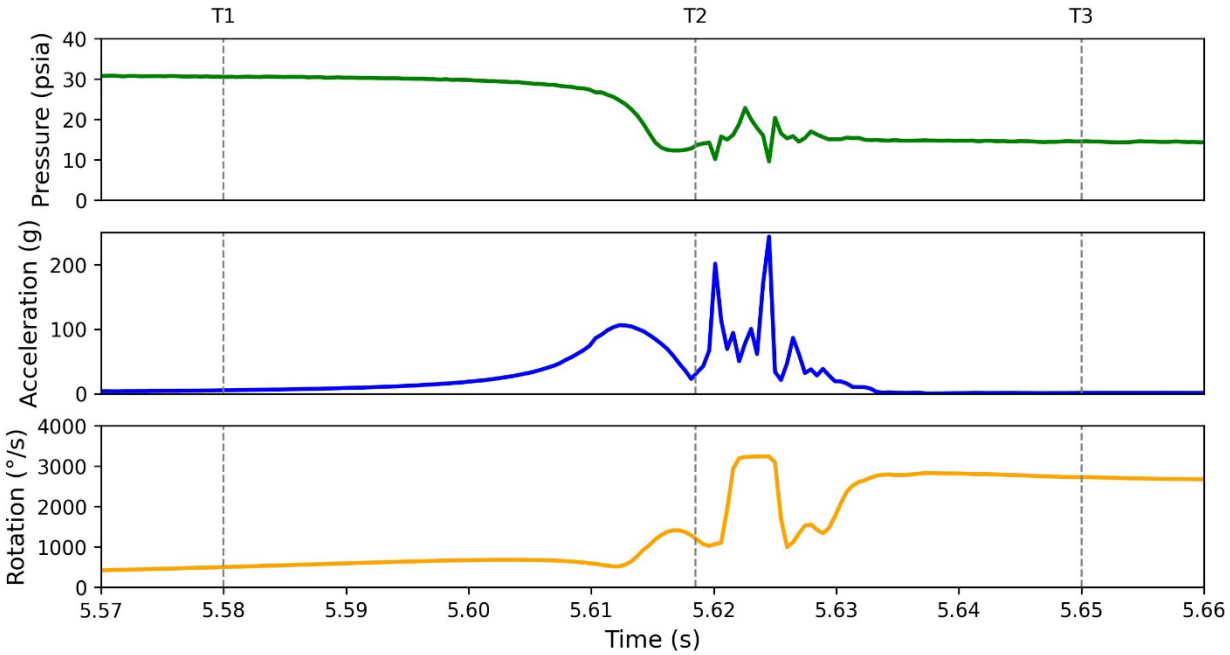

(b) T1-T3.

Figure 2-34. Typical Sensor Fish dataset example with timing marks showing (a) all five timing marks (T0-T4), and (b) around nozzle region timing marks (T1-T3).

Acceleration Events

The mean peak accelerations of the Sensor Fish collision events are presented in Table 2-15. The results indicate that the mean values of peak acceleration in the collision tests increased with

jet velocity and plate angle, and the mean values are higher than those of the shear events at the same jet velocity.

Table 2-15. Mean peak acceleration values for the Sensor Fish collision events.

Jet Velocity (fps) [m/s]	Plate Angle (°)	Valid Sensor Fish Releases (*n*)	Mean Values of Maximum Accelerations of Collision Events (g_0)
50 [15.2]	30	42	204
60 [18.3]	20	20	218
50 [15.2.]	20	46	188
40 [12.2]	20	27	171

Estimated Survival Rates

Following the methods described in section 2.1.3.4, the mean and 95th percentile values of M_V for collision lab testing are shown in Table 2-16. It should be noted that the M_V value for each Sensor Fish release was the maximum value among both the primary collision events with the plate and the secondary collision events with the tank wall under the non-submerged flow condition. Results show that M_V values increased with jet velocity and plate angle. Furthermore, based on the live fish (coho salmon) collision lab testing under the treatment of 50 fps-jet velocity and 20°-plate conducted in 2025, the calibrated mortal threshold of collision M_V was found to be 2.63 m/s. Accordingly, the cumulative distribution function curves of M_V for each collision lab test are shown in Figure 2-35, and the estimated 48-hr survival rates are shown in Table 2-17. Results show that estimated 48-hr survival rates for the other three treatments were 42.8% under 50 fps-jet velocity and 30°-plate, 47.2% under 60 fps-jet velocity and 20°-plate, and 100% under 40 fps-jet velocity and 20°-plate, while the accuracy of the estimates may be affected by the limited sample size.

Table 2-16. Values of Sensor Fish strike metric (M_V) for collision lab testing.

Jet Velocity (fps) [m/s]	Plate Angle (°)	Valid Sensor Fish Releases (*n*)	Mean Values of M_V (m/s) – [fps]	95th Percentiles of M_V (m/s) – [fps]
50 [15.2]	30	42	2.53 - [8.30]	3.49 - [11.45]
60 [18.3]	20	20	2.56 - [8.40]	3.37 - [11.06]
50 [15.2.]	20	46	1.80 - [5.91]	2.81 - [9.22]
40 [12.2]	20	27	1.21 - [3.97]	2.16 - [7.09]

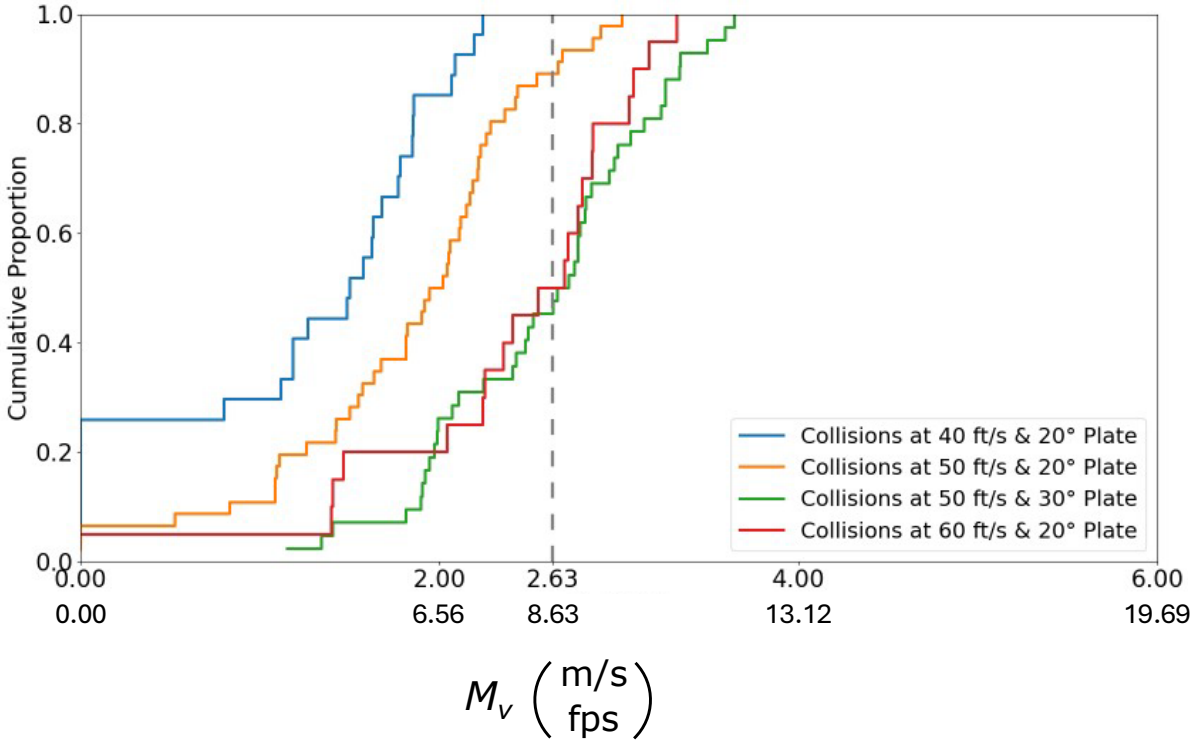

Figure 2-35. Applications of M_V for collision lab testing. The vertical gray dashed line shows the M_V (2.63).

Table 2-17. 48-hr survival rates, estimated from Sensor Fish Strike Metric (M_V) for collision lab testing.

Jet Velocity (fps) [m/s]	Plate Angle (°)	Valid Sensor Fish Releases (*n*)	Estimated 48-hr Survival Rates (%)	Coho Salmon 48-hr Survival Rates (%)
50 [15.2]	30	42	42.8	N/A
60 [18.3]	20	20	47.2	N/A
50 [15.2] **(threshold calibration)**	20 **(threshold calibration)**	46	90.7	90.7
40 [12.2]	20	27	100	100

2.2.2.3 Collision: CFD Modeling

This section summarizes the data and results of the CFD-particle flow simulations conducted for collision testing under unsubmerged jet conditions. Cylindrical DEM particles, analogous to Sensor Fish, were utilized to characterize the hydraulic conditions and strikes that live fish might encounter during collision events under non-submerged jet flow conditions. As extensively explained later in the Section 3.1.6 for computational model for GPR, the coefficient of normal restitution (NCR) was set to 0.10 in the DEM simulation setup. The lower NCR value facilitates the modeling of inelastic collisions, which are expected to occur in both Sensor Fish experiments and live fish collision testing.

Qualitative comparison of the free surface and jet velocity

As mentioned in Section 2.1.5.2, turbulent multiphase flow simulations were conducted for an unsubmerged jet striking to a 20º angled plate and three jet velocities. The water level in the shear tank was maintained below the nozzle and plate to ensure that the unsubmerged jet would strike the plate in air. Unlike the submerged jet simulations, a hybrid turbulence model, the DES, was employed. The flow simulations were conducted for a sufficient duration to allow the flow to achieve pseudo-steady-state conditions. Since no quantitative data on velocity or pressure drop was available from experimental studies, a qualitative comparison of the free surface behavior was performed. Figure 2-36 (a & b) shows the front and top views of the free surface evolution in the CFD simulations. As expected, the water jet striking the plate fragmented into droplets, slender jets, and splashes on the free surface. Upon impact with the inclined plate, the flow was directed toward the tank wall, resulting in chaotic flow patterns observed at the bottom of Figure 2-36 (b). Similar behavior was evident in experimental snapshots in Figure 2-36 (c), demonstrating qualitative agreement between the CFD simulations and experimental observations. Overall, both studies support consistent qualitative flow dynamics.

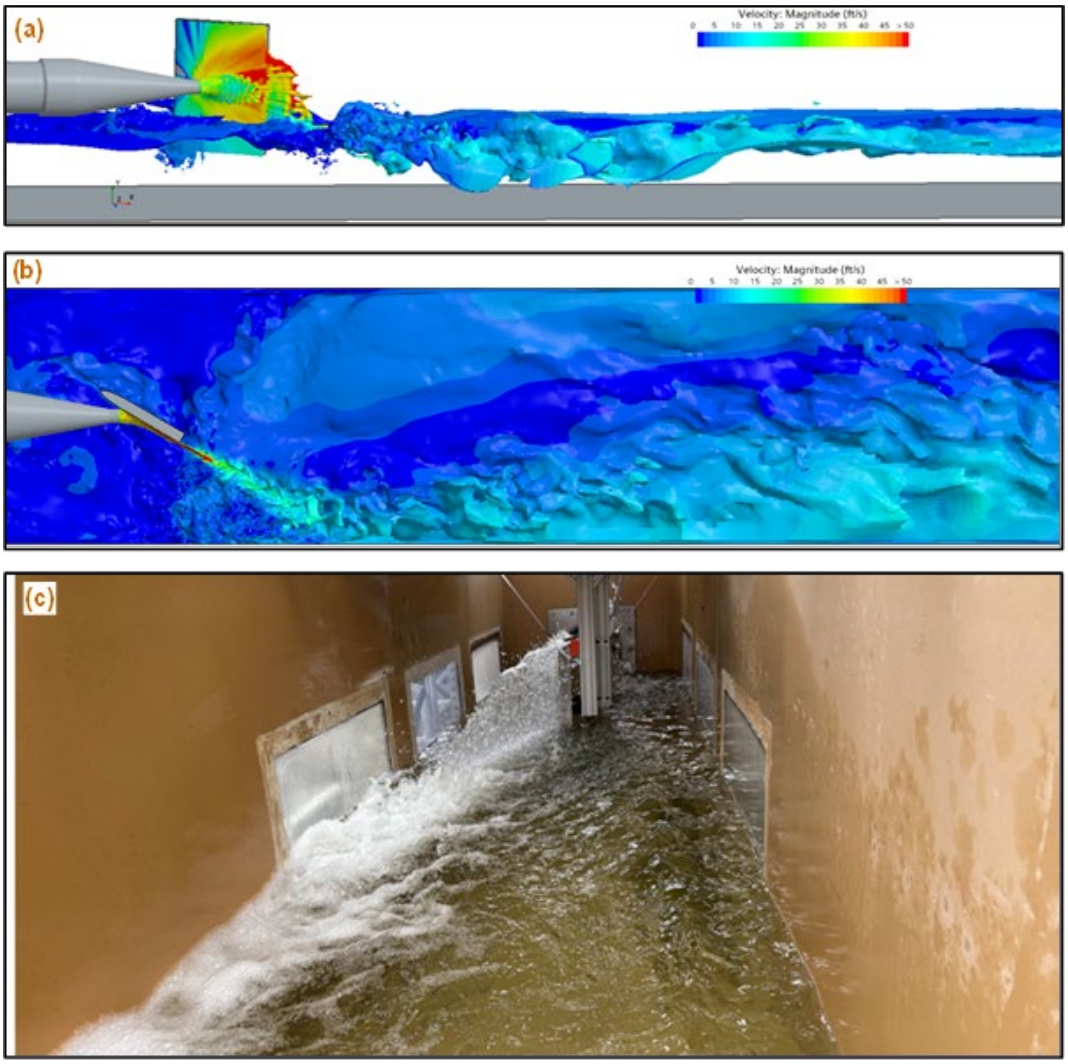

Figure 2-36. Qualitative comparison of free surface flow during unsubmerged jet testing in the shear tank. Color contours are used to illustrate: (a) the front view of the free surface, capturing jet formation and droplet behavior, and (b) the top view of the free surface, showcasing wavy flow patterns and velocity. (c) Experimental snapshots qualitatively validate the flow predictions.

Acceleration Events

Similar to previous studies conducted for HAHD, GPR, and shear testing, particle acceleration was calculated for each jet velocity during collision tests. The median and 95th percentile of the maximum acceleration experienced by particles during collision events are presented in Table 2-18. As expected, the median and 95th percentile values of peak acceleration increased with higher jet velocities. Additionally, the CFD-predicted severe acceleration values were compared with experimental data from Sensor Fish studies. The median peak acceleration demonstrated a strong correlation, as indicated by Pearson's r = 0.975 and p = 0.14. The relatively high p-value was attributed to the smaller sample size in the analysis. However, with a larger sample size, the correlation coefficient (r = 0.975) would indicate an excellent relationship between the CFD-predicted and Sensor Fish values. Overall, the CFD-predicted severe acceleration exhibited reasonable and strong correlation with Sensor Fish measurements.

Table 2-18. Acceleration of the particle for collision lab testing.

Jet Velocity (fps) [m/s]	Plate Angle (°)	Number of Particles	Median of Peak Acceleration for Severe Events (g_0)		95th Percentile of Peak Acceleration for Severe Events (g_0)	
			CFD	SF	CFD	SF
40 [12.2]	20	400	100	154	143	207
50 [15.2]	20	400	145	160	212	258
60 [18.3]	20	400	209	183	280	229

Prediction of the Acceleration Events and Survival Rates

Following the procedure described in the Sensor Fish Methods Section 2.1.3.4 and further employed in HAHD, GPR and shear testing, the median and 95th percentile values of M_V for collision lab testing are presented in Table 2-19. It is important to note that the M_V value for each particle was based on the maximum value observed during primary collision events with the plate under non-submerged flow conditions. As expected, both median and 95 percentile value of M_V increases with increased jet velocity. Additionally, the CFD-predicted M_V values were compared to those obtained from Sensor Fish studies for median and 95 percentile range. The median M_V value demonstrated a strong correlation, with Pearson's r = 0.996 and p = 0.05.

Table 2-19. Particle strike metric (M_V) for collision lab testing.

Jet Velocity (fps)	Plate Angle (°)	Number of Particles	Median of Strike Metric (M_V) (m/s) – [fps]		95th Percentile of Strike Metric (M_V) (m/s) – [fps]	
			CFD	SF	CFD	SF
40	20	400	2.471 - [8.10]	1.65 - [5.41]	3.32 - [14.80]	2.19 - [7.19]
50	20	400	2.65 - [8.69]	2.02 - [6.63]	4.51 - [15.78]	2.65 - [8.69]
60	20	400	4.09 - [13.41]	2.71 - [8.89]	5.62 - [18.43]	3.37 - [11.06]

The cumulative distribution function plot of M_V for each jet velocity is shown in Figure 2-37. Furthermore, based on live coho salmon testing from collision experiments conducted in 2025 at a jet velocity of 50 fps and a 20° plate angle, the calibrated mortality threshold value of M_V was determined to be 4.45 m/s (indicated by the vertical dashed-dot line in Figure 2-37). Using this mortality threshold, the 48-hr survival rates at various jet velocities were predicted and are presented Table 2-20. For the other two jet velocities, survival rates were predicted to be 23% for 60 fps and 100% for 40 fps. Notably, at a jet velocity of 40 fps, all three methods—CFD simulations, Sensor Fish studies, and live fish testing—reported 100% survival. However, the prediction accuracy could be further enhanced with larger sample sizes, which would allow for testing across a broader range of jet velocities, plate angles, and experimental scenarios. Limited sample sizes may introduce variability and impact the precision of survival rate estimates.

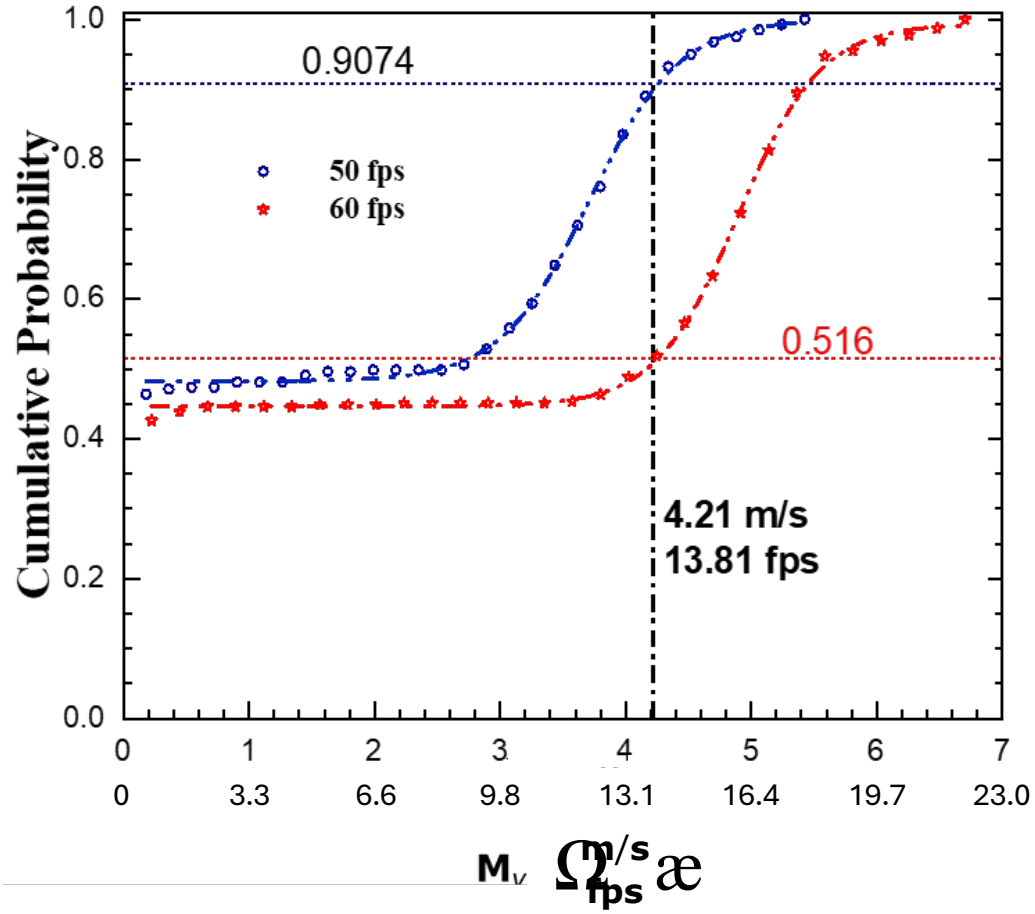

Figure 2-37. CFD-predicted cumulative exposure probabilities of M_V values during Collision Testing conducted at PNNL. The top horizontal blue dotted line represents coho salmon survival from laboratory experiments, while the vertical black dash-dot line indicates the CFD-predicted threshold value of M_V (4.45). The lower red dotted line represents the predicted survival probability based on the M_V threshold at the jet velocity of 60 fps.

Table 2-20. Comparison of CFD-predicted survival rates with Sensor Fish studies and live fish survival for collision lab testing.

Jet Velocity (fps) [m/s]	Plate Angle (°)	CFD-predicted survival rates (%)	Sensor Fish estimated survival rates (%)	Coho salmon 48-hr survival rates (%)
60 [18.3]	20	51.6	47.2	N/A
50 [15.2]	**20**	**90.7**	**90.7**	**90.7**
40 [12.2]	20	100	100	100

2.2.3 Integration of HBET and BioPA

PNNL has developed two similar methods for evaluating fish passage: the Biological Performance Assessment (BioPA) for CFD analysis (Richmond et al. 2014) and the Hydropower Biological

Evaluation Toolset (HBET) for Sensor Fish deployments (Hou et al. 2018). BioPA and HBET function similarly, generally by multiplying the probability of mortality at a given exposure level by the likelihood of that exposure occurring. With the new lab-derived biological response models (Sections 2.1.3.2 and 2.1.4.1), the models improve upon this method of application by allowing for detailed assessments tailored to specific fish length distributions, species coefficients, and balloon tag presence. This approach ensures a comprehensive evaluation of survival probabilities under varying conditions.

Previous biological response models predicted survival as a function of acceleration (g_0) when applied to Sensor Fish data or strain rate (s^{-1}) when applied to CFD data. Strike or collision events were based on acceleration for both CFD and Sensor Fish data. Additionally, previous biological response models applied within BioPA and HBET for strike/collision events were based on models designed to evaluate blade strike, which differed from the stationary boundary collisions more representative of HAHD and GPR conditions. This study was conducted to evaluate collision with a stationary boundary to better simulate the actual experiences of fish at these sites, addressing a critical gap identified in prior research and application of these models. This comparison aims to assess the consistency and accuracy of methods using data acquired from Sensor Fish or CFD simulations against the methods using live fish deployments in the field, specifically applying them to the tests conducted at HAHD and GPR.

2.2.3.1 Methods

The biological response models (Sections 2.2.1.1 and 2.2.2.1) estimate survival as a function of jet velocity. To convert these models to predict survival as a function of M_V for shear and collision, the Sensor Fish deployment in the laboratory study and the results from the CFD analysis of the lab study were used to develop a relationship to make this conversion (Table 2-21, Figure 2-38). These relationships vary depending on the stressor type (elevated shear or collision) and whether the Sensor Fish was equipped with balloon tags. The derived relationships, based on the previously shown exposure distributions, follow a quadratic form, providing a robust linkage between controlled laboratory conditions and field observations. This adjustment enhances the predictive accuracy of survival estimates by aligning laboratory-derived response models with the M_V metric.

Table 2-21. Quadratic equations used to convert jet velocity (V) to M_V for various testing conditions based off elevated shear and collision testing in the laboratory. NT = non-tagged; BT = balloon-tagged.

Data Method	M_V Condition	Equation
Sensor Fish and CFD	Collision NT	$M_V = 0.00074V^2$
	Shear NT	$M_V = 0.00128V^2$
Sensor Fish	Collision BT	$M_V = 0.00059V^2$
	Shear BT	$M_V = 0.00109V^2$

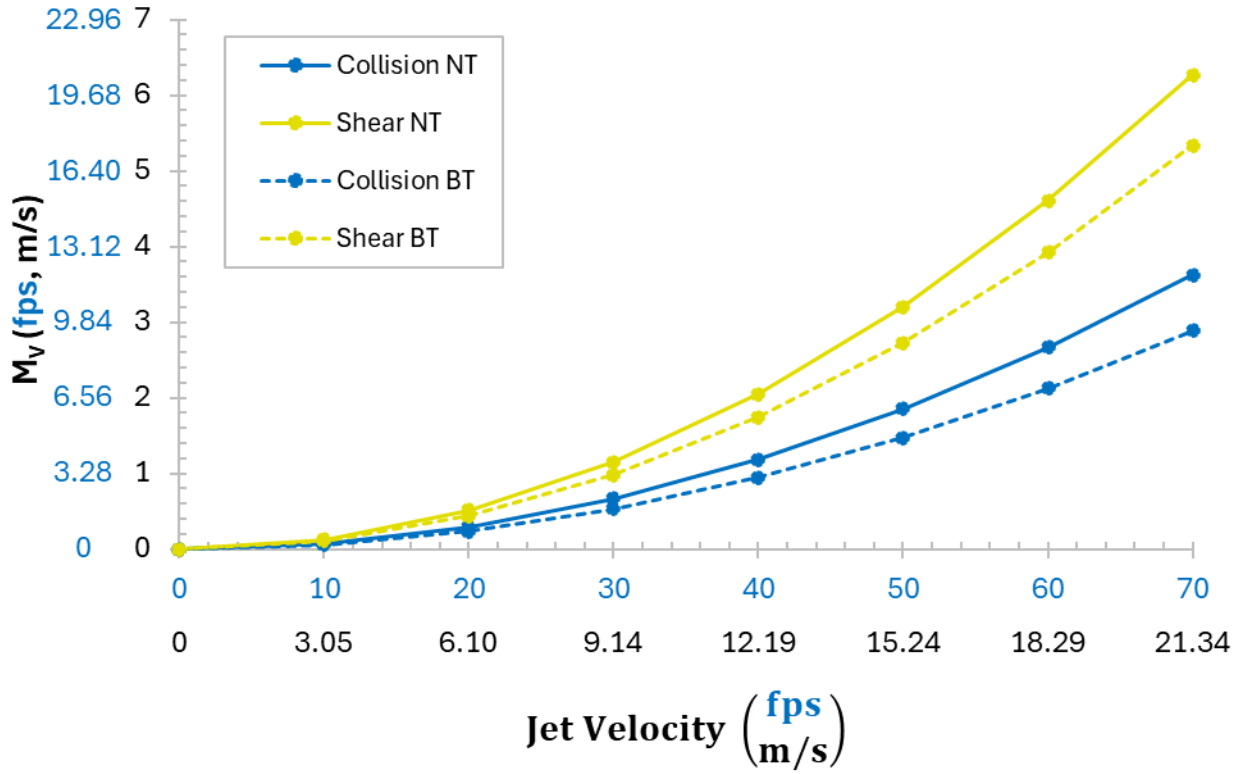

Figure 2-38. Graphical representation of the relationships between jet velocity and the various methods of measurements for elevated shear and collision events. Equations are displayed in Table 2-21. NT = non-tagged; BT = balloon-tagged.

The biological response models were systematically applied to field tests conducted at HAHD across multiple forebay elevations and flow treatments, as well as at GPR under varying operational scenarios. For HAHD, the models were calibrated using parameters for balloon-tagged coho salmon, mirroring the tagging protocol and fish length distribution used for each treatment during field deployments in February, April, and June 2024. Similarly, for GPR, the models were adjusted to assess non-tagged Chinook salmon, of fry and subyearling length distributions, to match the methods and parameters used during the field portion of the study.

3.0 Green Peter Dam: Direct Injury and Survival and Associated Hydraulic Conditions

The direct injury and survival and associated hydraulic conditions at Green Peter Dam (GPR) task was conducted at GPR, located on the South Santiam River in the Willamette Basin, Oregon. Green Peter Dam has a steep slope bypass pipe, and the 985 ft elevation fish horn (uppermost horn) was used for this task.

The objective was to assess direct immediate and 48-hr injury and survival of live fish and associated hydraulic conditions of the 985 ft horn at full flow under 17 ft of hydraulic head (i.e., the reservoir elevation was 1002 ft). Three age classes of Chinook salmon (fry, subyearling, and yearling) were intended to be used to assess fish injury and survival; however, the yearling Chinook salmon were diseased and could not be tested. Thus, only fry and subyearling Chinook salmon were evaluated. Live fish were tagged with PIT tags, and Sensor Fish were used to assess hydraulic conditions to estimate the following:

1. Hydraulic conditions and direct fish injury and mortality through the uppermost horn (985 ft el. pipe) of the bypass system.
2. Quantify strike severity using M_V metric and characterize each pipe region.
3. Characterize the acceleration events experienced throughout the bypass system.

3.1 Field Testing Methods

Live fish injury and survival assessments and Sensor Fish testing at GPR took place in May 2023. Chinook salmon of three age classes (fry, subyearling, and yearling) were obtained for the tests. Fry Chinook salmon were sourced from the Willamette Fish Hatchery (Oregon Department of Fish and Wildlife) in Oakridge, OR and the subyearling and yearling Chinook salmon were sourced from the Oregon State University's Wild Surrogate Fish Program facility in Corvallis, OR. However, the yearling Chinook salmon were diseased; thus, that age class was not tested.

3.1.1 Testing Conditions

Testing conditions of the juvenile steep slope bypass pipe were held constant over the testing period. The forebay reservoir elevation was 1002 feet above mean seal level (fmsl). The bypass horn pipe elevation was 985 fmsl, and the bypass flow control knife valve gate was 100% open.

The steep slope bypass exits at a juvenile fish collection facility located in the tailwaters of the dam, which contained a fish collection basket. The fish collection basket was comprised of a dewatering screen and a basket with metal grating on the sides. Additional sheets of perforated metal plate were attached to the sides of the basket to keep fish from escaping through the grating (Figure 3-1). Because fish could be recaptured in the juvenile fish collector, live fish and Sensor Fish did not need a balloon tag. Instead, only a PIT tag was implanted into fish for individual identification.

Figure 3-1. Multiple views of the juvenile collection basket at Green Peter. (A) A view of the juvenile collection basket out of water. (B) An aerial view of the juvenile fish collection basket in water, with the juvenile bypass pipe on the left flowing into the basket. The water is flowing out of the basket into the tailwaters on the right side of the picture.

3.1.2 Live Fish Tagging and Assessments

Tagging procedures for implanting PIT tags in fish were identical to methodology outlined in Section 2.1.3.2. After PIT tag implantation, fish were placed directly into a recovery bucket of fresh water, Then, the PIT tag ID was recorded and each individual fish was measured (mm fork length), weighed (g), assigned to a treatment or a control, and a pre-assessment of the fish was conducted (a body condition exam and photographs described in Appendix E). Once data was recorded, fish were returned to the recovery bucket.

Buckets of recovered test fish were placed into a holding tank supplied with flow-through water from the GPR forebay and allowed to further recover for a minimum of 30 minutes. These tanks were located in the tailrace of GPR. For treatment fish, buckets of fish were transported via a cart to the release site at the top of the dam. Control fish were also transported via a cart to the release site downstream of GPR.

The first post-release assessment evaluation of live fish occurred within 1-hr after recapture, and the second post-release assessment was conducted at approximately 48-hr after recapture. At each timepoint, fish were sedated (using the methods described in Section 2.1.3.2.) and assessed according to methods described in Appendix E. Afterwards, fish were transferred to holding tanks with flow-through water from GPR reservoir. Fish were euthanized in an overdose of MS-222 (250 mg/L) after the final 48-hr examination.

3.1.3 Release and Recapture

To release the fish, both the treatment and control sites comprised a basin with flow-through water connected to a 4-in flexible hose. The treatment release hose terminated near the intake of the

horn of the juvenile fish bypass pipe (approximately 9-in of separation from the exit of the release hose and the fish horn), so that released fish were immediately entrained into the horn and bypass pipe. The control release hose deposited fish into the bypass pipe just downstream of the underground exit. Once exiting the release hose, fish traveled a few meters along the open channel before passing over the perforated liner and into the collection basket in the juvenile fish collection facility (Figure 3-2). With each cohort of live fish, individually labeled Sensor Fish were also released to record data about hydraulic conditions.

Prior to release, each Sensor Fish was activated using a magnet, which initiated a five-second delay indicated by five LED blinks. After this delay, the Sensor Fish began recording data. Each unit was then tapped three times on the basin to generate three distinct acceleration magnitude signals, which served as a marker indicating that the Sensor Fish was about to be released into the release system. Sensor Fish deployed for the control releases followed the same activation and tapping procedure.

Immediately before treatment or control live fish or Sensor Fish were released, the fish collection basket was lowered to be below the exit of the bypass pipe. Approximately two minutes after the last individual live fish or Sensor Fish was released it was lifted out of the water. Live fish were netted out of the basket into buckets and transferred to staff for post-assessment. Sensor Fish were collected and deactivated with a magnet. The data was downloaded, and the Sensor Fish systems were reset before the next deployment. Sensor Fish data was analyzed throughout the testing period to evaluate sample quality and quantity of samples by testing condition.

Figure 3-2. The control release system at GPR. The hose on the left near the top of the blue release tank supplies flow-through water to the basin. Water is also supplied to the PVC Y-piece to provide constant flow through the release hose.

3.1.4 Live Fish Analyses

The data analysis and statistical methods for live fish injury and survival analysis described below are the same for all field live fish injury evaluations and survival analysis.

Injury assessment analyses used Fisher's exact tests to assess the occurrence of specific injuries to determine if there was a significant association between the groups (treatment vs. control) and the outcome (injury vs. no injury). A p-value of less than 0.05 was considered statistically significant, indicating that the observed results would be highly unlikely under the null hypothesis.

Survival estimates were conducted using the following statistical equations:

Passage survival (τ) was estimated as:

$$\tau = \frac{S_T}{S_C}$$

Where S_T is the survival of the treatment group, estimated as:

$$S_T = \frac{\left(\frac{a_T}{R_T}\right)}{\left(\frac{d_T + a_T}{R_T}\right)}$$

And S_C is the survival of the control group, estimated as:

$$S_C = \frac{\left(\frac{a_C}{R_C}\right)}{\left(\frac{d_C + a_C}{R_C}\right)}$$

Where a_T = the number of alive treatment fish,
R_T = the number of treatment fish released,
d_T = the number of dead treatment fish,
a_C = the number of alive control fish,
R_C = the number of control fish released, and
d_C = is the number of dead control fish.

The standard error of the passage survival estimate ($SE[\tau]$) was estimated as:

$$SE[\tau] = \left(\tau^2 \times \left(\left(\frac{\left(\frac{S_T(1-S_T)}{R_T}\right)}{{S_T}^2} \right) + \left(\frac{\left(\frac{S_C(1-S_C)}{R_C}\right)}{{S_C}^2} \right) \right) \right)^{1/2}$$

When survival of the control fish between 1 and 48-hr was greater than the survival of treatment fish, the 48-hr survival estimates of the treatment fish were greater than the 1-hr survival estimates. Because survival cannot increase from 1-hr to 48-hr (i.e, fish cannot come back to life), in these cases the 1-hr estimates were used for both 1 and 48-hr.

Fisher's exact tests were used to assess the occurrence of specific injuries to determine if there was a significant association between the groups (treatment vs. control) and the outcome (injury vs. no injury). A p-value of less than 0.05 was considered statistically significant, indicating that the observed results would be highly unlikely under the null hypothesis.

3.1.5 Sensor Fish Data Analyses

The Sensor Fish data analysis methods for GPR are the same as described in Section 2.1.3.4.

3.1.6 Computational Fluid Dynamics

The CFD data analyses methods are described in Appendix F.

3.2 GPR Field Testing Results

3.2.1 Live Fish Results

A total of 361 fry and 386 subyearling Chinook salmon were PIT-tagged at Green Peter for testing (Table 3-1). Of the tagged fish, 354 fry and 376 subyearling salmon successfully recovered from surgery and were released, supporting minimal mortality from tagging (<3%).

Table 3-1. General information about the fish sizes and release numbers for Chinook salmon released at GPR.

Life Stage	Fork length, mean and range (in)	Weight, mean and range (oz) [a]	Tagged (*n*)	Released alive (*n*)	Recovered after release (*n*)
Fry	2.20 (1.77–2.76) [b]	0.06 (0.02–0.13)[b]	361	354	278
Subyearling	3.15 (2.17–3.86) [c]	0.18 (0.05–0.35) [c]	386	376	340
Total	**–**	**–**	**747**	**730**	**618**

[a] The 0.002 oz weight of the PIT tag was not subtracted from the recorded weight of each fish as the tag weighed less than the precision of the scale.
[b] Excluding one tagged fish with missing length and weight measurements.
[c] Excluding four tagged fish with missing length and weight measurements.

Recovery rates of both fry and subyearling Chinook salmon were lower than expected for this study. Of the 354 PIT-tagged fry that were released, only 278 (78.5%) were recovered (Table 3-2). The 376 released subyearling Chinook salmon experienced a higher rate of recovery (90.4%; Table 3-2). However, it was expected that all released live fish would be recovered as there was a collection basket at the end of the release pipe. Additionally, previous fish injury studies at Green Peter recovered 100% of released fish at a similar size (41–70 mm FL steelhead), although different elevation pipes and gate openings were tested (Normandeau Associates, Inc. 2018).

Table 3-2. Recovery sample sizes and final disposition of fry and subyearling Chinook salmon released at GPR through 48-hr post-recollection.

Group	Cohort	Life Stage	
		Fry (*n*)	Subyearling (*n*)
Treatment	Released	179	190
	Recovered	145	176
	Alive after 1-hr	140	171
	Died within 1-hr	5	5
	Alive after 48-hr	136	140
	Died within 48-hr	9	36
Control	Released	175	186
	Recovered	133	164
	Alive after 1-hr	130	164
	Died within 1-hr	3	0
	Alive after 48-hr	124	131
	Died within 48-hr	9	33

During testing, it was observed that air pockets could form in the release system hose. The hose could become dislodged from one of the attachment points on the dam near the water surface, resulting in reduced water velocity. A combination of adding weights to the belly of the hose and keeping constant flow helped minimize the formation of air pockets. However, air pockets also formed in the release tank. To remedy this, water flow to the release hose was temporarily

reduced while the flow to the release tank was increased in order to allow the fish to be flushed out of the tank quickly.

The collection basket was also observed to have issues with keeping the small test fish contained. The basket was modified with smaller metal mesh on the side walls, and a cloth net was added to the top of the basket during testing to improve fish retention. However, these additions did not solve the containment problem. Additionally, the water velocity into the collection basket was fast, and when combined with a high volume of water with the 100% gate opening, led to observed turbulence in the basket for all released fish, regardless of treatment or control group. This turbulence may have contributed to injuries observed. Live fish injury results are detailed in Appendix E.

3.2.1.1 Survival

Survival estimates for both fry and subyearling Chinook salmon were greater after 48-hr than after 1-hr (Table 3-3). Therefore, the 1-hr survival estimates were used for analyses. Fish not recaptured by the juvenile collection basket after release were considered recaptured with an unknown fate because their final designation (survived/died) was unknown. Thus, they are not reflected in the survival analyses. It is important to consider that the fish used in this study were not depth acclimated prior to passage through the bypass facility. A fish's response to rapid decompression exposure is a function of acclimation pressure (a function of depth) and the lowest pressure (nadir) that they are exposed to during passage. The deeper fish are acclimated prior to passage increases the likelihood of barotrauma occurring and therefore these estimates may underestimate mortality due to barotrauma.

Table 3-3. Survival estimates for PIT-tagged Chinook salmon released at GPR in 2023 by life stage. The estimated standard error (SE) for each calculation is in parentheses.

	Passage Survival (SE)	
Life Stage	**Immediate (1-hr)**	**Overall (48-hr)**
Fry	0.988 (0.018)	0.988 (0.018)
Subyearling	0.972 (0.012)	0.972 (0.012)

3.2.2 Sensor Fish Results

This section provides an overview of Sensor Fish testing conducted at GPR under a forebay elevation of approximately 1002 ft, during which 261 valid treatment releases and 134 control releases were collected. Sensor Fish devices were calibrated prior to testing following PNNL's standard Sensor Fish operating procedures, confirming their pressure readings stayed within acceptable ranges from atmospheric pressure on the day of testing. Descriptions of the release pipe, 12-in pipe, 24-in pipe, and evaluator basin are provided to outline the physical conditions experienced by the Sensor Fish throughout the passage. Cumulative distribution functions and associated tables summarize the distribution of acceleration events and velocity-based strike metric M_V across regions of the passage system.

3.2.2.1 Treatments and Sample Sizes

During testing at GPR, the forebay reservoir elevation was approximately 1002 fmsl. A total of 261 valid datasets were acquired, alongside 134 control datasets (Table 3-4). The control Sensor Fish data was only used for checking the release pipe system and was not used for further analysis.

Table 3-4. Sensor Fish releases by study treatment at GPR.

Year	Average Forebay Reservoir Elevation (ft)	Bypass Pipe Elevation (ft)	Gate Valve Opening (%)	Valid Treatment Releases (*n*)	Valid Control Releases (*n*)
2023	1002	985	100	261	134

3.2.2.2 Timing Marks

The fish bypass passage system is divided into two regions, namely, the horizontal 12-in pipe region (that passes through the dam) and the 24-in steep slope pipe region on the downstream face of the dam (Figure 3-3).

- Release pipe (T0-T1): The beginning of this region is characterized by a rise in hydrostatic pressure as the Sensor Fish descends through the water column. An instantaneous pressure drop, indicative of the Venturi effect (i.e., where the water speeds up as it passes through a constricted section), marks the outlet of the release pipe.
- 12-in pipe (T1-T2): An instantaneous pressure drop, indicative of the change in flow conditions from the reservoir to the pipe, marks the 12-in pipe region, where the flow is pressurized. This is verified with CFD results.
- 24-in pipe (T2-T3): The pressure returns to near-atmospheric levels at the entrance to this region, subsequently resulting in increased rotational and acceleration magnitudes, followed by fluctuations in pressure readings. The traveling time during this region is approximately 16 seconds.
- Evaluator/Collection Basin: Acceleration, rotational velocity spikes, and pressure fluctuations are typical upon entry into the evaluator, as the Sensor Fish collides with the metal screens, which could potentially lead to fish injuries.

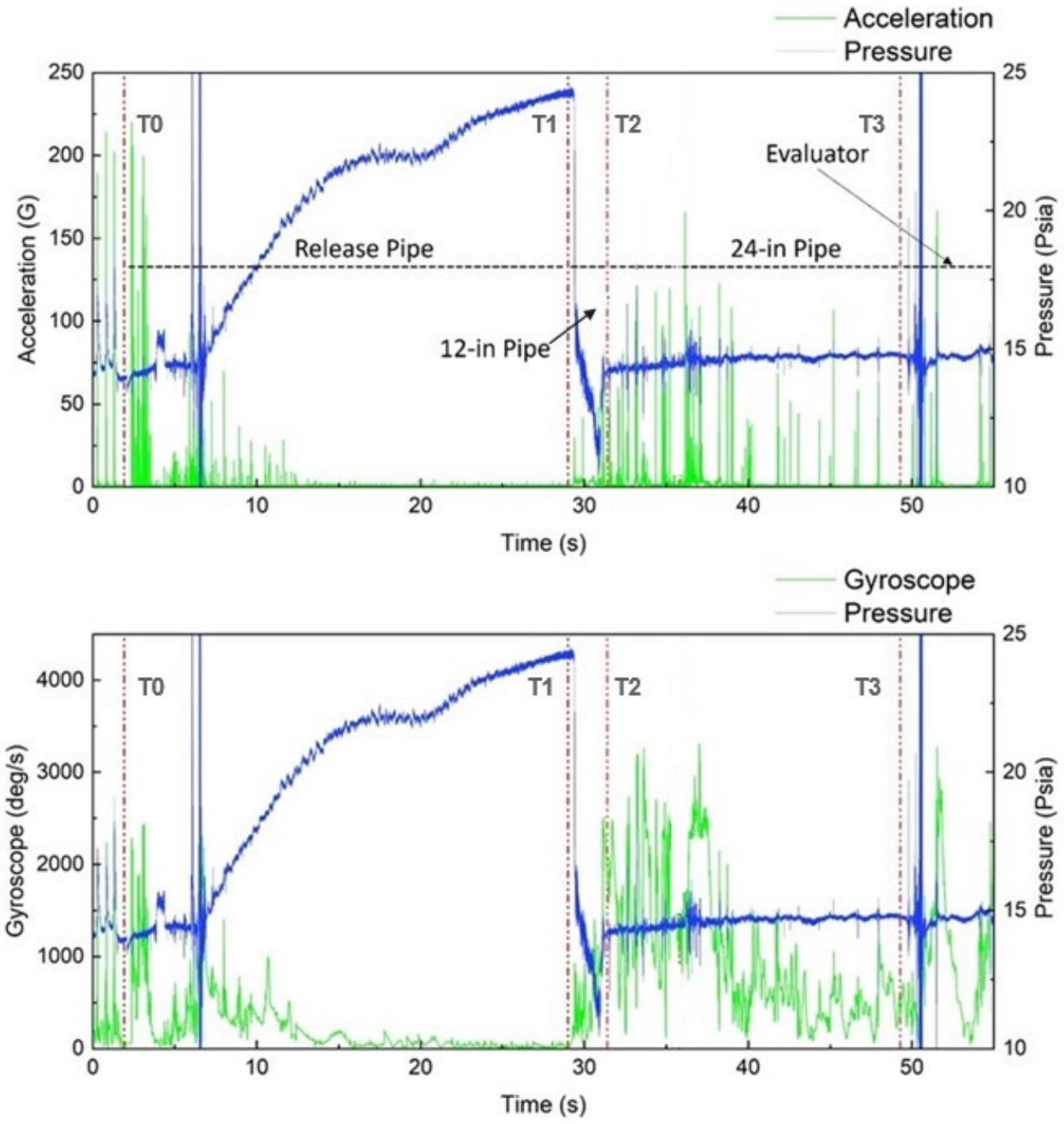

Figure 3-3. Representative passage data collected by a treatment-released Sensor Fish at GPR.

3.2.2.3 Severe Acceleration Events

The mean values of the maximum accelerations were 101 g_0 for the 12-in pipe and 193 g_0 for the 24-in pipe (Table 3-5). Moreover, the percentages of Sensor Fish releases at GPR experiencing severe acceleration events while passing through 12-in and 24-in pipes were 46.0% and 100%, respectively. The results indicate that the 24-in pipe region is more likely to cause fish injury due to higher magnitudes and frequencies of severe acceleration events. In addition, most of the severe events were attributed to strikes. Only one mild shear event with a low shear M_V value of 3.07 m/s was observed within the 24-in pipe region of GPR. As pressure exposure is not

considered a significant factor for fish mortality, we include only metrics based on acceleration events. Further analysis with pressure values is included in Appendix H.2. Figure 3-4 shows the distribution of the maximum acceleration event of the releases for the overall region at GPR.

Table 3-5. Severe acceleration events of Sensor Fish releases per treatment at GPR.

Average Forebay Reservoir Elevation (ft)	Bypass Pipe Elevation (ft)	Gate Valve Opening (%)	Valid Treatment Releases (*n*)	Mean Values of Maximum Accelerations (g_0)		Sensor Fish Releases with Severe Events (%; ≥ 95 g_0)		
				12-in pipe	24-in pipe	12-in pipe	24-in pipe	Overall
1002	985	100	261	101	193	46.0	100.0	100.0

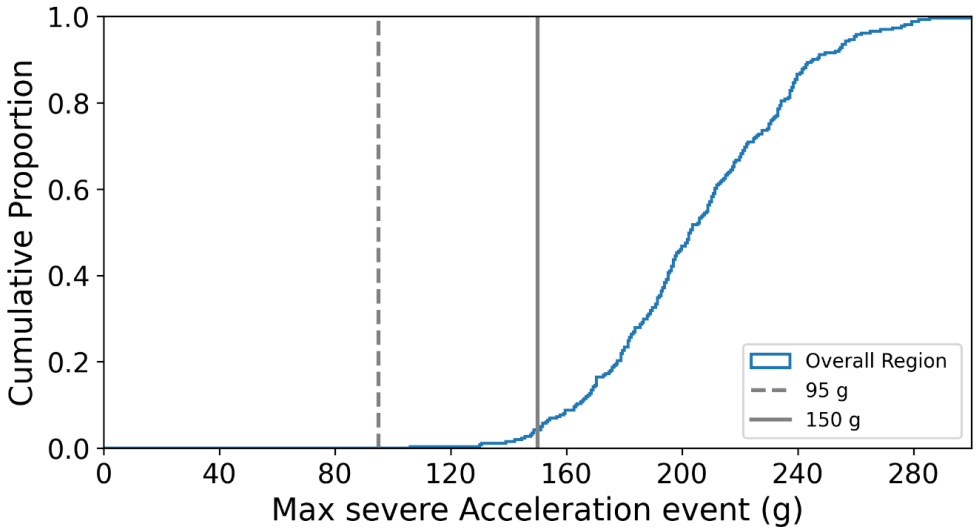

Figure 3-4. Cumulative distribution of Max severe acceleration events for GPR fish passage.

3.2.2.4 Survival Rates Estimated from Strike Metrics

Following the procedure described in Section 3.1.5, the mean and 95th percentile values of M_V for each hydraulic region of the tunnel passage (i.e., 12-in and 24-in pipe regions) are shown in Table 3-6. Results show that the 24-in pipe region yielded higher M_V values, which indicates higher severity of strikes/collisions. Moreover, according to the collision lab testing for both Sensor Fish and live fish (coho salmon) in 2025, the calibrated mortal threshold of M_V was found to be 2.63 m/s. More specifically, this value was calibrated from a total of 46 Sensor Fish samples, with a jet velocity at 50 fps and a 20° angle plate. A total of 60 live fish releases were used for this calibration. In addition, considering the similar flow conditions between steep pipe flow at GPR and the spillway flow, another mortal threshold of M_V was found to be 4.25 m/s based on the Sensor Fish and live fish (Chinook salmon) tests conducted at the removable spillway weir of Ice Habor Dam in 2015 (Duncan et al. 2018). Thus, throughout this report two different M_V values will be shown, 2.63 m/s from lab testing, and 4.25 m/s from Ice Harbor Dam study (Appendix I).

Table 3-6. Values of Sensor Fish strike metric (M_V) for each pipe region at GPR.

Average Forebay Reservoir Elevation (ft)	Bypass Pipe Elevation (ft)	Gate Valve Opening (%)	Valid Treatment Releases (*n*)	Mean Values of M_V (m/s) –[fps]		95th Percentile of M_V (m/s) – [fps]	
				12-in pipe	24-in pipe	12-in pipe	24-in pipe
1002	985	100	261	0.46 - [1.51]	1.68 - [5.51]	1.40 - [4.59]	3.03 - [9.94]

The cumulative distribution function curves of M_V for each pipe region are shown in Figure 3-5, and the estimated 48-hr survival rates are shown in Table 3-7. Results show that all the M_V values that occurred in the 12-in pipe region were lower than the mortal thresholds of 2.63 m/s and 4.25 m/s, and hence the estimated 48-hr survival rate for this region was 100%. However, the 24-in pipe region would cause fish injuries and mortalities, as it yields a 48-hr survival estimate percentage of 91.23 and 98.37 under the 2.63 m/s and 4.25 m/s M_V thresholds, respectively. Moreover, as indicated by Figure 3-6, about 80% of mortal collision events occurred in the bend region (middle region).

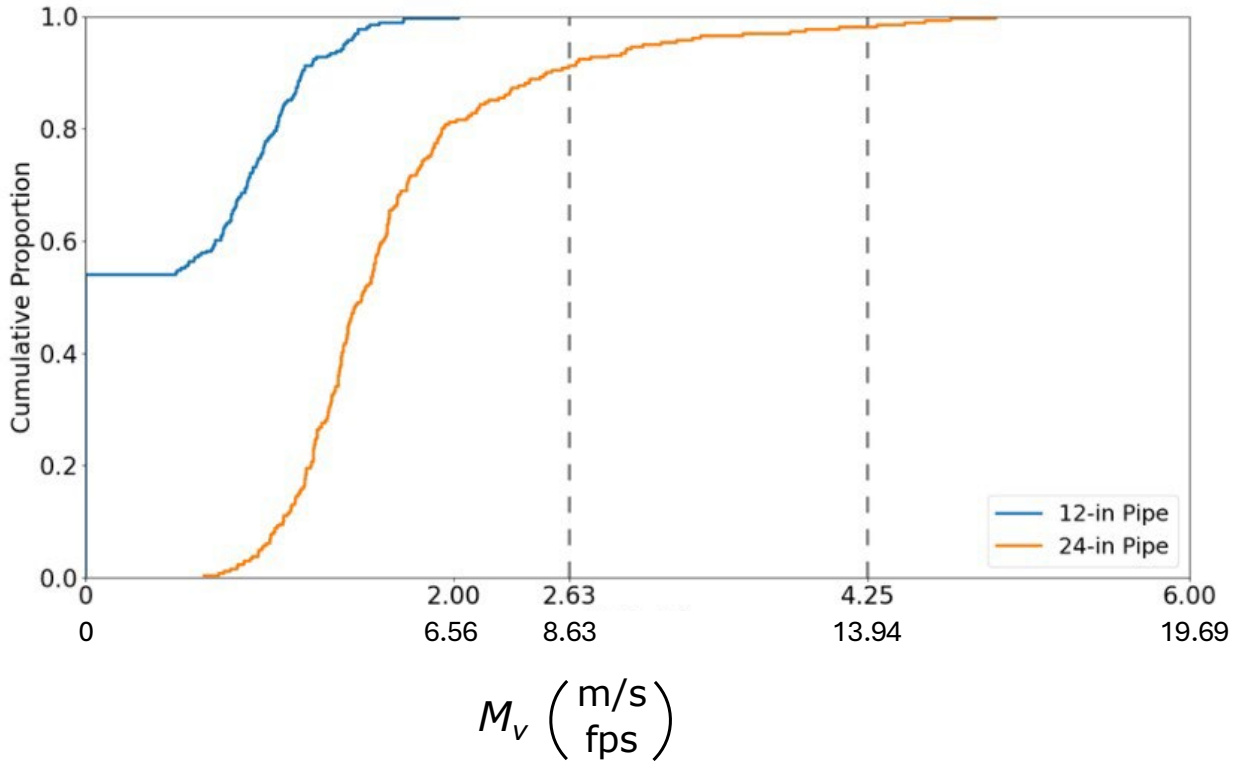

Figure 3-5. Applications of M_V for different pipe regions of GPR fish passage. The dotted gray lines represent mortality thresholds derived from two independent studies: a threshold of 2.63 calibrated from collision laboratory testing conducted in 2025 using coho salmon, and a threshold calibrated from Ice Harbor Spillway field testing conducted in 2015 using yearling Chinook salmon.

Table 3-7. Survival percentages at 48-hr estimated from different Sensor Fish strike metrics (M_V) at GPR.

Average Forebay Reservoir Elevation (ft)	Bypass Pipe Elevation (ft)	Gate Valve Opening (%)	Valid Treatment Releases (*n*)	48-hr Survival with Mortal Threshold of 2.63 m/s – [8.63 fps] (%)		48-hr Survival with Mortal Threshold of 4.25 m/s – [13.94 fps] (%)	
				12-in pipe	24-in pipe	12-in pipe	24-in pipe
1002	985	100	261	100.0	91.23	100.0	98.37

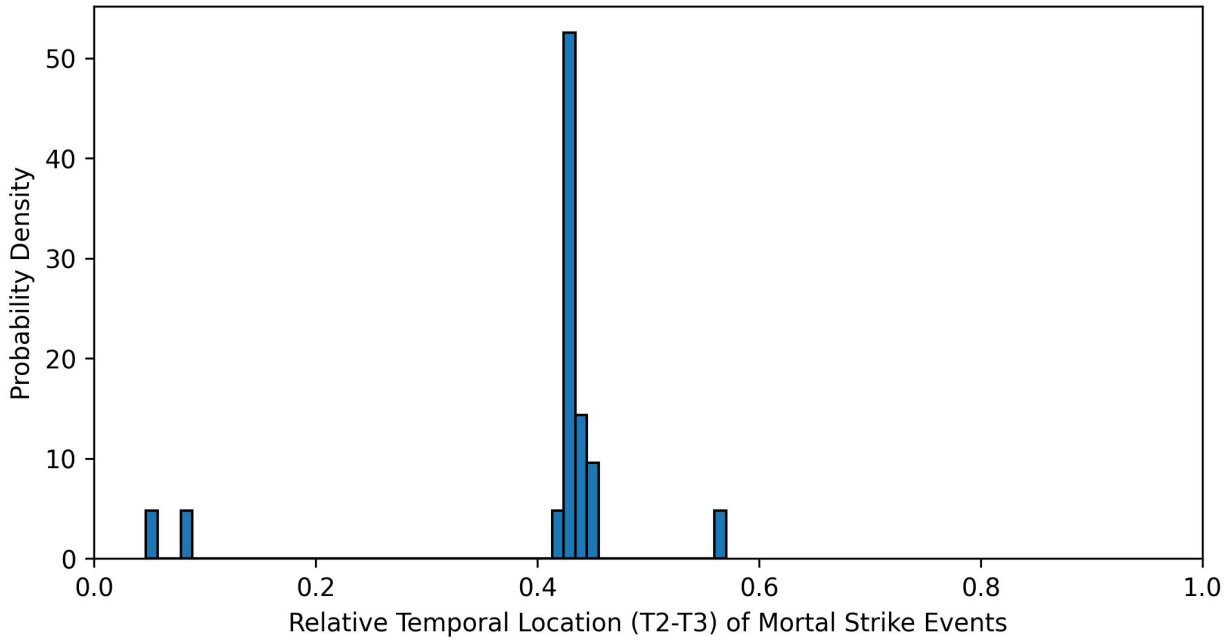

Figure 3-6. Histogram of relative temporal locations of mortal strike events (M_V ≥ 2.63 m/s) for 24-in pipe region (T2-T3) at GPR.

3.2.3 CFD-particle Modeling Results

The BioPA CFD modeling for GPR used the BioPA toolset, developed by PNNL, to estimate the hydraulic environment of the FPF design using CFD model results.

The objective was for PNNL to develop baseline CFD models of the GPR bypass pipe. The BioPA toolset (Singh et al. 2021) was then applied to the analysis, and the documentation would serve as a basis for a tutorial of steps used in development. The BioPA toolset was also used to review the Corps' CFD model outputs and provide feedback on the format of the CFD models and results. This enabled the Corps to utilize BioPA for future designs or examine differing flow cases for existing designs.

3.2.3.1 Simulation Framework and Particle Release

In line with the field study conducted using Sensor Fish and live fish at GPR, the CFD-particle simulations were conducted to investigate the hydraulic conditions. The VOF flow simulations were conducted for a sufficient duration to achieve the flow pseudo-steady state in terms of discharge rate and free surface of water as described in Section 3.1.6. The particle flow simulations were then conducted using DEM method. The forebay reservoir elevation and bypass pipes elevation were approximately 1002 ft and 985 ft respectively, to be consistent with the live fish and Sensor Fish field deployments. A total of 600 cylindrical particles having the same design and dimensions and density of the sensor fish was released from the outlet of 4" flexible hose. For efficient particle simulations, the parcel-depletion scheme was used where particles were automatically deleted upon the prescribed domain of interest. The CFD-particle simulations were performed until all particles left the exit of the bypass pipe. The particles data was only used for checking the release pipe system and collector region was excluded in further analysis.

3.2.3.2 Comparison of the Pressure Distribution with the Sensor Fish Field Study

Similar to the CFD simulations conducted for HAHD (Appendix F), the CFD-predicted absolute pressure histories for streamline and particle trajectories were plotted and compared with Sensor Fish data in Figure 3-7. The comparison shows consistent trends and results aligning well. Initially, the hydrostatic pressure observed across streamlines, particle trajectories, and Sensor Fish measurements was approximately 22 psia. Following this, a notable drop in hydrostatic pressure below atmospheric levels occurred in the middle of the 12-in pipe, which then gradually rose to atmospheric pressure at the exit of the 12-in pipe, stabilizing at 14.7 psia due to the atmospheric conditions at the top of the 24-in pipe. Note that the top of 24-in pipe is exposed to air. Additionally, three pressure spikes were observed in all three cases. These spikes correspond to the junction of the lower three 12-in pipes (shown in Figure 3-8), where the upstream valve was completely closed, resulting in an absence of water flow within those pipes. A particle/sensor fish may also collide with wall at that location. Another slight pressure bump was identified in the bend region of the 24-in pipe, where the presence of a hydraulic jump is likely. In this region, the horizontal contributes to flow deceleration, leading to the pressure increase there. Overall, the absolute pressure profiles obtained from Sensor Fish measurements, CFD-predicted streamlines, and particle trajectories exhibit close agreement in terms of both the timing and magnitude of pressure fluctuations.

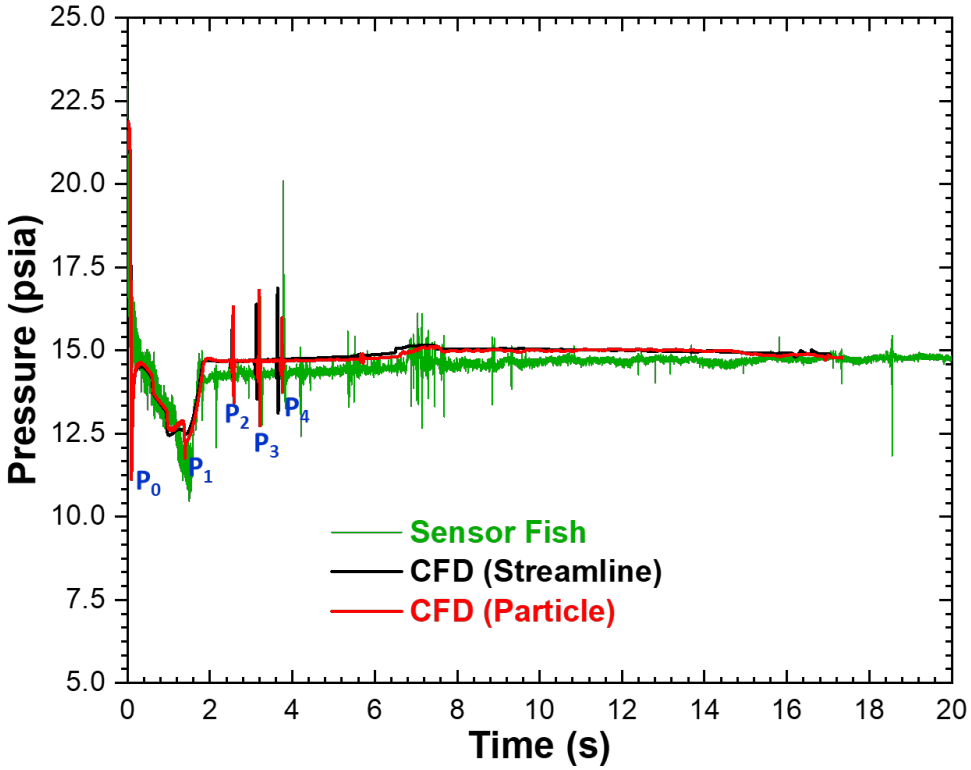

Figure 3-7. Comparison of the CFD-predicted pressure using streamline and cylindrical particles with field data using Sensor Fish for GPR. Results for CFD prediction and Sensor Fish studies match well for pressure and location of lowest pressure.

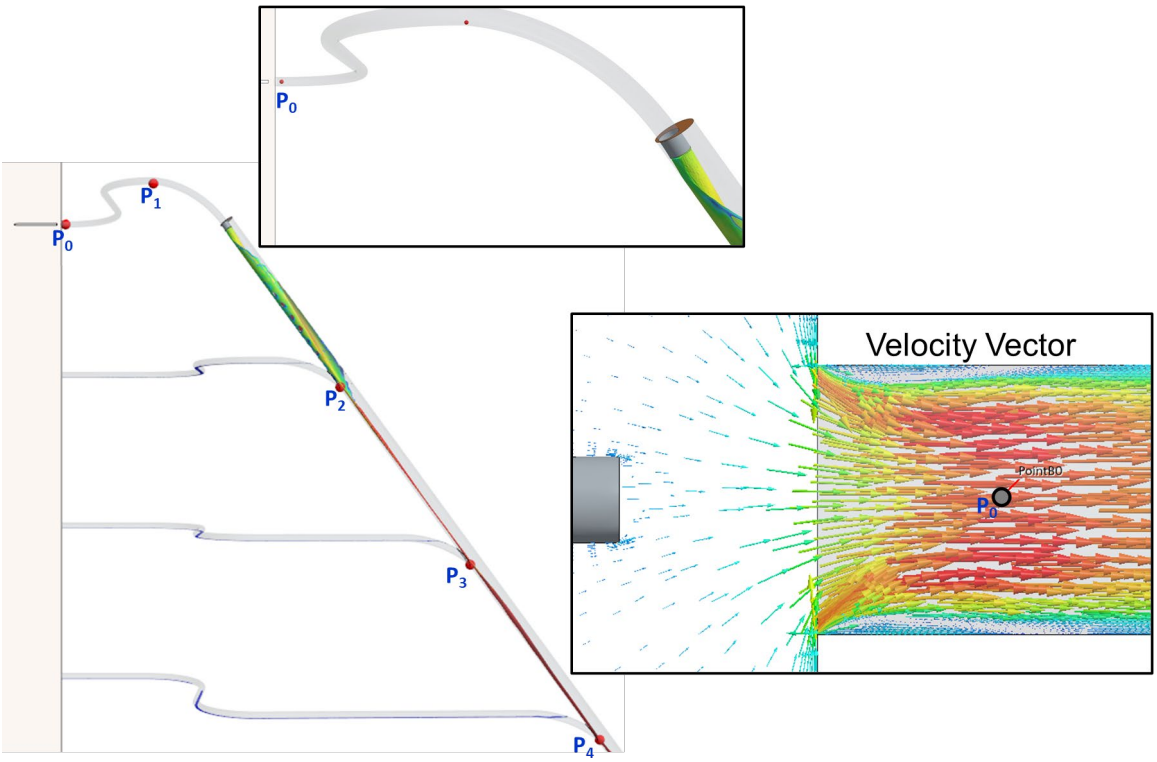

Figure 3-8. The locations of points (P) representing the pressure fluctuation in the bypass pipe for GPR. Both CFD simulations and Sensor Fish studies show pressure fluctuation at these locations. The exploded view at the top inset shows the presence of nadir pressure point P_0 in CFD simulations, which is attributed to the sharp edge at the inlet of the 12-in pipe and the forebay wall. The vector plot in the bottom-right inset depicts the formation of a vena-contracta near the wall, resulting in the nadir pressure in close proximity to the forebay wall.

3.2.3.3 Nadir Pressure Event

Nadir pressure is a critical stressor that can lead to barotrauma injuries in fish, especially acclimated species. As shown in Figure 3-7 and Figure 3-8, a single cylindrical particle experiences pressure lower than atmospheric pressure at multiple locations in the high-head bypass pipe within the GPR system, particularly in the 12-in pipe and at the junction of the 12-in and 24-in pipes. The reduced pressure at point P_0 in Figure 3-8 is an artifact of sharp edge boundary where the 12-in pipe connects to the upstream wall. This sharp edge creates vena-contracta, resulting in lower pressure within the 12-in pipe. However, in the existing GPR design, a diffuser is used to connect the valve with 12-in pipe, facilitating a smooth flow entrance to the 12-in pipe. Therefore, the pressure readings at point P_0 were excluded when sampling nadir pressure for 600 cylindrical particles. Figure 3-9 shows the cumulative exposure distribution of nadir pressure within the GPR system. The lowest CFD predicted nadir pressure was found to be 8.75 psia, which closely aligns with field studies conducted using Sensor Fish, where the lowest nadir pressure was approximately 9 psia. This consistency between CFD simulations and field data reinforces the reliability of the CFD predictions in assessing barotrauma risk under operating conditions. Under the current operating conditions, surface-acclimated fish are unlikely to experience barotrauma injuries, but a portion of deeper depth acclimated fish may be exposed to pressure decompressions that could cause injury and mortality.

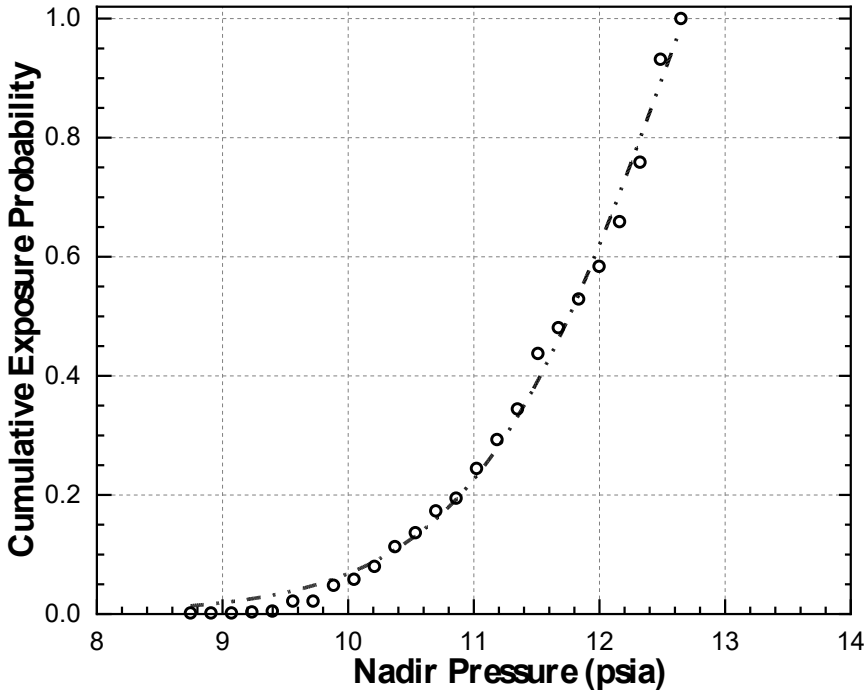

Figure 3-9. The cumulative exposure probability of CFD-predicted Nadir Pressure for high head fish bypass pipe for GPR.

3.2.3.4 CFD-predicted Severe Acceleration Events

Similar to the Sesnsor Fish studies, severe accelaration events were computed for each section of the bypass pipeline for all particles. However, the results for severe events are only presented for 12-in and 24-in pipe. Table 3-8 presents that the mean values of the maximum accelerations, and shows they were 101 g_0 for the 12-in pipe and 193 g_0 for the 24-in pipe. Moreover, predcted Sensor Fish releases at GPR experiencing severe acceleration events while passing through 12-in and 24-in pipes were 5.32% and 100%, respectively. The results indicate that the 24-in pipe region is more likely to cause fish injury due to higher magnitudes and frequencies of severe acceleration events. In addition, most of the severe events were attributed to strikes.

Table 3-8. CFD-predicted severe acceleration events (≥ 95 g_0) and particle strike metric (M_V) for GPR.

Average Forebay Reservoir Elevation (ft)	Bypass Pipe Elevation (ft)	Gate Valve Opening (%)	Number of Particles (n)	95th Percentile of M_V (m/s) – [fps]		Particles with Severe Events (%; ≥ 95 g_0)	
				12-in pipe	24-in pipe	12-in pipe	24-in pipe
1002	985	100	601	1.50 - [4.92]	3.65 - [11.98]	1.67	100

3.2.3.5 CFD-predicted Survival Rates Estimated from Strike Metrics

Using the method outlined for Sensor Fish studies in Section 2.1.6, the M_V value was calculated for each particle within different regions of the bypass pipelines. As previously noted, the flow environment at the GPR differs slightly from that at the HAHD, potentially leading to higher rebound velocities for particles. In field studies, strikes involving live fish and Sensor Fish often behave as real-world inelastic collisions. Under such conditions, particles rebound with a lower velocity than the velocity of strike. To implement this physics in the simulation, the coefficient of normal restitution (NCR) in the discrete element method (DEM) setup was iteratively reduced to model idealized inelastic collisions. The coefficient of normal restitution specifically quantifies the ratio of the relative velocity of separation to the relative velocity of approach before and after an impact in normal direction. The cumulative probability distribution of M_V was subsequently calculated and compared to the Sensor Fish studies for 12-in and 24-in pipes. Figure 3-10 presents the comparison of cumulative exposure probabilities of M_V for the 24-in pipe. In this figure, the horizontal blue dotted line indicates 95% fish survival, while the vertical green and red dashed lines represent M_V threshold values derived from Sensor Fish experiments and CFD simulations, respectively. As expected, the 95th percentile values of M_V decrease with lower NCR values, with the trends of both plots converging. This behavior can likely be attributed to the shallow water with high velocity present in the 24-in pipeline (Figure 3-10), which allows particles to rebound with increased velocities in air at higher NCR values. At NCR value of 0.10, the variation in the cumulative exposure probability of M_V follows a similar trend, although the CFD-predicted M_V values remain higher compared to those obtained from Sensor Fish experiments.

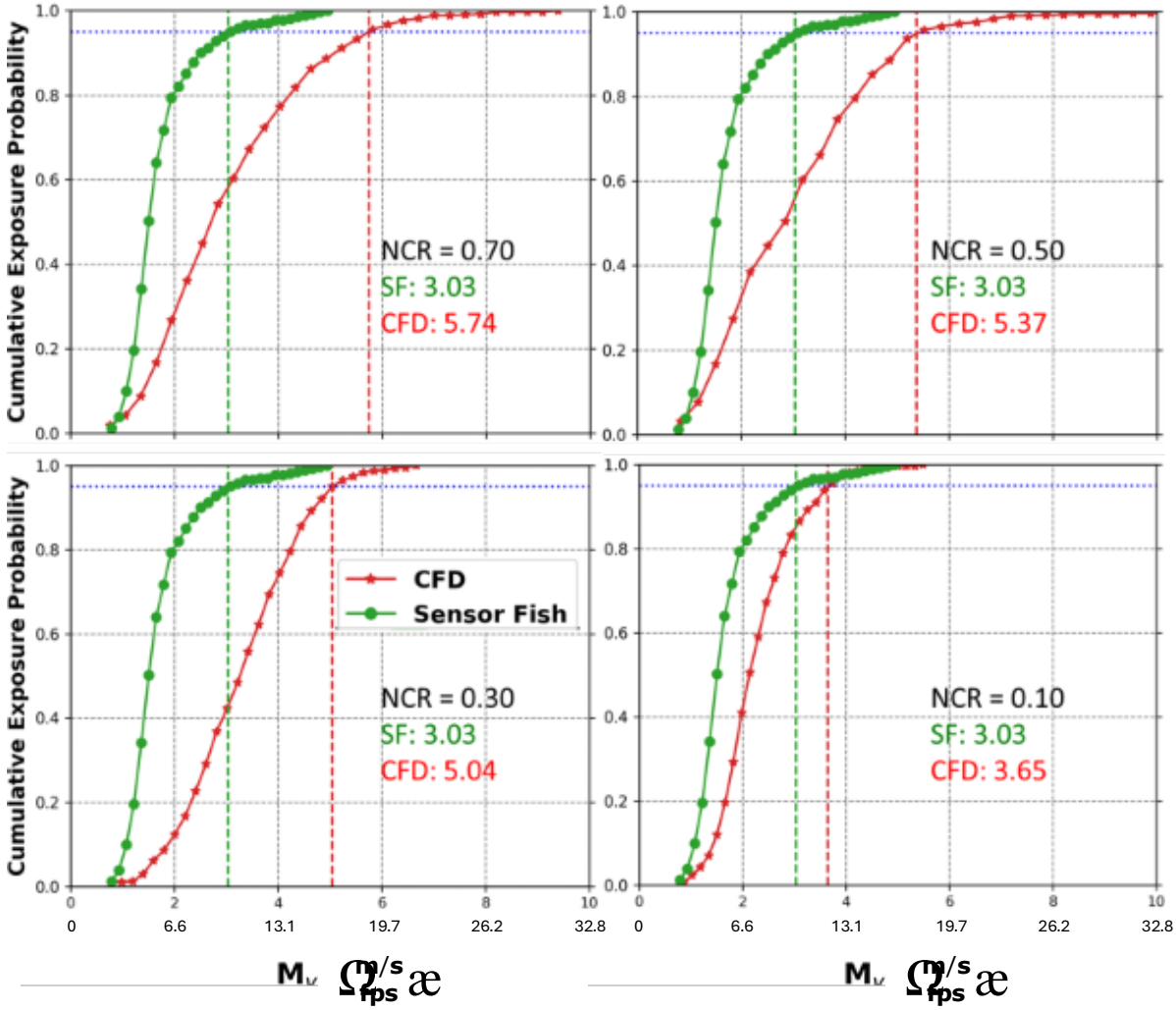

Figure 3-10. Comparison of CFD-predicted and Sensor Fish-estimated cumulative exposure probabilities for M_V at GPR in 24-in pipe at different NCR values. The horizontal blue dotted line represents 95% fish survival, while the vertical green and red dashed lines represent the threshold values of M_V obtained from Sensor Fish experiments and CFD simulations, respectively. The legend shows the M_V value in metric units.

The comparison of the cumulative exposure probability of M_V for a 12-in pipe are shown in Figure 3-11. As expected, the 95th percentile values of M_V decrease with decreasing NCR values. The observed variation in the exposure plots follows a distinct trend for CFD and sensor fish studies. In the CFD simulations, M_V was calculated for all particles, regardless of whether their acceleration exceeded 95 g_0. In contrast, the Sensor Fish study considered only severe events, specifically instances where acceleration was greater than 95 g_0. Consequently, the Sensor Fish exposure probability began at 56%, while the CFD-predicted M_V values started at 0%. Further, the impact of NCR became negligible beyond a value of 0.30. This phenomenon may be attributed to the submerged motion of particles (as shown in the inset of Figure 3-11) and their collisions with the pipe walls. In submerged conditions, particle movements slow rapidly after collisions due to momentum dissipation caused by the higher drag exerted by water. At NCR = 0.10, the M_V values predicted by CFD (1.50) were found to be in close agreement with the corresponding value

(1.40) derived from Sensor Fish studies. As a result, the CFD simulation conducted at NCR value of 0.10 was used for predicting fish survival.

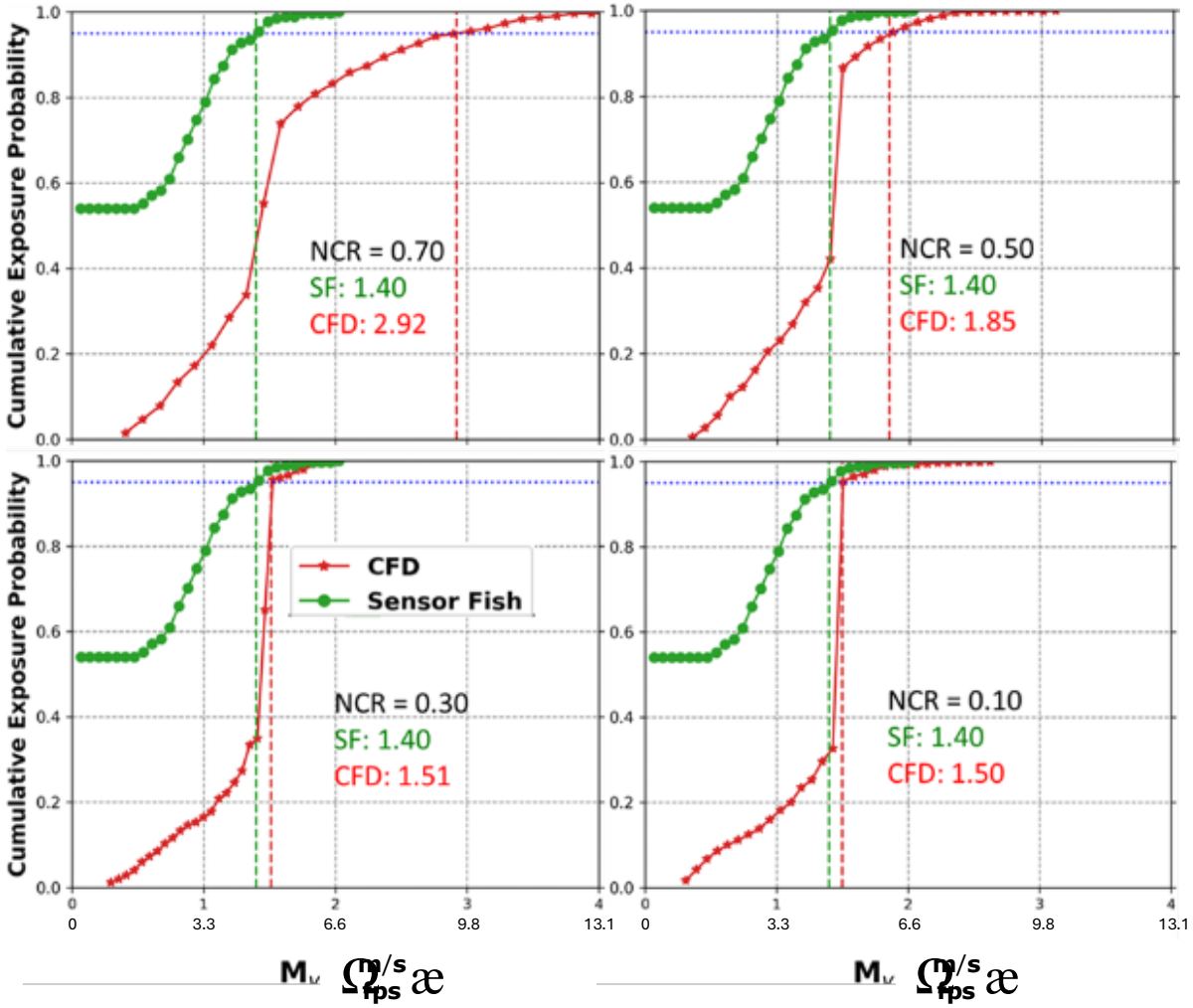

Figure 3-11. Comparison of CFD-predicted and Sensor Fish-estimated cumulative exposure probabilities for M_V at GPR in 12-in pipe at different NCR values. The horizontal blue dotted line represents 95% fish survival, while the vertical green and red dashed lines represent the threshold values of M_V obtained from Sensor Fish experiments and CFD simulations, respectively. The legend shows M_V value in metric units.

The 95th percentile values of M_V for each region of the bypass passage (i.e., 12-in and 24-in pipes) are shown in Figure 3-12. The 24-in pipe shows higher M_V values, which indicates higher severity due to strikes/collisions. Results indicate that the 24-in pipe exhibited higher M_V values, signifying greater severity due to strikes and collisions. This increased severity could be attributed to higher flow acceleration caused by the steep slope of the 24-in pipe, which results in elevated water velocities. Additionally, the shallow, high-velocity flow conditions in the 24-in pipe (Figure 3-12) exacerbate collisions and particle-wall interactions such as dragging, and high-intensity bouncing of particles off the pipe walls.

In laboratory testing for unsubmerged jet collision designed to replicate flow field conditions at the GPR, idealized collisions of Sensor Fish and live fish (coho salmon) under unsubmerged jet flow conditions established a mortal threshold of 4.45 m/s. Further comparisons of the CFD-predicted exposure probability of M_V with the Sensor Fish studies are presented in Table 3-9. Moreover, similar flow conditions between the steep pipeline flow at GPR and the spillway flow were observed. Based on Sensor Fish and live fish (Chinook salmon) testing conducted at the removable spillway weir of Ice Harbor Dam in 2015 (Duncan et al., 2018), another mortal threshold for M_V was identified as 4.25 m/s. The cumulative distribution function (CDF) curves of M_V predicted by CFD and calculated through Sensor Fish studies for the 24-in pipe are shown in Figure 3-12, while the corresponding estimated 48-hr survival rates are summarized in Table 3-9. Results indicate that all M_V values in the 12-in pipe were below the mortal threshold, ensuring an estimated 100% survival rate within this region; consequently, exposure plots for this region were not presented for sake of brevity. However, in the 24-in pipe—particularly within the bend region—poses significant risks for fish injuries and mortalities.

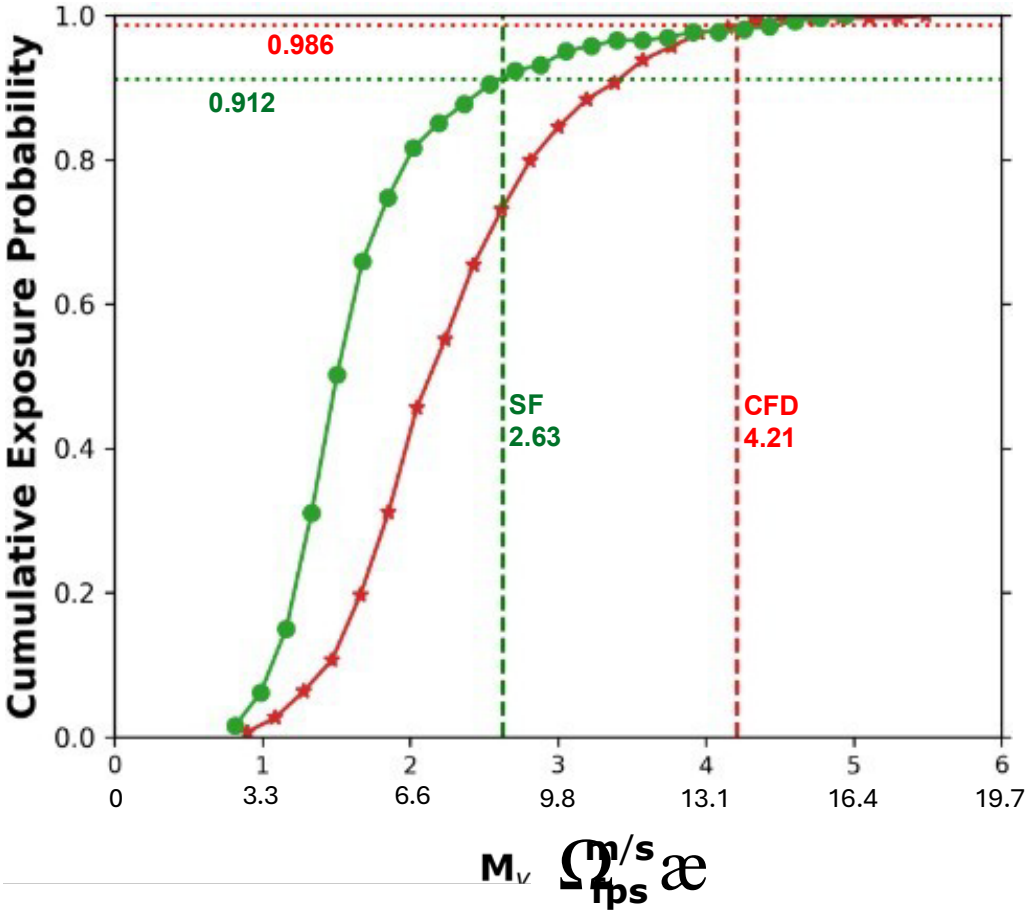

Figure 3-12. Comparison of CFD-predicted and Sensor Fish-estimated cumulative exposure probabilities for M_V at GPR. The vertical green and red dashed lines represent the threshold values of M_V obtained from Sensor Fish experiments and CFD simulations, respectively. The horizontal red and green dotted lines indicate the corresponding survival rates of Coho salmon observed in the CFD simulations and Sensor Fish studies, respectively. M_V value in the plot are in metric unit.

Table 3-9. Survival percentages at 48-hr at GPR, estimated from laboratory collision strike metrics (M_V).

Average Forebay Reservoir Elevation (ft)	Bypass Pipe Elevation (ft)	Gate Valve Opening (%)	Number of Particles (*n*)	48-hr Survival with Mortal Threshold of 4.21 m/s – [13.81 fps] (%)		
				12-in pipe	24-in pipe	Overall
1002	985	100	600	100.0	98.60	98.60

4.0 Howard A. Hanson Dam: Direct Injury and Survival and Associated Hydraulic Conditions

The objective of the Direct Injury and Survival and Associated Hydraulic Conditions at HAHD task was to assess direct immediate (with 1-hr) and 48-hr injury and survival of live fish and associated hydraulic conditions of the HAHD radial flow control gate and horseshoe tunnel. However, after an evaluation of the survival estimate data, immediate survival provided a better estimate of survival than 48-hr survival due to the confounding issues with the 48-hr survival estimates (i.e., greater than 100% survival and fish condition issues).

Coho salmon and Chinook salmon were used for this task at various juvenile life stages to assess fish injury and survival, and Sensor Fish were used to assess hydraulic conditions. Live fish and Sensor Fish were tagged with balloon tags to inform the following questions:

1. At what depth/discharge does 2% mortality occur associated with the radial gate?
2. At what depth/discharge does 2% mortality occur associated with the outlet tunnel?
3. What are the pressure changes, accelerations, and duration of passage associated with the existing project configuration?

Three hydrostatic head conditions and three flow conditions (regulated by the tunnel entrance radial gate) were tested; however, reservoir refill, pool elevation, Corps Water Management, and river flows determined the final set of head and flow conditions that were evaluated during testing.

The proposed hydrostatic head conditions were:

1. Less than 50 ft of head
2. 50 – 100 ft of head
3. Greater than 100 ft of head

The proposed flow condition categories were:

1. *Low*: 600 cfs or less
2. *Medium*: 600 –1,200 cfs
3. *High*: 1,200 cfs or more

For the CFD modeling, the objective was for PNNL to develop a baseline CFD-particle simulation framework for the existing HAHD tunnel. The CFD simulation data will be used to sample hydraulic stressors associated with fish mortality and survival within the HAHD tunnel. The BioPA toolset (Singh et al., 2021) was applied to the analysis, and the documentation serves as a tutorial outlining the steps involved in the framework's development.

CFD simulations were conducted for the same cases as the field studies described above. Results of these simulations will be compared to data obtained from Sensor Fish field studies, enabling translation of Sensor Fish thresholds into CFD simulations. The translated threshold can then be integrated into the BioPA framework, facilitating predictions of fish survival in New proposed HAHD designs.

4.1 Field Testing Methods

Field testing for the HAHD task was conducted in spring 2023 (April and June) and in winter and spring 2024 (February, April, and June). Field testing at HAHD targeted nine conditions: three hydrostatic head categories (≤50 ft, 50–100 ft, >100 ft) and three flow conditions (≤600 cfs, 600–1200 cfs, >1200 cfs). Five conditions were examined during the two deployments in 2023 (April

and June), but due to environmental constraints and uncertainties in fish recovery, data from 2023 tests was primarily used for method refinement (methods and results from 2023 deployments are presented in Appendix D).

The field work conducted in 2024 aimed to build upon the findings and methodological refinements from 2023 (Appendix D) to further assess the fish passage conditions at HAHD. Eight of the nine conditions were evaluated over the three deployments (February, April, and June); high head/low flow was not feasible due to environmental conditions. The process involved attaching self-inflated balloon tags to live fish and Sensor Fish with self-inflating balloon tags, releasing treatment and control groups through distinct systems, and recovering them to assess injury, survival, and hydraulic conditions.

4.1.1 Live Fish Tagging and Assessments

Juvenile coho salmon used for the 2024 field tests were obtained from WDFW Soos Creek Hatchery for all three field deployments. Fish were held at HAHD in flow-through tanks filled with reservoir water and were monitored daily for temperature and DO. Feed was withheld for 24-hr prior to tagging.

Prior to tagging, fish were anesthetized to sedation (as described in Section 2.1.3.2). A uniquely numbered balloon tag ID and PIT tag ID were recorded for each fish. Fish were measured (mm FL), weighed (g), assigned as a treatment or control, and a pre-assessment of the fish was conducted (as described in Appendix E). The fish was then placed in a transfer container with anesthesia water and handed to the surgeon with its tags.

The PIT tags were implanted and the balloon tags were affixed using the techniques described in Section 2.1.3.2. Tagged fish were placed in recovery buckets (maximum three fish per bucket to prevent tag tangling) with fresh water and held in flow-through post-tagging recovery tanks for at least 30 minutes before release.

Post-release at the assessment trailer, balloons were cut off live fish to restore normal swimming. Within 1-hr of recapture, fish were anesthetized in an 80 mg/L MS-222 bath, identified via PIT tags, and assessed (as described in Appendix E). Once assessed, fish were placed in a fresh-water Bonar tote to recover from anesthesia, then transported in batches to flow-through recovery tanks ~0.5 miles downstream. Fish were held for 48-hr to monitor delayed mortality, reassessed, and euthanized with an overdose of MS-222 (250 mg/L).

4.1.2 Release and Recapture

Live fish and Sensor Fish were released in treatment and control groups to evaluate passage conditions through the HAHD 19-ft horseshoe tunnel, with the control group accounting for handling and release effects. Treatment releases used a system located on the deck within the HAHD forebay, while control releases occurred downstream of the tunnel exit in the tailrace. Balloon tags were activated prior to release and after passage and balloon tag inflation, fish were recollected in the tailwaters downstream of the dam.

4.1.2.1 Release Systems

The treatment release system (Figure 4-1) was installed on the deck within the forebay at an elevation of 1142 ft, using a portable flow-through release tank with an inflow hose supplied by a sump pump in the reservoir and a release hose secured to handrails to maintain a parallel or declining angle. The release hose was attached to a bracket on the bulkhead gate near the 19-ft tunnel intake, ensuring fish were entrained without obstruction. The control release system

(Figure 4-2) was installed on the west bank below the tailrace, using a submersible pump, powered by a generator, to flush river water through a flex hose into a PVC connector on a stand, then through a ~50-ft release hose positioned to avoid inclines and ensure underwater exit, minimizing fish obstruction.

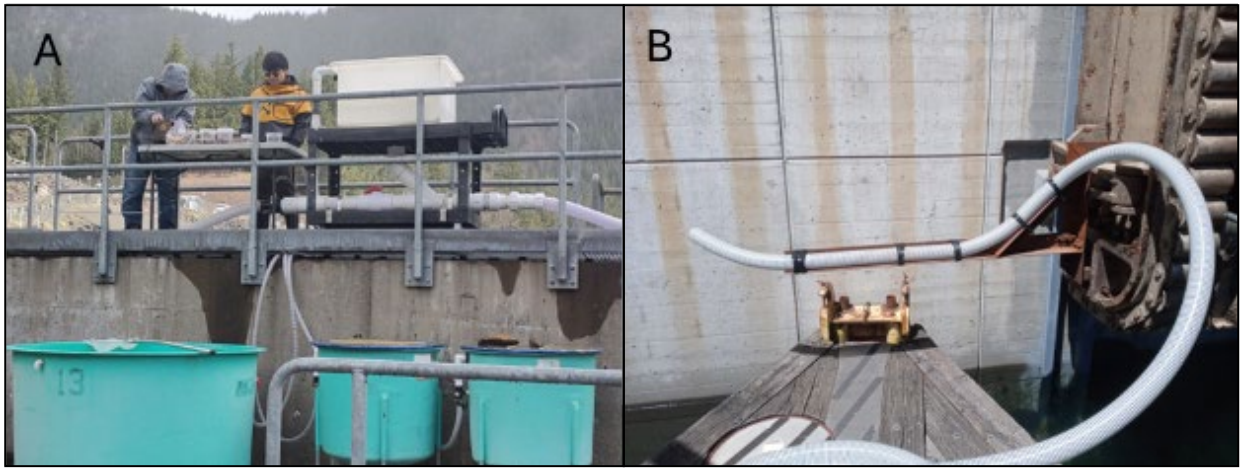

Figure 4-1. The treatment release system at HAHD. (A) View of the system installed on the 1142-ft deck, showing the portable release tank (white translucent tub) on a black cart. The inflow hose is attached to a PVC Y-piece and the release hose extending into the forebay on the right. Holding tanks and pre-release recovery tank are in the foreground. (B) Close-up of the release hose end attached to a bracket on the bulkhead gate at the 19-ft tunnel intake, prior to lowering to depth.

Figure 4-2. The control release system at HAHD. (A) View from the east bank of the Green River, showing the wider white release hose (left) and the white hose connected to a submersible pump (right) that flushes water through the release hose. (B) Close-up view of the system, with the flex hose attached to the top of the PVC Y-piece linked to the submersible pump and the release hose attached to the bottom for water flow.

4.1.2.2 Release Procedures

Each fish release was conducted individually, with release times and initial sightings communicated via radio and recorded by downstream crews. For treatment releases, tagged fish were moved in buckets from post-tagging recovery tanks to a table by the release tank, where balloons were inflated, and live fish or Sensor Fish were hand-released into the tank's standpipe and flushed through the release hose. For control releases, live fish and Sensor Fish were transported in buckets within a Bonar tote (filled with fresh river water) to the release site by truck. Balloons were inflated and held until ~¾ maximum size (~1 minute) to match treatment group balloon size at capture and ensure successful recovery. Fish or Sensor Fish were then hand-placed into the PVC fitting on the release system for entrainment through the release hose. Control releases occurred in closer succession due to the shorter, unobstructed hose compared to the treatment system.

4.1.2.3 Recapture

Live fish and Sensor Fish were recovered on shore and by kayak using dip nets. Recaptured live fish were quickly assessed for body condition and behavior. Shore caught fish were then placed in 4-gallon lidded buckets (maximum three fish per bucket) to prevent tangling. Full buckets were hand-transported to the assessment trailer ~0.25 miles downstream. Kayak-collected fish were moved in zippered, insulated fish bags via trolley and the transitioned to buckets for transport to the assessment trailer.

Once recovered, Sensor Fish were deactivated with a magnet and retained by netters until the cohort was complete. Sensor Fish data was downloaded, the systems were reset, and new balloons were attached for the next deployment. Sensor Fish data was analyzed throughout the testing period to evaluate sample quality and quantity of samples by testing condition.

4.1.3 Live Fish Analyses

The data analysis and statistical methods used for HAHD live fish injury and survival analyses in 2023 and 2024 were the same as used at GPR, described in Section 3.1.4.

4.1.4 Sensor Fish Data Analyses

The Sensor Fish data analysis methods for HAHD were the same as those used for GPR and the laboratory testing, described in Section 2.1.3.4.

4.2 HAHD Results

4.2.1 Live Fish Results

4.2.1.1 2023 Tagging

During the April and June 2023 field deployments at HAHD, an initial balloon tagging method was applied to facilitate live fish recapture. However, low recapture rates, including multiple instances of balloons recovered without attached fish, indicated poor tag retention. Because of this poor retention, survival rates from these deployments were considered unreliable, and the data were excluded from the final HAHD survival estimates. Although several tagging methods were tested in the field, none proved adequate. This prompted a controlled laboratory study of tagging procedures and tag retention, which resulted in the development of an improved balloon-tag attachment method that was applied in 2024. The complete 2023 field assessment and laboratory tag-retention study are detailed in Appendix D.

4.2.1.2 2024 Tagging

The testing at HAHD in 2024 occurred during three periods: from February 13 to 20, 2024, from April 8 to 12, 2024, and from June 3 to 7, 2024.

Fish length and weight increased with each deployment in 2024 due to expected growth (Table 4-1). Though fish size was observed to affect mortality rates according to results from laboratory testing (Section 2.2), these fish sizes are assumed to represent the size of fish that would pass the dam throughout the year.

Table 4-1. General information about the fish sizes and release numbers for juvenile Chinook salmon released at HAHD in 2024.

Season	Fork Length mean and range (in)	Weight, mean and range (oz)	Tagged (*n*)	Released Alive (*n*)	Recovered after Release (*n*)
February (Low Pool)	4.21 (3.58–5.04)	0.48 (0.32–0.79)	342	333	316 [a]
April (Mid Pool)	4.53 (3.66–5.28)[b]	0.57 (0.35–0.86) [b]	391	390	383 [c]
June (High Pool)	5.08 (4.29–6.30)	0.78 (0.48–1.36) [d]	358	334	310
Total	**4.61 (3.58–6.30)**	**0.61 (0.32–1.36)**	**1,091**	**1,058**	**1,009**

[a] Excludes 10 fish which were released in poor condition and recovered, but therefore not assessed. It also excludes one fish which was marked as recaptured but does not have any post-assessment data.
[b] Excludes two tagged fish with missing length and weight measurements.
[c] Inclusive of one fish which was recaptured 21-hs after its initial release.
[d] Excludes one tagged fish with missing weight measurement.

Fish tagged during February and April 2024 recovered with minimal mortality (≤2%). In June, 6% (*n* = 23) of tagged fish did not recover from surgery and were therefore not released. This mostly occurred on the afternoon of June 5, when the average morning pre-testing holding tank temperature was 11.7 °C (Appendix D). The most likely explanation for the unexpected mortality is the temperature of the anesthesia water used during tagging rose to uncomfortable levels for the fish because of high air temperature, exacerbating the stress of the tagging process. The failure of fish to recover was discovered in the flow-through holding tank during the 30-minute recovery period, and all water sources used for tagging were immediately swapped.

Of the nine proposed testing conditions, eight were tested at HAHD in 2024 (Table 4-2). The only category that was unavailable for data collection was < 600 cfs flow (low flow) during high pool reservoir elevation. This combination was not possible to test due to environmental conditions and necessary dam operations.

Table 4-2. Detailed testing conditions for each day of fish deployments at HAHD in 2024.

Date	Mean Daily Pool Elevation (ft)	Reservoir Elevation Category	Flow Condition (cfs)	Flow Category	Gate Opening (in)	Tailwater Depth (ft)
2/13/2024	1,091.9	Low	1,220	High	32	6.6
2/14/2024	1,090.5	Low	1,194	High	32	6.6
2/15/2024	1,087.8	Low	1,212	High	33	6.6
2/16/2024	1,087.1	Low	753	Med	20	5.7
2/17/2024	1,089.2	Low	430	Low	10	4.9
2/18/2024	1,091.3	Low	388	Low	9	4.8
2/19/2024	1,091.8	Low	784	Med	20	5.8
4/8/2024	1,141.7	Med	1,233	High	23	6.7
4/9/2024	1,141.4	Med	1,233	High	23	6.7
4/10/2024	1,142.7	Med	832	Med	15	5.9
4/11/2024	1,144.1	Med	837	Med	15	5.9
4/12/2024	1,145.3	Med	446	Low	7	5.0
6/3/2024	1,162.7	High	1,251	High	21	6.7
6/4/2024	1,162.8	High	1,253	High	21	6.7
6/5/2024	1,166.1	High	1,263	High	21	6.7
6/6/2024	1,167.4	High	1,269	High	21	6.7
6/7/2024	1,168.1	High	1,035	Med	17	6.3

Live fish recovery rates greatly increased from 2023 to 2024. The season with the most unrecovered fish was June, with 7.5% of released fish that went unrecovered. During high pool testing, seven balloon tags were recovered without a fish attached, one fish was recovered with no balloon tag, and 17 fish were never recovered. Tagging methods did not change during 2024, so it is unlikely that surgeon error contributed to the decrease in recovery. One reason for the lower recovery rates in June 2024 could be consistently high flows, which reached a maximum of 1,269 cfs (Table 4-2). It is possible the high flows carried the fish downstream past recovery crews before the fish could be spotted or before it was brought to the surface by the balloon tag.

Injuries

Injuries that occurred during passage through HAHD were recorded and analyzed but not used for the final survival estimates. The results from the injury assessments are detailed in Appendix E.3.

Survival

During testing in February 2024, six balloon-tagged treatment fish were caught in the hydraulic jump (i.e., a rapid transition from fast, shallow supercritical flow to deeper, slower subcritical flow) located immediately downstream of HAHD. Three of these fish were dead or moribund at the time of the post-release assessment. Because the hydraulic jump is an artifact of HAHD, injuries or mortality that occurred as a result of the hydraulic jump should be treated as injury or mortality

caused by dam passage. However, if the injuries or mortality incurred within the hydraulic jump were the result of the fish being attached to an inflated balloon, then the mortality should not be attributed to dam passage. Therefore, survival was estimated in two different ways for the testing that occurred in February. The first method assumed that fish caught in the hydraulic jump may have experienced injuries or mortality as a result of the inflated balloon, and the six fish were censored from the survival analysis. The second method assumed that any mortality incurred by fish caught in the hydraulic jump was a result of HAHD passage, and the six fish were included in the survival estimation. The first method (hydraulic jump = censored) has the potential to underestimate mortality if the mortality incurred because of being caught in the hydraulic jump independent of balloon attachment. The second method (hydraulic jump = included) has the potential to overestimate mortality if the mortality incurred as a result of being caught in the hydraulic jump was due to balloon attachment.

For most forebay and flow condition testing combinations, both 1-hr and 48-hr survival decreased as flows increased (Table 4-3). The only exceptions to this pattern occurred during low pool / low flow and medium pool / medium flow. If the hydraulic jump was included as an effect of dam passage, survival estimates during low pool / low flow were less than those at low pool / medium flow (Table 4-3). Medium pool testing in April showed relatively equal survival estimates during both low flow and medium flow conditions, with 80.0% (± SE) survival at both 1-hr and 48-hr for those flows (Table 4-3).

In general, the highest survival estimates were found during low pool, and lowest survival estimates were found during high pool. The lowest 48-hr survival estimates occurred during high pool / high flow, with an estimate of 75.9% ± 4.4%. At the preferable low pool testing conditions, high flow survival at 48-hr was only 85.7% ± 5.4%, roughly 10% less than estimates for medium flow, regardless of hydraulic jump censoring. In instances when the 48-hr survival estimate was greater than the 1-hr survival estimate, the 48-hr survival estimate was changed to equal the 1-hr survival estimate (Table 4-3).

As with the testing conducted at GPR, the fish used in the HAHD deployments were not depth acclimated prior to passage through the tunnel. This may lead to an underestimation of mortality due to rapid decompression. However, based off the Sensor Fish data (Section 4.2.2), pressures were rarely recorded at values significantly less than surface pressure. Therefore, minimal mortality is likely caused by rapid decompression not only for surface acclimated fish, but also likely depth acclimated fish.

Table 4-3. Survival estimates for balloon-tagged live fish at HAHD in 2024, separated by testing month and testing bins (forebay elevation / flow conditions). The hydraulic jump calculations are only relevant for February 2024. The estimated standard error (SE) for each calculation is in parentheses.

Month	Testing Condition Bins (forebay el. / flow)	*n*	Hydraulic jump = censored		Hydraulic jump = included	
			Immediate 1-hr survival	Overall 48-hr survival	Immediate 1-hr survival	Overall 48-hr survival
February	Low / Low	48	0.979 (0.021)	0.979 (0.021)	0.923 (0.037)	0.923 (0.037)
	Low / Med	45	0.951 (0.042)	0.945 (0.051)	0.954 (0.040)	0.949 (0.049)
	Low / High	42	0.929 (0.040)	0.857 (0.054)	0.929 (0.040)	0.857 (0.054)
April	Med / Low	50	0.800 (0.057)	0.800 (0.057)	0.800 (0.057)	0.800 (0.057)
	Med / Med	66	0.803 (0.049)	0.803 (0.049)	0.803 (0.049)	0.803 (0.049)
	Med / High	54	0.769 (0.062)	0.769 (0.062)	0.769 (0.062)	0.769 (0.062)
June	High / Med	50	0.778 (0.074)	0.778 (0.074)	0.778 (0.074)	0.778 (0.074)
	High / High	107	0.776 (0.049)	0.759 (0.053)	0.776 (0.049)	0.759 (0.053)

4.2.2 Sensor Fish Results

This section provides an overview of Sensor Fish testing conducted at HAHD, during which 449 valid treatment releases and 122 control releases were collected. Sensor Fish devices were calibrated prior to testing following PNNL's standard Sensor Fish operating procedures, confirming their pressure readings stayed within acceptable ranges from atmospheric pressure on the day of testing. Cumulative distribution functions and associated tables summarize the distribution of acceleration events and velocity-based strike metric M_V across regions of the passage system.

4.2.2.1 Treatments and Sample Sizes

In February, the forebay reservoir elevation ranged between 1087.1 and 1091.9 ft (NGVD 29), and the gate openings were 9 in, 10 in, 20 in, and 32 in. In April, the forebay reservoir elevation ranged between 1141.4 and 1145.3 ft, and the gate openings were 7 in, 15 in, and 23 in. In June, the forebay reservoir elevation ranged between 1162.7 to 1168.1 ft, and the gate openings were 17 in and 21 in. A total of 449 valid datasets and 122 control datasets were acquired (Table 4-4). The control Sensor Fish data was only used for checking the release pipe system and was not used for further analysis.

Table 4-4. Treatment Sensor Fish releases by study treatment at HAHD during 2024.

Year	Average Forebay Reservoir Elevation (ft) *	Gate Opening (in)	Valid Treatment Releases (*n*)
2024	1091.3	9	30
	1089.2	10	29
	1089.9	20	58
	1090.0	32	38
	1145.3	7	28
	1143.4	15	64
	1141.5	23	52
	1168.1	17	40
	1164.8	21	110

Note: The forebay elevation is the average value from the operation data during the period for Sensor Fish testing.

4.2.2.2 Timing Marks

The fish passage is divided into five regions, and the overall tunnel region extends from the gate opening to the downstream tunnel transition (Figure 4-3).

- Gate opening (T1-T2): This region is marked by the peak hydrostatic pressure followed by a pressure drop as the Sensor Fish is drawn into the tunnel gate opening.
- Upstream tunnel transition (T2-T3): Immediately after the Sensor Fish enters the gate, the pressure quickly returns to nearly atmospheric levels because of the presence of air and shallow water inside the tunnel. A pressure elevation (pressure bump) near the end of this region indicates the tunnel slope. This is verified with Computational Fluid Dynamics (CFD) results. Additional markers include a sharp increase in both rotational and acceleration magnitudes.
- Tunnel (T3-T4): The entrance to this region is selected based on a pressure tremor caused by water volume expansion once the splitter wall ends, accompanied by simultaneous increases in acceleration and rotational magnitudes.
- Downstream tunnel transition (T4-T5): This region features a slope resembling the upstream tunnel transition, resulting in a pressure elevation (pressure bump) and a sharp increase in rotational and acceleration magnitudes. This is also verified with CFD results.
- Stilling basin (T5-T6): This region demonstrates a gradual increase in pressure correlating with the water's depth and intensified water turbulence, leading to higher rotational magnitudes.

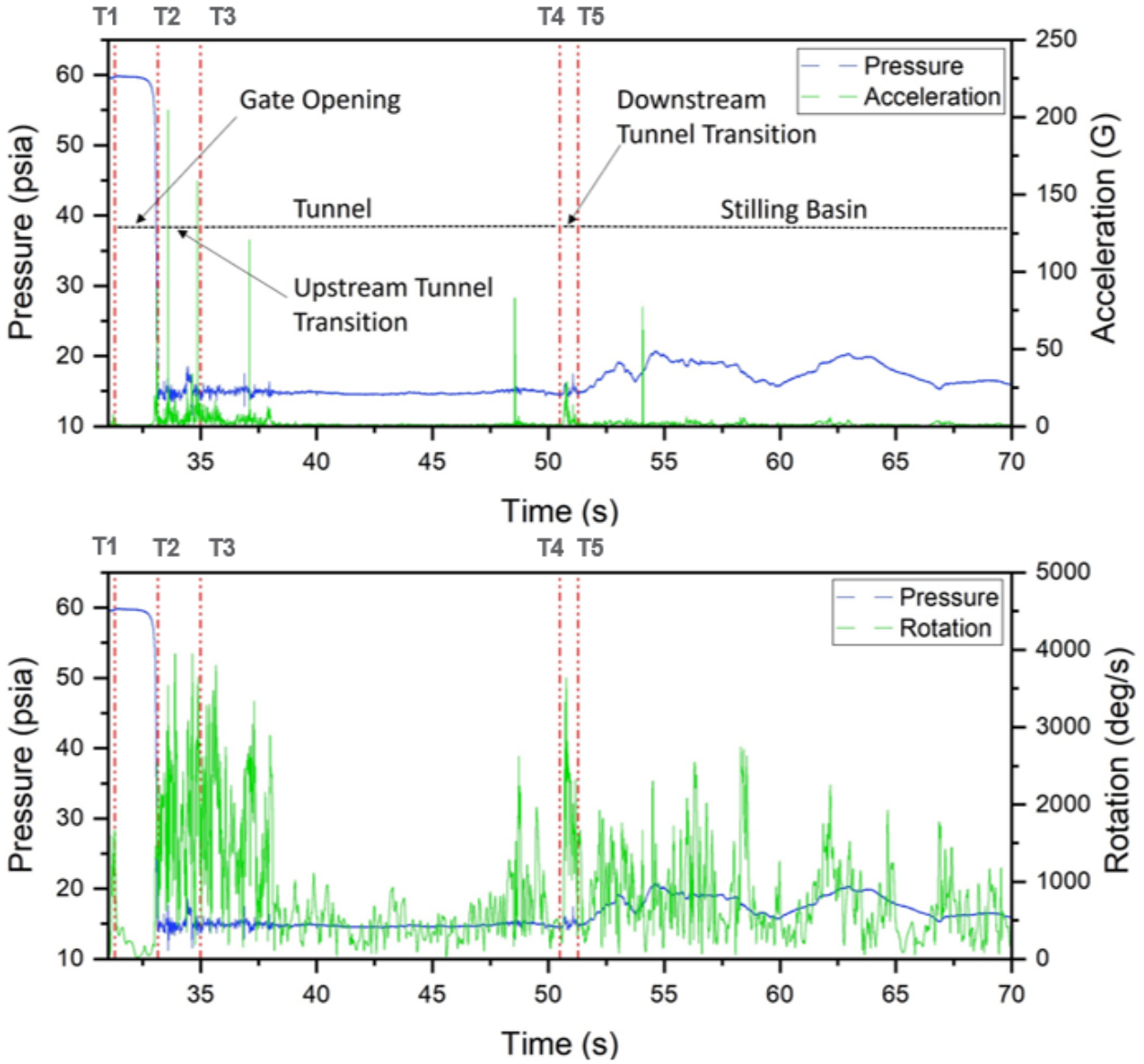

Figure 4-3. Representative passage data collected by a treatment-released Sensor Fish at HAHD in 2025.

4.2.2.3 Severe Acceleration Events

Severe acceleration events during fish passage usually result from collisions with hydraulic structures or exposure to shearing flows. The mean values of the maximum acceleration of each Sensor Fish release and the percentages of Sensor Fish releases that encountered severe acceleration events (i.e., acceleration peak ≥ 95 g_0) per treatment while passing through each hydraulic region are presented in Table 4-5 and Table 4-6, respectively. Most of the severe events were attributed to strikes. Only three mild shear events with low shear M_V values of 3.39, 2.30, and 3.17 m/s were observed within the gate opening region of HAHD.

Sensor Fish results show that the mean values of maximum accelerations and the percentage of Sensor Fish releases with severe acceleration events in the gate opening region was relatively low, suggesting minimal occurrences of collisions on the radial gate. In contrast, the upstream

tunnel transition and tunnel regions exhibited a higher acceleration magnitude and a higher percentage of Sensor Fish releases with severe acceleration events. This trend indicates a greater likelihood of potential collisions, such as grinding against the tunnel floor or collisions with the tunnel wall. In addition, the magnitude and the occurrence of severe events during downstream tunnel transitions were notably lower, indicating a reduced frequency of such events in this region. Furthermore, as the forebay reservoir elevation increased, the percentage of Sensor Fish releases with severe acceleration events tended to increase.

Table 4-5. Mean values of maximum accelerations of Sensor Fish releases per treatment at HAHD in 2024.

Year	Average Forebay Reservoir Elevation (ft)	Gate Opening (in)	Valid Treatment Releases (*n*)	Gate Opening Region (g_0)	Upstream Tunnel Transition (g_0)	Gate & Upstream Tunnel Transition (g_0)	Tunnel (g_0)	Downstream Tunnel Transition (g_0)	Overall Tunnel Region (g_0)
2024	1091.3	9	30	62	40	80	80	20	119
	1089.2	10	29	42	66	89	83	17	128
	1089.9	20	58	24	49	57	108	27	121
	1090.0	32	38	23	46	56	92	35	117
	1145.3	7	28	72	118	128	157	15	171
	1143.4	15	64	52	116	124	113	25	153
	1141.5	23	52	42	95	104	108	45	141
	1168.1	17	40	50	125	132	107	33	153
	1164.8	21	110	50	87	98	59	34	115

Table 4-6. Percentage of Sensor Fish releases at HAHD in 2024 that experienced severe acceleration events (acceleration peak ≥ 95 g_0) per treatment.

Year	Average Forebay Reservoir Elevation (ft)	Gate Opening (in)	Valid Treatment Releases (*n*)	Gate Opening Region (%)	Upstream Tunnel Transition (%)	Gate & Upstream Tunnel Transition (%)	Tunnel (%)	Downstream Tunnel Transition (%)	Overall Tunnel Region (%)
2024	1091.3	9	30	13.3	13.3	26.7	46.7	0.0	63.3
	1089.2	10	29	3.4	34.5	37.9	48.3	0.0	69.0
	1089.9	20	58	0.0	25.9	25.9	58.6	0.0	67.2
	1090.0	32	38	0.0	23.7	23.7	52.6	5.3	63.2
	1145.3	7	28	3.6	67.9	71.4	89.3	0.0	96.4
	1143.4	15	64	4.7	65.6	67.2	62.5	3.1	84.4
	1141.5	23	52	0.0	44.2	44.2	67.3	13.5	76.9
	1168.1	17	40	5.0	67.5	70.0	57.5	5.0	80.0
	1164.8	21	110	10.0	44.5	50.9	27.3	4.5	62.7

4.2.2.4 Survival Rates Estimated from Strike Metrics

To better quantify the biological effect of severe strikes between fish and hydraulic structures, the velocity-based strike metric (M_V) considers both magnitudes of accelerations around the peak and the duration of the severe strike events. Following the procedure described in Section 3.1.5, the mean and 95th percentile values of M_V for each hydraulic region of the tunnel passage (i.e., gate opening, upstream tunnel transition, gate and upstream tunnel transition combined, tunnel, and downstream tunnel transition) and each treatment are shown in Table 4-7 and Table 4-8, respectively. Results show that the upstream tunnel transition and tunnel regions yielded higher M_V values, which indicates higher severity of strikes/collisions. Moreover, the calibrated mortal threshold of M_V was found to be 1.27 m/s, which corresponds to the highest correlation (r = 0.65 and p = 0.07 for the overall tunnel region) between Sensor Fish estimates and the coho salmon 48-hr survival rates from HAHD 2024. Thus, the coho salmon with M_V values above 1.27 m/s are likely to be killed during the passage, otherwise the coho salmon are likely to survive through the passage. The cumulative distribution function curves of M_V for each treatment are shown in Figure 4-4, and the estimated 48-hr survival rates are shown in Table 4-9. Specifically, the Pearson correlation coefficient between Sensor Fish estimates and the coho salmon 48-hr survival rates from HAHD 2024 was 0.86 (p = 0.005) for the upstream tunnel transition region, which implies that this is the region of concern in terms of fish injuries and mortalities. Also, similar to the trend indicated by the percentage of Sensor Fish releases with severe acceleration events (Table 4-9), the estimated survival rates tended to decrease with the increase of the forebay reservoir elevation.

Table 4-7. Mean values of Sensor Fish strike metric (M_V) per treatment at HAHD in 2024.

Year	Average Forebay Reservoir Elevation (ft)	Gate Opening (in)	Valid Releases (*n*)	Gate Opening Region (m/s) [fps]	Upstream Tunnel Transition (m/s) [fps]	Gate & Upstream Tunnel Transition (m/s) [fps]	Tunnel (m/s) [fps]	Downstream Tunnel Transition (m/s) [fps]	Overall Tunnel Region (m/s) [fps]
2024	1091.3	9	30	0.38 [1.25]	0.15 [0.49]	0.52 [1.71]	0.37 [1.21]	0.00 [0.00]	0.80 [2.62]
	1089.2	10	29	0.06 [0.20]	0.36 [1.18]	0.43 [1.41]	0.41 [1.35]	0.00 [0.00]	0.70 [2.30]
	1089.9	20	58	0.00 [0.00]	0.21 [0.69]	0.21 [0.69]	0.58 [1.90]	0.00 [0.00]	0.67 [2.20]
	1090.0	32	38	0.00 [0.00]	0.23 [0.75]	0.23 [0.75]	0.53 [1.74]	0.09 [0.30]	0.68 [2.23]
	1145.3	7	28	0.08 [0.26]	0.76 [2.49]	0.84 [2.76]	0.92 [3.02]	0.00 [0.00]	1.18 [3.87]
	1143.4	15	64	0.05 [0.16]	0.76 [2.49]	0.79 [2.59]	0.74 [2.43]	0.03 [0.10]	1.12 [3.67]
	1141.5	23	52	0.00 [0.00]	0.51 [1.67]	0.51 [1.67]	0.63 [2.07]	0.13 [0.43]	0.84 [2.76]
	1168.1	17	40	0.08 [0.26]	0.74 [2.43]	0.80 [2.62]	0.61 [2.00]	0.05 [0.16]	0.99 [3.25]
	1164.8	21	110	0.11 [0.36]	0.49 [1.61]	0.56 [1.84]	0.28 [0.92]	0.05 [0.16]	0.71 [2.33]

Table 4-8. 95th percentile values of Sensor Fish strike metric (M_V) per treatment at HAHD in 2024.

Year	Average Forebay Reservoir Elevation (ft)	Gate Opening (in)	Valid Treatment Releases (*n*)	Gate Opening Region (m/s) [fps]	Upstream Tunnel Transition (m/s) [fps]	Gate & Upstream Tunnel Transition (m/s) [fps]	Tunnel (m/s) [fps]	Downstream Tunnel Transition (m/s) [fps]	Overall Tunnel Region (m/s) [fps]
2024	1091.3	9	30	3.07 [10.07]	1.11 [3.64]	3.07 [10.07]	1.09 [3.58]	0.00 [0.00]	3.07 [10.07]
	1089.2	10	29	0.00 [0.00]	1.22 [4.00]	1.62 [5.31]	1.06 [3.48]	0.00 [0.00]	1.62 [5.31]
	1089.9	20	58	0.00 [0.00]	0.95 [3.12]	0.95 [3.12]	1.59 [5.22]	0.00 [0.00]	1.59 [5.22]
	1090.0	32	38	0.00 [0.00]	1.10 [3.61]	1.10 [3.61]	1.25 [4.10]	0.17 [0.56]	1.50 [4.92]
	1145.3	7	28	0.00 [0.00]	1.45 [4.76]	1.79 [5.87]	1.62 [5.31]	0.00 [0.00]	1.88 [6.17]
	1143.4	15	64	0.00 [0.00]	1.79 [5.87]	1.79 [5.87]	1.94 [6.36]	0.00 [0.00]	2.04 [6.69]
	1141.5	23	52	0.00 [0.00]	1.65 [5.41]	1.65 [5.41]	1.31 [4.30]	0.98 [3.22]	1.65 [5.41]
	1168.1	17	40	0.05 [0.16]	1.61 [5.28]	1.67 [5.48]	1.51 [4.95]	0.04 [0.13]	1.90 [6.23]
	1164.8	21	110	1.17 [3.84]	1.56 [5.12]	1.59 [5.22]	1.36 [4.46]	0.00 [0.00]	1.66 [5.45]

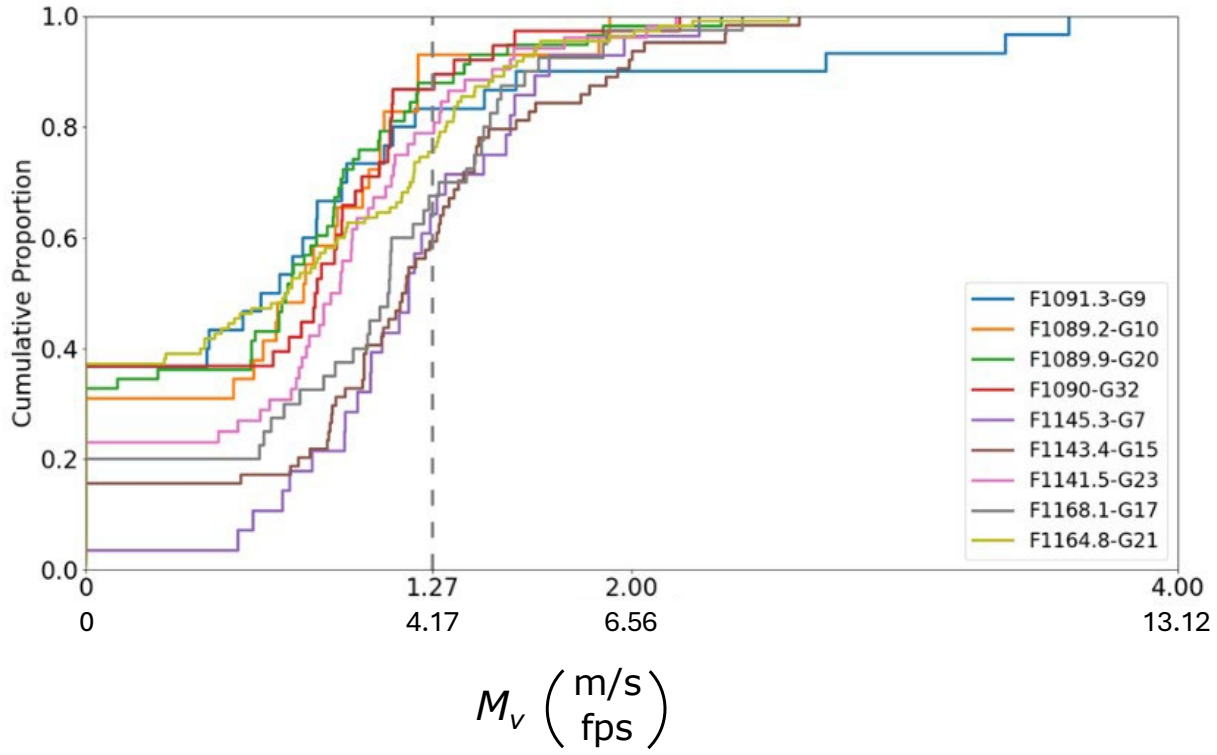

Figure 4-4. Applications of M_V for different treatments of HAHD fish passage (Note: the legend is in the form of "Forebay Elevation in feet- Gate Opening in inches", and the mortal threshold in a dotted gray line was calibrated based on data from HAHD 2024).

Table 4-9. 48-hr survival rates, estimated from Sensor Fish Strike Metric (M_V) at HAHD in 2024.

Year	Average Forebay Reservoir Elevation (ft)	Gate Opening (in)	Valid Treatment Releases (*n*)	Gate Opening Region (%)	Upstream Tunnel Transition (%)	Gate & Upstream Tunnel Transition (%)	Tunnel (%)	Downstream Tunnel Transition (%)	Overall Tunnel Region (%)
2024	1091.3	9	30	89.88	98.1	84.77	100	100	84.17
	1089.2	10	29	98.88	96.8	93.37	100	100	93.37
	1089.9	20	58	100	100	100	88.62	100	88.62
	1090.0	32	38	100	97.3	97.3	95.34	97.75	89.38
	1145.3	7	28	98.45	83.45	79.87	81.67	100	65.59
	1143.4	15	64	99.88	77.52	75.96	78.49	100	59.95
	1141.5	23	52	100	85.99	85.99	94.07	99.34	80.61
	1168.1	17	40	98.05	85.82	83.32	85.74	99.38	68.32
	1164.8	21	110	97.02	84.43	81.71	92.28	100	76.11

4.2.3 CFD-particle Modeling Results for HAHD

Computational flow simulations were conducted to investigate the free surface flow and CFD-particle flows in HAHD using the commercial CFD software STAR-CCM+. Multiphase flow simulations were conducted utilizing the VOF method to investigate hydrodynamics, free surface evaluations, pressure distribution, and severe events based on the 95 g_0 criteria using independent field studies using Sensor Fish.

The CFD-particle simulations were conducted in two steps:

- Turbulent free surface flow simulations using VOF method.
- Eulerian-Lagrangian Simulations using coupled CFD-DEM method for particle trajectory.

4.2.3.1 Comparison of the predicted discharge rate with Field measurement

The discharge rate predicted by CFD simulations was computed and compared with USACE data across various operating conditions (forebay water elevation and gate opening). Note that water discharge rate was regulated by the gate openings for a given forebay water elevation. These data are summarized in the Table 4-10. As seen from the Table 4-10, data for the discharge rates in are in good agreement (<10%) at different forebay elevations and gate openings.

Table 4-10. Comparison of CFD-predicted discharge rates at different operating conditions.at HAHD.

Year	Average Forebay Reservoir Elevation (ft)	Average Downstream Reservoir Elevation (ft)	Gate Opening (in)	Discharge Rate (USACE) (cfs)	Discharge Rate CFD (cfs)
	High Head Release, June 2024				
2024	1168.1		17	1,259	1,200
	1164.8		21	1,035	1,000
	Medium Head Release, April 2023				
2023	1,137.8		24	1,260	1,231.37
	1,137.8		16	823	820.27
	1,137.8		8	480	424.97
	Low Head Release, February 2024				
2024	1,090		32	1,209	1,166
	1,090		20	768.5	710
	1,090		10	409	353

4.2.3.2 Comparison of CFD-predicted Streamlines and Field Data using Sensor Fish

The CFD-predicted absolute pressures along streamlines were compared to the field data with Sensor Fish to investigate the hydraulic conditions in the flow domain including upstream forebay, tunnel and stilling basin. That comparison allowed approximately identification of distinct regions within the tunnel of HAHD. Due to anticipated uncertainty in the location of the exit of the flexible hose for Sensor Fish release, CFD predicted streamline data were generated at distinct locations around the approximate the exit of Sensor Fish release hose (P_{inj}). CFD-predicted streamlines included nine initial points, labeled P1 through P8, with P_{inj} representing the approximate location of the outlet of Sensor Fish release hose (Figure 4-5).

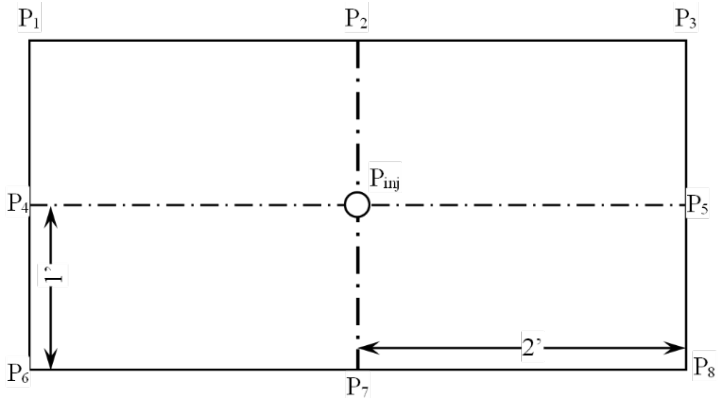

Figure 4-5. Initial seeding locations of the streamlines P1 through P8 and Pinj (approximate location of Sensor Fish release hose outlet).

VOF simulations were conducted for two gate openings. In these cases, roughness of the wall increased to 2 mm. The increased wall roughness led to increased skin drag, and flow velocity was expected to slow. Once flow achieved the quasi-steady state, the trajectory of streamlines was computed although it should be noted that injection locations were kept the same (Figure 4-6). The CFD-predicted absolute pressure histories were plotted and compared to Sensor Fish data, which showed the trend to trends and correlations in both gate openings. In this case, both results matched well at both gate openings. Initially, the hydrostatic pressure across all streamlines was observed to be approximately 72 psia. This was followed by a sudden drop in hydrostatic pressure to near-atmospheric levels of 14.7 psia (near the radial gate), followed by a pressure jump in the transition zone before the end of the splitter wall and tunnel entrance. Note that the downward slope led to flow deceleration and subsequent slightly pressure bump appears. In the tunnel region, pressure reams approximately constant at the atmospheric conditions in both cases. At the transition and diverging section, pressure bumps appear again. Subsequently, pressure grows higher in the stilling basin. The pressure for Sensor Fish and CFD-predicted streamlines closely matched in terms of time and pressure bump values.

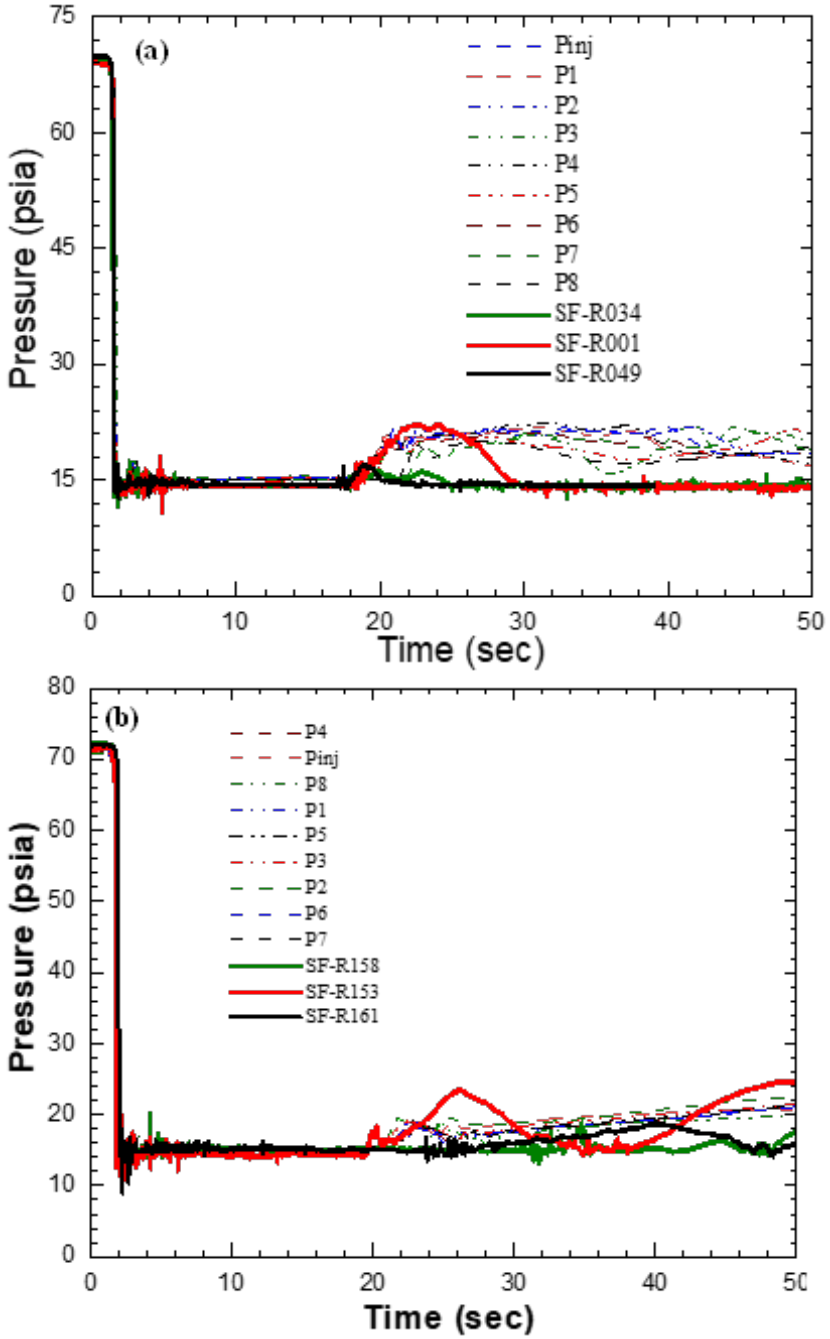

Figure 4-6. Comparison of the CFD-predicted pressure using streamline with field study data using sensor Fish. (a) 21” and (b) 17” gate openings at high forebay elevation in June 2024. Both results matched well for the two gate openings. The higher bump in the pressure in Sensor Fish may have been due to collision.

4.2.3.3 CFD-particle Simulations for Predictions of Stressors

Once flow filled in, the fish passage was validated against the comparison of the field study and coupled CFD-DEM simulations were conducted to sample the stressors data for BioPA analyses. 600 cylindrical particles with the same dimension of the sensor fish were randomly injected in 10 seconds. The particles were periodically injected at a given time interval to avoid inter-particle

collisions. The flow particle simulations were conducted until the particles left the flow domain. The parcel depletion model was chosen for efficient simulations in which the particle depleted once the particle crosses the domain of interest. A temporal snapshot for the particles and collision events at various regions of the HAHD passage is shown in Figure 4-7.

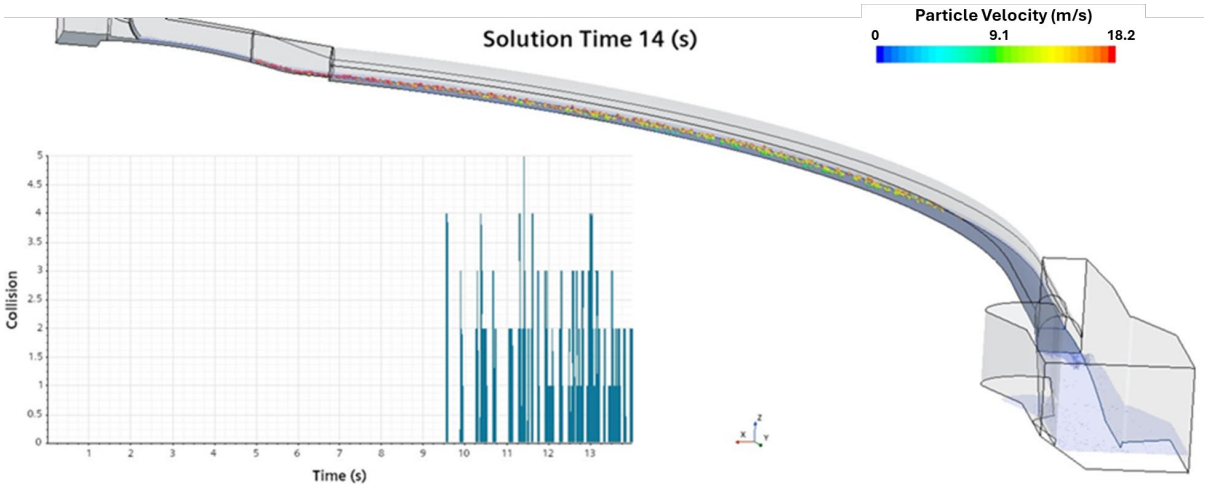

Figure 4-7. Free surface of water (light blue) and particles (i.e., surrogates for fish), velocity in a full scale model of existing HAHD fish passage. The histogram shows the history of collision of particles with the rigid structure of HAHD fish passage.

In the Sensor Fish data, severe acceleration events in fish passage usually resulted from collisions of Sensor Fish with hydraulic structures or exposure to high shear flows. Inline to the Sensor Fish study, acceleration of the particles was computed from the velocity data in the trajectory files, and the computed acceleration was nondimensionalized by gravitational acceleration. Furthermore, the severe acceleration event was computed based on Sensor Fish criteria in which the value of normalized acceleration is greater than 95 acceleration ($g_0 \geq 95$). The percentage of the particles that encountered the severe acceleration event was also computed.

The mean values of the maximum acceleration of each Sensor Fish release and the percentages of Sensor Fish releases that encountered severe acceleration events (i.e., ≥ 95 g_0) per treatment while passing through each hydraulic region are presented in Table 4-11 and Figure 4-10, respectively. Most of the severe events were attributed to strikes. Only three mild shear events with low shear M_V values of 3.39, 2.30, and 3.17 m/s were observed within the gate opening region of HAHD.

4.2.3.4 Nadir Pressure Distribution

The distribution of nadir pressure is a key parameter for evaluating the risk of barotrauma injuries in fish as they pass through water resource facilities. Both the magnitude and the rate of change in nadir pressure exposure are significant factors influencing barotrauma risk. Consequently, the shape of the exposure plot for nadir pressure is essential for assessing the conditions fish encounter during passage.

In this context, the nadir pressure, its rate of change, and the duration of passage are closely tied to the existing HAHD design and have been computed across various operating conditions. Figure 4-8 presents the cumulative exposure probability distribution for nadir pressure under different operating scenarios, showing a consistent trend across all cases. Notably, the data

indicates minimal variation (< 2 psia) for nadir pressure as discharge rate changes except for the case of the 17-in gate opening and higher forebay water elevation (1164.8 ft). As a result, not only surface-acclimated fish, but likely also depth acclimated fish, are unlikely to experience injuries associated with barotrauma under these conditions.

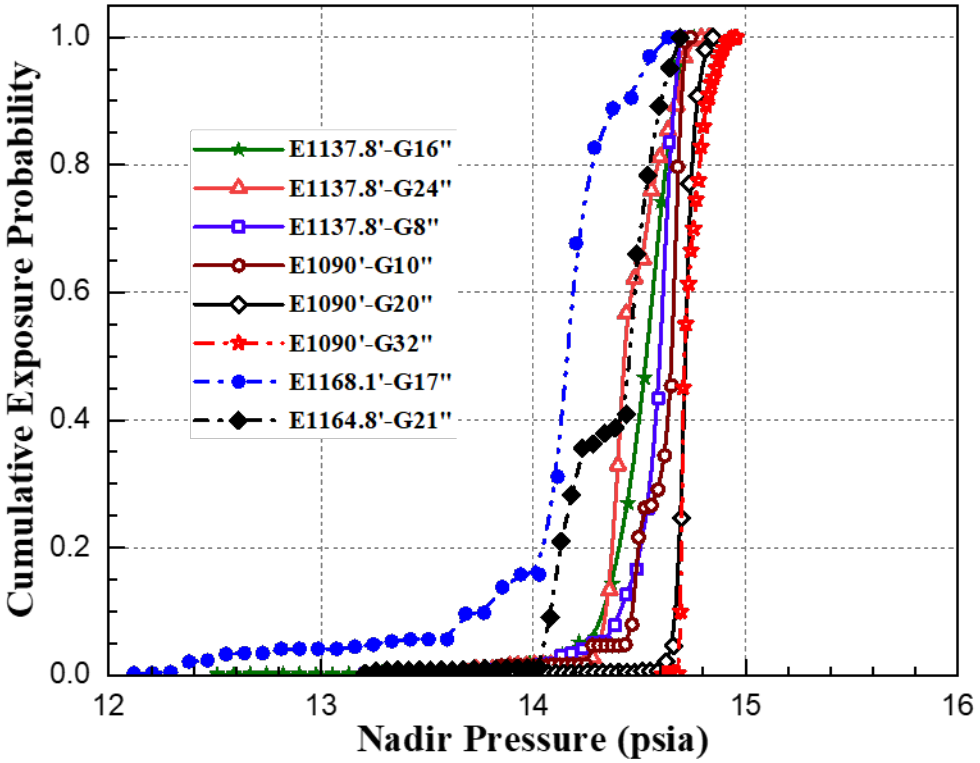

Figure 4-8. The plot shows the cumulative exposure probability of CFD-predicted Nadir Pressure under various operating conditions for HAHD fish passage. The legend is formatted as described in the document "E: Forebay Elevation in feet, and G: Gate Opening in inches."

4.2.3.5 Predicted Survival Rates computed from Strike Metrics

In the Sensor Fish study, the velocity-based strike metric (M_V) was employed to quantify the biological impact of severe strikes between fish and hydraulic structures. The M_V metric accounts for both the magnitude of peak accelerations and the duration of severe events. Larger peak durations were classified as severe shear events, while shorter durations were categorized as collision events.

One of the objectives of the CFD-particle flow simulations was to compare predicted results with Sensor Fish studies, thereby validating the computational modeling approach and enhancing confidence level its accuracy. Accordingly, a similar procedure for calculating M_V, as described in Section 2.1.3.4, was applied to each particle. Subsequently, the exposure probability of M_V values was computed for each region within the tunnel passage of the HAHD. The 95th percentile values of M_V in cumulative exposure distribution correspond to M_V value for horizontal green line (Figure 4-9) for each hydraulic region (i.e., gate opening, upstream tunnel transition, gate, tunnel, downstream diverging tunnel transition, and stilling basin) under eight operating conditions are presented in Table 4-11. The results indicate that the gate and tunnel regions exhibited higher M_V values, suggesting that these areas are more prone to severe strikes or collisions.

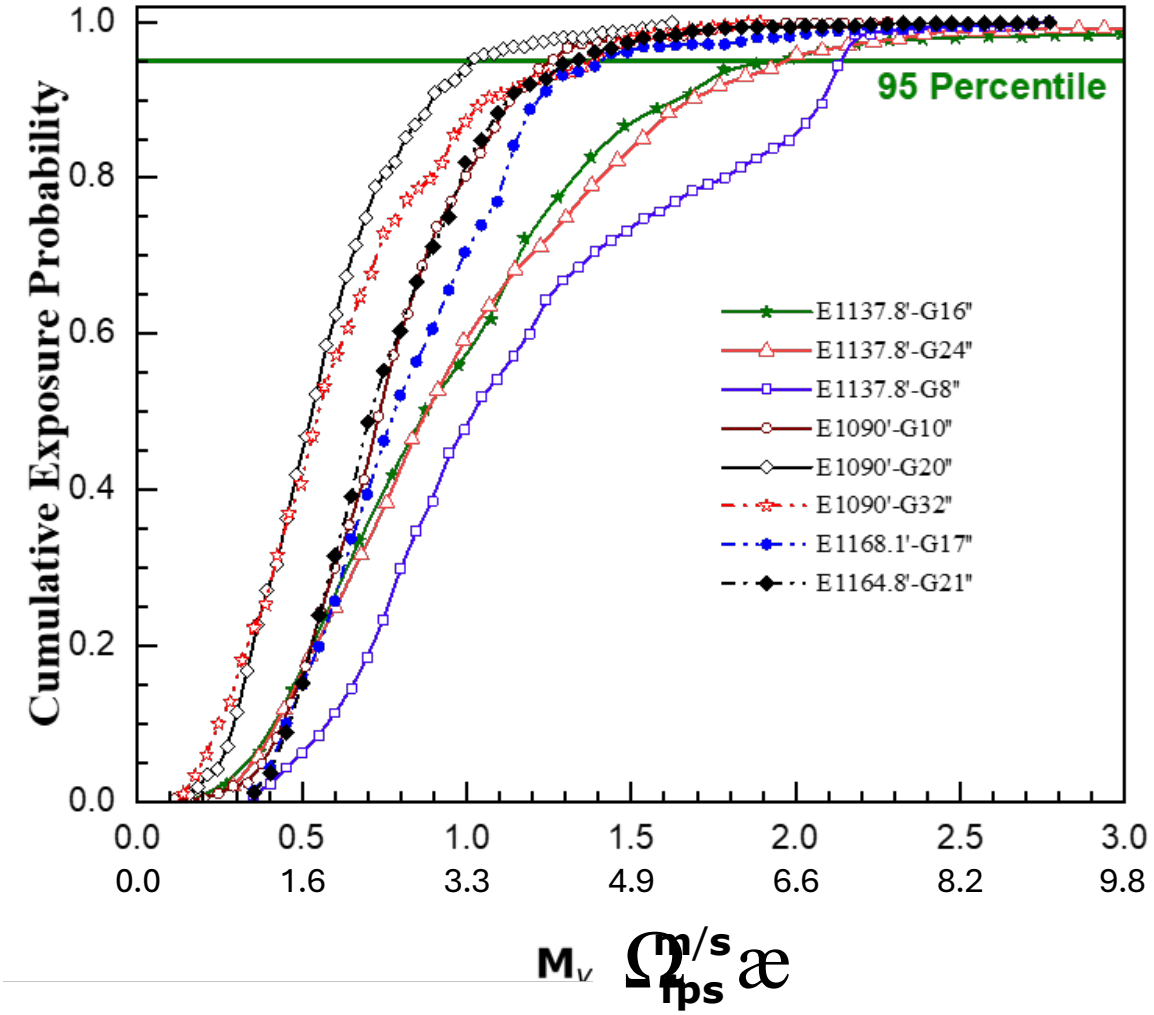

Figure 4-9. The plot shows the cumulative exposure probability of CFD-predicted M_V strike under various operating conditions for the HAHD fish passage system. The horizontal green line represents the 95th percentile of the exposure probability. The legend is formatted as 'E: Forebay Elevation (feet), G: Gate Opening (inches).'"

Table 4-11. 95th percentile values of CFD-predicted strike metric (M_V) by average forebay reservoir elevation during testing at HAHD.

Year	Average Forebay Reservoir Elevation (ft)	Gate Opening (in)	Discharge (cfs)	Gate Opening Region (m/s) [fps]	Upstream Tunnel Transition (m/s) [fps]	Tunnel (m/s) [fps]	Diverging (m/s) [fps]	Basin Region (m/s) [fps]	Overall Tunnel Region (m/s) [fps]
2023	1137.8	8	400	2.19 [7.19]	0.80 [2.62]	1.68 [5.51]	0.78 [2.56]	1.24 [4.06]	2.19 [7.19]
	1137.4	16	800	1.40 [4.59]	0.81 [2.66]	1.70 [5.58]	0.55 [1.80]	1.49 [4.89]	1.70 [5.58]
	1137.8	24	1,200	1.04 [3.41]	1.05 [3.44]	1.73 [5.68]	0.57 [1.87]	1.57 [6.13]	1.73 [5.68]
2024	1089.2	10	400	1.02 [3.35]	0.48 [1.57]	1.25 [4.10]	0.84 [2.76]	0.69 [2.26]	1.25 [4.10]
	1089.9	20	800	0.59 [1.94]	0.24 [0.79]	1.00 [3.28]	0.65 [2.13]	1.10 [3.61]	1.10 [3.61]
	1090.0	32	1,200	0.66 [2.17]	0.58 [1.90]	1.19 [3.90]	0.51 [1.67]	1.16 [3.81]	1.19 [3.90]
2024	1168.1	17	1,000	1.48 [4.86]	0.66 [2.17]	1.62 [5.31]	0.68 [2.23]	1.46 [4.79]	1.62 [5.31]
	1164.8	21	1,200	0.01 [0.32]	0.14 [0.46]	0.53 [1.74]	0.47 [1.54]	0.04 [0.13]	0.53 [1.74]

*CFD analysis for medium forebay elevation was conducted on 2023 conditions, while Sensor Fish and live fish results are from 2024. Both conditions represent the medium forebay elevation and discharge rate was regulated by adjusting the gate opening.

In addition to calculating the cumulative exposure probability for individual regions, the exposure probability for the overall tunnel passage was also computed and is presented in Table 4-12 and Figure 4-10. Sensor Fish studies accounted for uncertainties in live fish results from HAHD 2023, and the Sensor Fish-calibrated mortality threshold of M_V was identified as 1.27 m/s. This threshold was derived based on the highest correlation between Sensor Fish estimates and coho salmon 48-hr survival rates from HAHD 2024. Consequently, coho salmon exposed to M_V values exceeding this threshold are likely to experience mortality, while those with values below the threshold are likely to survive the passage. The predicted survival rate is presented in Table 4-13 based on the shear threshold 1.78 m/s.

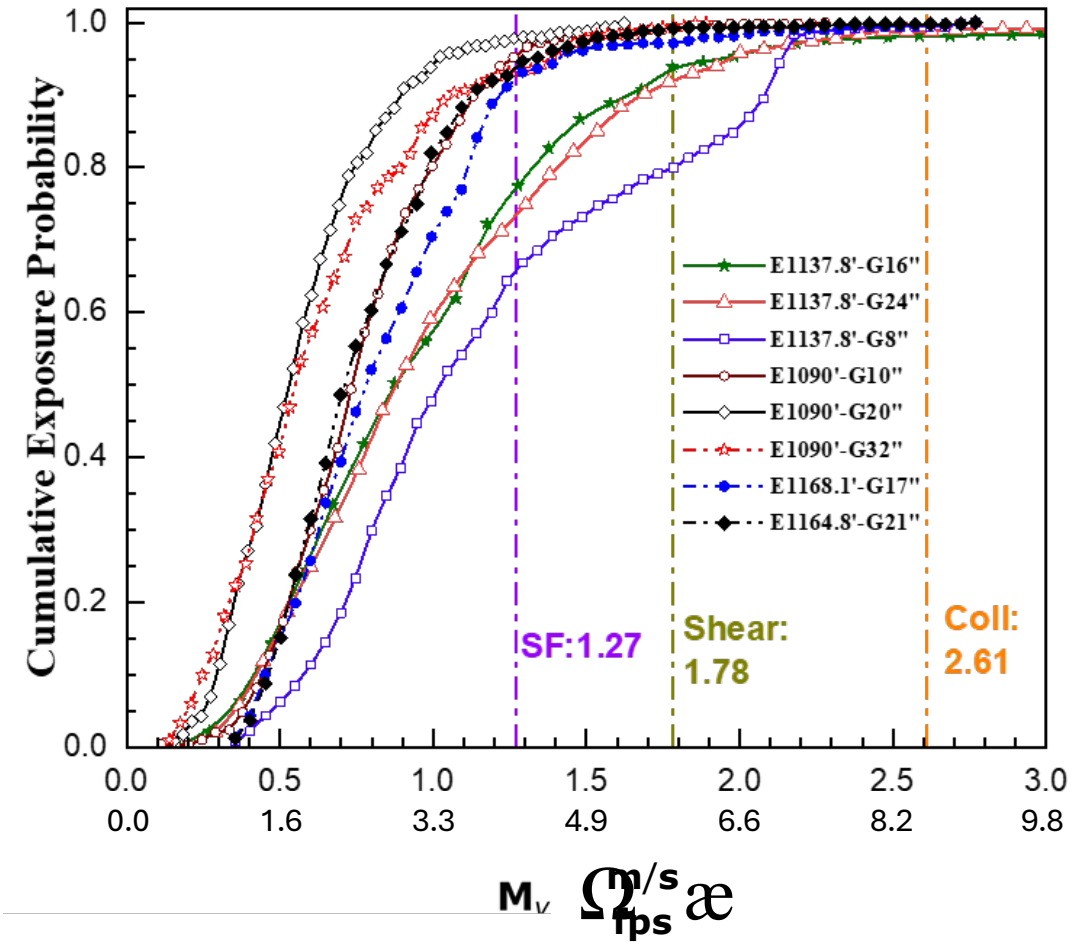

Figure 4-10. The plot shows the cumulative exposure probability of CFD-predicted M_V under various operating conditions for HAHD fish passage. The three vertical lines denote the calibrated mortality thresholds for Sensor Fish (SF) derived from HAHD, shear, and collision (coll) tests, based on submerged shear lab testing conducted in 2024. The legend is formatted as “E: Forebay Elevation in feet, and G: Gate Opening in inches.”

Table 4-12. 48-hr survival rates estimated from CFD-predicted Strike Metric ($M_V = 1.78\ m/sec$) for various sections of the HAHD tunnel and by average forebay reservoir elevation during testing at HAHD.

Year	Average Forebay Reservoir Elevation (ft)	Gate Opening (in)	Approximate Discharge (~cfs)	Gate Opening Region	Upstream Tunnel Transition	Tunnel	Diverging	Basin Region	Overall Tunnel Region
2023	1137.8	8	400	50.3	100	96	100	96.90	99.2
	1137.4	16	800	99	99.7	96.1	100	96.70	100
	1137.8	24	1,200	99.3	98.95	95.69	99.78	97.05	99.45
2024	1089.2	10	400	100	100	99.10	100	100	80.03
	1089.9	20	800	100	100	100	100	99.40	93.5
	1090.0	32	1,200	100	100	99.60	100	98.44	91.95
2024	1168.1	17	1, 000	99.15	100	96.25	100	97.5	94.05
	1164.8	21	1,200	100	100	100	100	100	95.7

This threshold was used in the CFD studies, and mortal thresholds derived from submerged jet conditions as shear test at a plate angle of 10º were also used. In this scenario, M_V values outside the nozzle region were selected, assuming similar flow conditions at HAHD. The threshold value was defined as $M_V = 1.78$ m/s for un-collided particles and $M_V = 2.61$ m/s for collided particles, with the thresholds corresponding to shear and collision events, respectively. These values were subsequently utilized to predict the overall survival probability of fish. The survival predictions using these three thresholds are detailed in Table 4-13. Specifically, using a Pearson's correlation coefficient between predicted survival using three threshold values and coho salmon 48-hr survival rates, the overall survival of HAHD was found to be more than 0.90 ($p < 0.005$). Furthermore, consistent with trends observed in Sensor Fish releases showing severe events, the estimated survival rates decreased as forebay reservoir elevation increased when using the three thresholds. This was preliminary work conducted to isolate collision as a single stressor, but results indicate that significant shear events also occurred. The results of this testing was not used for final predictions, and additional laboratory testing was conducted with the jet non-submerged to better isolate collision events.

Table 4-13. 48-hr survival rates for HAHD estimated from CFD-predicted Strike Metric (M_V) obtained from the submerged jet laboratory testing with a 10° plate angle at PNNL.

Year	Average Forebay Reservoir Elevation (ft)	Gate Opening (in)	Discharge (~cfs)	48-hr Live Fish Survival	Predicted Survival[b]		
					M_V = 1.78 m/s	M_V = 2.61 m/s	M_V = 1.27 m/s (SF)
2024	1089.2	10	400	92.3	99.2	100	96.0
	1089.9	20	800	95.6	100	100	98.0
	1090.0	32	1,200	85.7	99.45	100	93.3
2023	1137.8	8	400	80[a]	80.03	99.6	66.3
	1137.4	16	800	80[a]	93.5	98.3	77.1
	1137.8	24	1,200	76[a]	91.95	99.1	74.05
2024	1168.1	17	1, 000	77.8	94.05	98	72.2
	1164.8	21	1,200	75.9	95.7	99.4	84
Correlation coefficient between Live Fish and Predicted Survival					0.539	0.648	0.816
p-value					0.168	0.083	0.0135

[a] The live fish survival study in year 2023 had some limitations such as downstream fish collection and overall fish condition; therefore, survival data for these cases corresponded with year 2024. However, forebay elevation was slightly higher, but gate opening was lower.

[b] The survival of the fish also depends on the size and species types. Live fist testing to generate these survival predictions was for juvenile coho salmon.

5.0 BioPA Survival Estimates

The BioPA analysis was conducted using the biological response models developed for shear and collision from the laboratory testing and the biological response model for rapid decompression from Brown et al. (2012) for juvenile Chinook salmon (Table 5-1). The analysis showed strong agreement between Sensor Fish and CFD-based survival estimates, demonstrating the consistency of these methods across different data sources (Figure 5-1). For GPR, both Sensor Fish methods and CFD-particle modeling closely aligned with live fish survival estimates, validating the method's predictive accuracy under those testing conditions. However, at HAHD, Sensor Fish and CFD estimates indicated higher survival probabilities than the live fish survival, particularly during the April and June 2024 deployments (medium and high flows; Figure 5-1). This discrepancy is likely due to challenges with balloon-tag retention in the field tests. Compared with the February 2025 deployment, a higher proportion of fish lost their balloon tags in April and June. Per study protocol—based on laboratory tag-retention experiments—any fish for which only the balloon tag was recovered was classified as a mortality for the survival estimates. If field conditions caused greater tag loss for surviving fish than observed in the laboratory, this assumption would overestimate mortality and artificially lower reported live-fish survival.

Table 5-1. Probability of mortality due to rapid decompression equation from Brown et al. (2012) with coefficients.

Coefficient	Definition	Equation
P_M	Probability of Mortality	$P_M = \frac{e^{-5.56+3.85\left(\ln\frac{P_A}{P_N}\right)}}{1+e^{-5.56+3.85\left(\ln\frac{P_A}{P_N}\right)}}$
P_A	Acclimation Pressure	
P_N	Nadir Pressure	

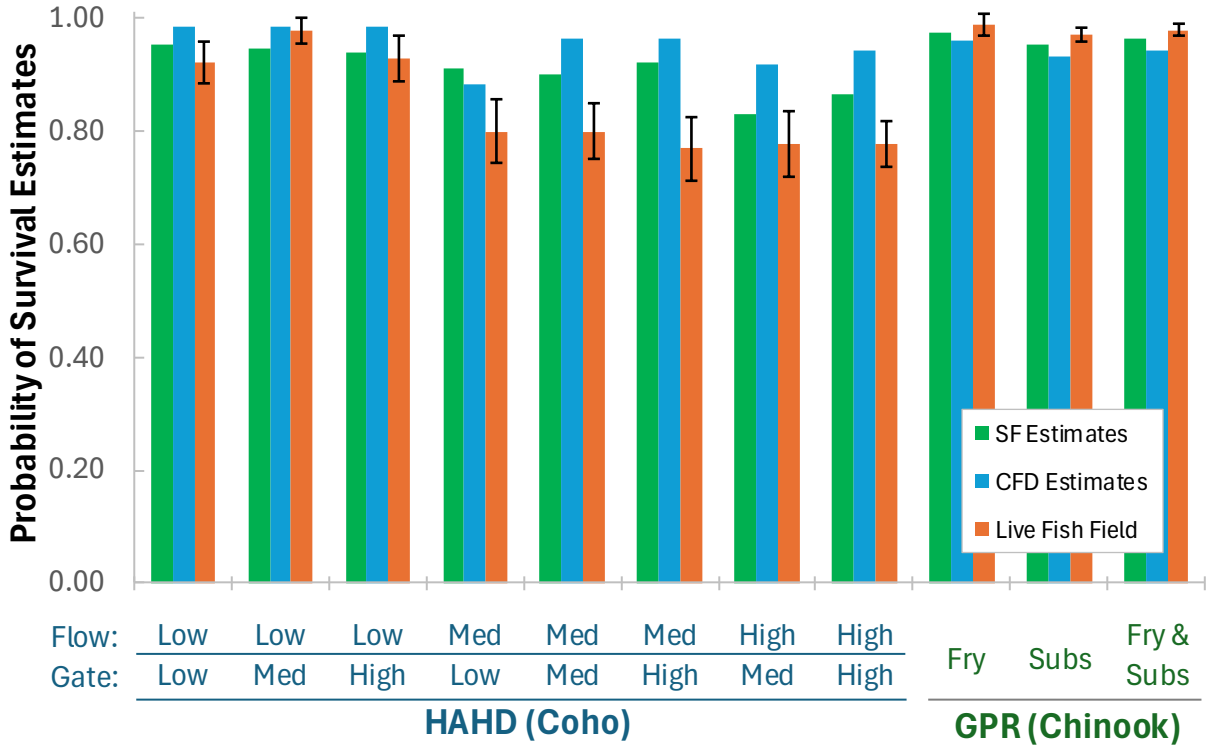

Figure 5-1. Comparison of survival estimates using lab-derived biological response models applied Sensor Fish and CFD data for the various treatments at HAHD and GPR and compared to the live fish field data. Biological response models used parameters to best match the field deployments. Biological response models applied to HAHD were set to evaluate balloon-tagged coho salmon and non-tagged Chinook salmon at GPR. Each model was applied using length distributions from each treatment tested during the live fish field deployments. For the application of CFD data, there is not a conversion of Jet Velocity to M_V that considers the presence of a balloon tag which differs from the application of Sensor Fish data.

A key additional factor is that CFD modeling used particles representing untagged Sensor Fish and therefore could not account for the increased injury and mortality risk associated with balloon tags, which laboratory studies showed is significant. Sensor Fish measurements, by contrast, inherently included this balloon-tag effect. This explains why CFD predictions at HAHD were most often higher than Sensor Fish predictions (Figure 5-1). Further uncertainty in the live-fish survival estimates may also arise from differences in fish condition between the laboratory tag-retention study and the field trials. It is suspected that the lab tested fish were in better condition prior to testing due to improved holding conditions and the lack of transport and additional handling stresses prior to testing which may have led to lower survival estimates for live fish deployments.

Finally, when applying these results using the BioPA and HBET methods, overall passage survival was calculated by multiplying the independent mortality probabilities associated with each of the three primary stressors (strike, shear, and barotrauma) for every individual particle or Sensor Fish trajectory. This multiplicative approach compounds any error or bias present in the individual stressor estimates. Moreover, because the dose-response relationships for each stressor were derived from separate laboratory experiments, potential interactions or cumulative effects among multiple stressors are not captured. Consequently, confidence is considerably higher in the

estimated survival probability for any single stressor than in the combined three-stressor survival estimate (Table 5-2). Across nearly all treatments and methods at both projects (Table 5-1), collision/strike was overwhelmingly the dominant source of predicted mortality, typically accounting for 80–100 % of the total mortality risk, while shear and barotrauma contributed negligibly (survival routinely ≥ 0.995–1.000).

Table 5-2. Probability of survival estimates for CFD and Sensor Fish data for the various treatments at HAHD and GPR compared to live fish field deployments survival estimates. Estimates include in survival probability for individual stressors (collision, shear, and pressure) and the probability of survival when individual stressors are combined.

Treatment	Live Fish		Probability of Survival			
	1-hr survival*	SE	Collision	Shear	Pressure	Combined Stressors
Sensor Fish						
Howard A. Hanson Dam						
Low Pool - Low Flow	0.923	0.037	0.958	1.000	0.996	0.954
Low Pool - Med Flow	0.978	0.022	0.950	1.000	0.996	0.946
Low Pool - High Flow	0.929	0.040	0.943	1.000	0.996	0.940
Med Pool - Low Flow	0.800	0.057	0.915	1.000	0.995	0.910
Med Pool - Med Flow	0.800	0.049	0.905	1.000	0.996	0.901
Med Pool - High Flow	0.769	0.057	0.926	1.000	0.996	0.922
High Pool - Med Flow	0.778	0.059	0.832	1.000	0.995	0.829
High Pool - High Flow	0.776	0.040	0.868	1.000	0.995	0.864
Green Peter Dam						
Fry	0.988	0.018	0.987	1.000	0.986	0.974
Subyearlings	0.972	0.012	0.966	1.000	0.986	0.953
Fry & Subyearling	0.979	0.011	0.976	1.000	0.986	0.962
CFD						
Howard A. Hanson Dam						
Low Pool - Low Flow	0.923	0.037	0.990	1.000	0.996	0.986
Low Pool - Med Flow	0.978	0.022	0.990	1.000	0.996	0.987
Low Pool - High Flow	0.929	0.040	0.989	1.000	0.996	0.985
Med Pool - Low Flow	0.800	0.057	0.900	0.985	0.996	0.883
Med Pool - Med Flow	0.800	0.049	0.969	0.998	0.996	0.964
Med Pool - High Flow	0.769	0.057	0.968	0.998	0.996	0.963
High Pool - Med Flow	0.778	0.059	0.929	0.997	0.996	0.917
High Pool - High Flow	0.776	0.040	0.947	0.998	0.996	0.942
Green Peter Dam						
Fry	0.988	0.018	0.970	1.000	0.990	0.961
Subyearlings	0.972	0.012	0.937	1.000	0.990	0.930
Fry & Subyearling	0.979	0.011	0.952	1.000	0.990	0.944

* 1-hr survival assumes balloon tag only recovered due to tag loss indicates mortality.

5.1 Survival Estimates for Subyearling Chinook Salmon at HAHD

To better understand the survival estimates for the target species, subyearling Chinook salmon, biological response models for blade strike, fluid shear, and rapid decompression (barotrauma) were applied to the stressor-exposure histories derived from Sensor Fish measurements and CFD-particle tracking at HAHD. For these estimates, the variables applied used nontagged subyearling Chinook salmon with the same length distribution as fish released in the GPR field studies (excluding fry).

For the rapid-decompression model, fish were assumed to be acclimated at the surface (0 m depth). This represents the scenario that produces the highest predicted survival (i.e., lowest barotrauma mortality). Nadir pressures recorded by Sensor Fish and predicted by CFD at HAHD were only modestly below atmospheric pressure; under the surface-acclimation assumption, barotrauma mortality was therefore negligible across all treatments (survival routinely ≥ 0.99; Figure 5-2, Table 5-2). The true acclimation depth of subyearling Chinook salmon approaching HAHD is unknown. If fish are acclimated to greater depths (e.g., ~10 m), the same nadir pressures could induce higher barotrauma mortality than estimated here.

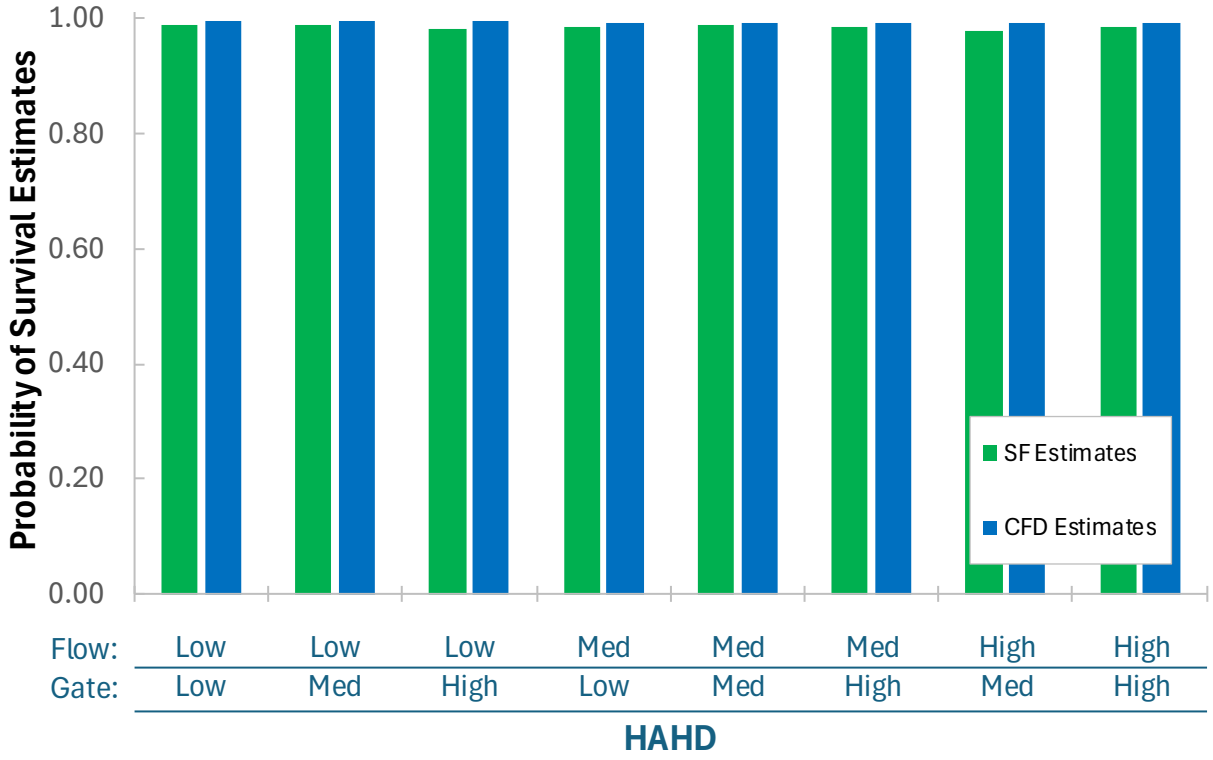

Figure 5-2. Comparison of survival estimates using lab derived biological response models applied Sensor Fish and CFD data for the various treatments at HAHD. Biological response models used parameters to match the targeted species of interest, Chinook salmon. Parameters used include Chinook as the species, fish length distribution matching the subyearling Chinook used at GPR during field testing, and no balloon tag attached.

Consistent with patterns observed when the models were applied to match the live fish deployments, collision was the dominant source of predicted mortality for subyearling Chinook salmon at HAHD, whereas contributions from shear and rapid decompression were minimal.

Combined direct passage survival for subyearling Chinook salmon was high under all tested pool-elevation and flow combinations, ranging from 0.977–0.998 (Sensor Fish) to 0.991–0.995 (CFD), with all estimates exceeding 97 % (Table 5-3, Figure 5-2). Based on these estimates, when the BioPA analysis is applied using non-tagged Chinook salmon, survival does not appear to be an issue. Survival was >97% for CFD and Sensor Fish modeling. This may indicate that at HAHD passage is the issue, as opposed to survival after passage. Fish are not passing HAHD, which may potentially be due to the depth of the tunnel entrance (Liss Larson et al. 2025).

Table 5-3. Probability of survival estimates for CFD and Sensor Fish data for the various treatments at HAHD, applied to nontagged subyearling Chinook matching the subyearling length distribution used during the GPR live fish deployments. Estimates include in survival probability for individual stressors (collision, shear, and pressure) and the probability of survival when individual stressors are combined.

Treatment	Probability of Survival			
	Collision	Shear	Pressure	Combined Stressors
Sensor Fish				
Low Pool - Low Flow	0.992	1.000	0.996	0.988
Low Pool - Med Flow	0.992	1.000	0.996	0.988
Low Pool - High Flow	0.985	1.000	0.996	0.981
Med Pool - Low Flow	0.989	1.000	0.995	0.984
Med Pool - Med Flow	0.985	1.000	0.996	0.987
Med Pool - High Flow	0.989	1.000	0.996	0.985
High Pool - Med Flow	0.982	1.000	0.996	0.977
High Pool - High Flow	0.982	1.000	0.995	0.985
CFD				
Low Pool - Low Flow	0.998	1.000	0.996	0.995
Low Pool - Med Flow	0.998	1.000	0.996	0.995
Low Pool - High Flow	0.998	1.000	0.996	0.994
Med Pool - Low Flow	0.995	1.000	0.996	0.991
Med Pool - Med Flow	0.997	1.000	0.996	0.993
Med Pool - High Flow	0.996	1.000	0.996	0.991
High Pool - Med Flow	0.996	1.000	0.996	0.992
High Pool - High Flow	0.997	1.000	0.996	0.992

6.0 Conclusions

Live fish results from laboratory shear and collision tests, GPR bypass pipe passage, and the HAHD tunnel passage demonstrated high immediate (1-hr) survival rates across most conditions, with variability in the overall (48-hr) survival influenced by confounding factors. In laboratory collision tests, coho salmon exhibited 100% immediate survival at 40 fps jet velocities and 90.7% at 50 fps (n=30–54 treatment), while shear tests showed nearly 100% immediate survival (>95%) for both coho and Chinook salmon up to 50 fps, dropping at higher velocities due to species-specific sensitivities (Chinook salmon generally higher than coho salmon). Key lab findings included minimal tag effects overall, though balloon-tagged fish had slightly lower immediate survival probabilities compared to non-tagged counterparts.

At GPR, Chinook salmon fry and subyearlings achieved immediate survival rates exceeding 98% through the steep slope bypass (985 ft elevation, 100% flow control valve opening, with 48-hr survival at 98.8% and 97.2% (n=179–190 treatment), though fish condition and recovery issues in the juvenile fish collector potentially introduced some uncertainty in the results. At HAHD, immediate survival for coho salmon was generally high (>90%) through the 19-ft tunnel across forebay elevations (1089–1168 ft) and gate openings (8–32 in), but 48-hr survival varied from 75.9% to 100% (n=20–107 treatment), with lower rates at higher elevations and intermediate gate openings. These results provide baseline estimates but highlight that immediate survival metrics offer a more reliable indicator of passage effects than delayed assessments due to post-release confounding factors.

Field study limitations included challenges with balloon tags at HAHD, such as no depth acclimation (tags activated immediately before release to minimize disruption), tag retention issues leading to balloons recovered without fish or vice versa, and unrecovered fish. These factors contributed to low recapture rates in 2023, though improved attachment methods tested in lab retention studies enhanced 2024 performance. Balloon presence was found to increase the probability of mortality during lab shear testing, making observed survival rates conservative compared to non-tagged fish of interest.

Sensor Fish results from laboratory shear and collision tests, GPR bypass pipe passage, and the HAHD tunnel passage showed that collision events are the primary contributors to predicted fish injury and mortality, as indicated by the percentage of severe acceleration events and the velocity-based strike metric (M_V). Shear events were rare, and when they did occur, the corresponding shear M_V values were very low and not associated with fish mortality based on live-fish testing. During the laboratory shear tests, non-tagged Sensor Fish exhibited higher mean values of maximum acceleration and higher shear M_V values than tagged Sensor Fish, indicating a measurable tag effect on the recorded shear response under controlled conditions. Barotrauma was negligible under the evaluated conditions.

At GPR, the 24-in steep slope bypass pipe exhibited a higher percentage of severe acceleration events and high collision M_V values than the 12-in horizontal pipe, with most severe events occurring in the bend region at the base of the steep slope pipe. At HAHD, the upstream tunnel transition and tunnel regions produced the highest percentage of severe acceleration events and the highest collision M_V values, while the gate opening and downstream tunnel transition regions showed substantially lower values for both metrics.

For the design of a new HAHD steep slope bypass like the GPR bypass, these findings suggest that collision risk should be minimized by avoiding abrupt geometric transitions, including sharp bends and rapid changes in slope or alignment, that increase the likelihood of fish–structure contact. Emphasis should be placed on maintaining smooth longitudinal and lateral transitions

through bypass pipes to reduce the frequency of severe acceleration events and limit M_V magnitudes observed during passage.

High-resolution CFD modeling simulations were performed to predict the hydrodynamics and hydraulic stressors affecting fish survival in fish passage systems. Extensive CFD simulations were conducted to model complex flow physics, particularly particle movement in free surface flow. Coupled CFD-DEM simulations were utilized to compute particle trajectories and sample hydraulic stressors. The size and shape of the particle, serving as a surrogate for fish, were consistent with field studies conducted using Sensor Fish. The CFD particle simulations followed a two-step process. First, extensive multiphase flow simulations were carried out using the VOF method, which is highly suitable for modeling stratified flows like open channel flows. Subsequently, the DEM method was applied to calculate particle trajectories and collisions between particles and various structures within the fish passage system. Severe events were identified based on particle shear and collisions with rigid structures. The intensity of these events was quantified using a novel strike metric derived from velocity (M_V) data measured by Sensor Fish.

In the primary phase, CFD simulations were carried out to validate the free surface characteristics and pressure drop in a 1:25 laboratory-scale model of the existing HAHD. The multiphase flow simulations, performed using the VOF method, showed good agreement with the laboratory-scale model in terms of free surface wave behavior, water depth along the tunnel walls, and conditions at the tunnel exit. The predicted water levels on the left and right sides of the tunnel corresponded closely to experimental values, with a deviation of approximately 10%. Additionally, the comparison of water surface levels at the tunnel exit indicated good consistency between the CFD simulations and experimental results, apart from a minor discrepancy observed on the right side.

CFD simulations were performed at PNNL to assess shear and collision stressors. The CFD-predicted velocities near the nozzle exit showed reasonable agreement (within 10%) with experimental measurements at lower jet velocities (< 20 fps). Subsequent extensive CFD-DEM simulations were conducted to determine the mortal threshold of M_V for shear and collision testing. DEM parameters for particle-wall interaction were calibrated to better align the M_V threshold with Sensor Fish data. The cumulative probability distributions of M_V from CFD simulations qualitatively matched well those from Sensor Fish data for both collision and shear tests. These cumulative exposure probability distributions were then used to establish mortality thresholds through live fish testing with coho and Chinook salmon (with collision testing performed specifically on coho salmon). The resulting mortality thresholds were applied to predict fish survival rates for HAHD and GPR.

Computational Fluid Dynamics-particle simulations were conducted using 600 particle datasets to evaluate the hydraulic and biological conditions of the physical model for HAHD downstream juvenile fish passage under varying operating conditions, including forebay water elevation and gate opening to achieve the desired discharge rate. Consistent with Sensor Fish studies, severe events were identified based on particle acceleration and a novel strike metric derived from velocity M_V data recorded by Sensor Fish. At lower forebay water elevations and discharge rates, particles predominantly collided with the tunnel floor. As discharge rates increased, particle collisions shifted toward the outer wall of the tunnel, an outcome that was anticipated. The nadir pressure distribution calculated under these conditions indicated that barotrauma was negligible. Additionally, the M_V values recorded during severe events were found to be very low, suggesting minimal fish mortality, as confirmed by live fish testing.

Further, CFD-particle simulations using 600 particles were conducted for the GPR bypass at the highest water elevation and full valve opening. Severe events were observed in the 24-in steep

slope pipe, particularly near the bend where the pipe transitions to a horizontal orientation. The 24-in pipe exhibited very shallow water layers due to its steep slope, leading to severe events caused by particle collisions with pipe walls. In contrast, the 12-in horizontal pipe showed lower M_V values, as particles remained fully submerged in water. Additionally, nadir pressure was found in the 12-in pipe; however, magnitude is not low enough for barotrauma injury. Using the calibrated M_V threshold (4.21 m/s) from laboratory collision testing, the predicted survival rates based on CFD simulations corresponded closely with results from live fish tests.

The live fish injury assessment, Sensor Fish, and BioPA modeling tasks spanned over three years (2023–2025). The data collected was successfully analyzed and correlated to determine thresholds that can aid in future modeling of fish passage at HAHD. The results presented in this report are the final findings from the field and laboratory studies.

Future studies may look to incorporate a biological-response curve (as a function of M_V), as the M_V threshold is a set value. Therefore, it does not allow for adjustment based on species or length. Results from the live fish field and laboratory testing have demonstrated that these variables may be contributing factors to fish survival. A biological-response curve, rather than an M_V threshold, may match up better for correlations or explain some of the differences in fish survival, because the M_V might change based on length and species. Ultimately, understanding and incorporating the differences between field and lab, and live fish, Sensor Fish, and CFD modeling, and using those to establish an appropriate threshold value for M_V is critical for the design of the new HAHD fish passage project.

7.0 References

Brown RS, TJ Carlson, AJ Gingerich, JR Stephenson, BD Pflugrath, AE Welch, MJ Langeslay, ML Ahmann, RL Johnson, JR Skalski, and AG Seaburg. 2012. *Quantifying mortal injury of juvenile Chinook salmon exposed to simulated hydro-turbine passage*. Transactions of the American Fisheries Society, 141(1), pp.147-157.

Deters KA, RS Brown, JW Boyd, MB Eppard, and AG Seaburg. 2012. *Optimal suturing technique and number of sutures for surgical implantation of acoustic transmitters in juvenile salmonids*. Transactions of the American Fisheries Society 141(1): 1-10.

Deng Z, TJ Carlson, JP Duncan, and MC Richmond. 2007. *Six-degree-of-freedom sensor fish design and instrumentation*. Sensors 7(12): 3399-3415.

Deng ZD, J Lu, MJ Myjak, JJ Martinez, C Tian, SJ Morris, TJ Carlson, D Zhou, and H Hou. 2014. *Design and implementation of a new autonomous sensor fish to support advanced hydropower development.* Review of Scientific Instruments 85 (11).

Duncan JP, ZD Deng, JL Arnold, T Fu, BA Trumbo, TJ Carlson, and D Zhou. 2018. *Physical and ecological evaluation of a fish-friendly surface spillway*. Ecological Engineering 110: 107-116.

Dassault Systems. 2022. SOLIDWORKS V. 2022. Dassault Systems.

Hosmer DW Jr, and S Lemeshow. 2000. *Applied logistic regression*. John Wiley and Sons, New York, NY.

Hou H, ZD Deng, JJ Martinez, T Fu, JP Duncan, GE Johnson, J Lu, JR Skalski, RL Townsend, and L Tan. 2018. *A hydropower biological evaluation toolset (HBET) for characterizing hydraulic conditions and impacts of hydro-structures on fish*. Energies 11(4): 990.

Huang T, A Salalila, A Meyers, T Fu, J Martinez, H Hou, and ZD Deng. 2025. *Velocity-and pressure-based metrics for estimating strike injuries during fish passage through hydro turbines*. Results in Engineering 25: 104535.

Liss Larson SA, Fischer ES, Zionce EL, Harnish RA, Fu T, Ham KD, Carver JM, Deng ZD. 2025. *Evaluation of Howard A. Hanson Dam Juvenile Fish Passage and Survival Study: Downstream Passage and Survival (Acoustic Telemetry) Task*. PNNL-37338. Final Report submitted by the Pacific Northwest National Laboratory to the U.S. Army Corps of Engineers, Seattle, Washington.

Neitzel DA, MC Richmond, DD Dauble, RP Mueller, RA Moursund, CS Abernethy, GR Guensch, and GF Cada. 2000. *Laboratory studies on the effects of shear on fish*. EERE Publication and Product Library, Washington, DC (United States).

Normandeau Associates, Inc. 2018. *High head passage at Green Peter Dam: fish injury and survival evaluation*. Report prepared for U.S. Army Corps of Engineers Portland District, Portland, OR.

Normandeau Associates, Inc. 2019. *Biological Fish Injury and Survival Evaluation of the New Fish Weir at Foster Dam, 2018.* Report prepared for U.S. Army Corps of Engineers Portland District, Portland, OR.

Normandeau Associates, Inc. 2019. *Direct survival and injury of juvenile spring Chinook salmon passed through a newly installed turbine runner at Ice Harbor, 2019*. Report prepared for U.S. Army Corps of Engineers Walla Walla District, Walla Walla, WA.

Pflugrath BD, RP Mueller, KA Deters, SM Watson, AD Schneider, and ZD Deng. 2025. *Maximizing Safe Passage for Large Fish: Evaluating Survival of Rainbow Trout through a Novel Hydropower Turbine*. Environmental and Sustainability Indicators. DOI: 10.1016/ j.indic.2025.100801.

Richmond MC, JA Serkowski, C Rakowski, B Strickler, M Weisbeck, and C Dotson. 2014. *Computational tools to assess turbine biological performance*. Hydro Review, 33(6), pp.88-98.

Salalila A, J Martinez, A Tate, N Acevedo, M Salalila, and ZD Deng. 2023. *Balloon Tag Manufacturing Technique for Sensor Fish and Live Fish Recovery*. J. Vis. Exp. (200): e65632.

Salalila A, ZD Deng, JJ Martinez, J Lu, and LJ Baumgartner. 2019. *Evaluation of a fish-friendly self-cleaning horizontal irrigation screen using autonomous sensors*. Marine and Freshwater Research 70(9): 1274-1283.

Siemens Digital Industries Software. 2022. *STAR-CCM+, v. 17.06*, Siemens Product Lifecycle Management Software Inc: USA.

Singh RK, BD Pflugrath, and K DeSomber. 2021. *Tutorial Guide: Biological Performance Assessment (BioPA) Toolset for High Head Passage.* Report prepared for the U.S. Department of Energy.

Singh RK, P Romero-Gomez, A Colotelo, WA Perkins, and MC Richmond. 2022. *Computational studies of hydraulic stressors for biological performance assessment in a hydropower plant with Kaplan turbine*. Renewable Energy 199: 768-781.

Pacific Northwest National Laboratory

902 Battelle Boulevard
P.O. Box 999
Richland, WA 99354

1-888-375-PNNL (7665)

www.pnnl.gov